2014-08-20

# Genetically Designed Bacterial Biosystems for Environmental and Biomedical Applications

Leslie D. Knecht
*University of Miami*, lesanndole@gmail.com

UNIVERSITY OF MIAMI

# GENETICALLY DESIGNED BACTERIAL BIOSYSTEMS FOR ENVIRONMENTAL AND BIOMEDICAL APPLICATIONS

By

Leslie D. Knecht

A DISSERTATION

Submitted to the Faculty
of the University of Miami
in partial fulfillment of the requirements for
the degree of Doctor of Philosophy

Coral Gables, Florida

December 2014

UNIVERSITY OF MIAMI

A dissertation submitted in partial fulfillment of
the requirements for the degree of
Doctor of Philosophy

# GENETICALLY DESIGNED BACTERIAL BIOSYSTEMS FOR ENVIRONMENTAL AND BIOMEDICAL APPLICATIONS

Leslie D. Knecht

Approved:

| | |
|---|---|
| _____ | _____ |
| Sylvia Daunert, Ph.D. | Leonidas Bachas, Ph.D. |
| Professor of Biochemistry and Molecular Biology | Professor of Chemistry |
| _____ | _____ |
| Angel Kaifer, Ph.D. | M. Brian Blake, Ph.D. |
| Professor of Chemistry | Dean of the Graduate School |

_____
Sapna Deo, Ph.D.
Professor of Biochemistry and Molecular Biology

KNECHT, LESLIE (Ph.D., Chemistry)
Genetically Designed Bacterial Biosystems for Environmental and Biomedical Applications (December 2014)

Abstract of a dissertation at the University of Miami.

Dissertation supervised by Professor Sylvia Daunert.
No. of pages in text. (173)

Nature has endowed us with eloquently designed biosystems which can be applied to a number of analytical applications. Advances in biotechnology have allowed for bacteria and the proteins found therein to be exploited throughout the years for the development of designer analytical systems. Herein, we have exploited genetically designed bacterial whole-cell systems and proteins for biomedical and environmental applications. First, we have demonstrated the use of a whole-cell sensing system based on the quorum sensing regulatory protein LasR as a tool to elucidate interkingdom communication and better understand host-microbiome interactions. Specifically, the role of serotonin as a bacterial signaling molecule was investigated *in vitro* by examining virulence phenotypes of the opportunistic pathogen *P. aeruginosa* such as elastase production and biofilm formation. Next, we show the applications of genetically encoded biosensors integrated into diverse organisms -bacteria and worms- for *in situ* and remote detection of arsenic. To this end, first we demonstrate the utility of the genetically encoded biosensor incorporated in bacterial cells for the detection of arsenic in environmental samples and organoarsenicals, a class of arsenical compounds used as chemical warfare agents. The preservation and transport of the sensor was enhanced by forming bacterial spores, which were deposited on paper strips and used as inexpensive, transportable, on-site detection. In addition, we incorporated the genetically encoded biosensor into a model living organism,

*Caenorhabditis elegans* as a model for remote sensing capabilities. From this work, we exploit spores as packaging for whole-cell biosensors and incorporate them into wax printed paper strips for the development of on-site analytical detection systems. Finally, we employ a thermophilic dehalogenase from *Sulfolobis tokodaii* to demonstrate remote activation of enzymatic activity via iron oxide nanoparticles co-encapsulated with the enzyme in a hydrogel.

It’s not that I’m so smart, it’s just that I stay with problems longer. - Albert Einstein

**Acknowledgments**

I have been blessed in my life to be surrounded by inspirational people. It is these people that have carried me, both emotionally and intellectually, to my Ph.D. First and foremost, I thank my Ph.D. advisor Dr. Sylvia Daunert. She has been the force surrounding and pushing me to be my best for years. If I had not met her as an undergraduate, I would have never learned the excitement and fulfillment that research and teaching could bring me. For that, I am forever grateful to her. I also thank my committee members Dr. Bachas, Dr. Kaifer, and Dr. Deo. Your guidance throughout my research, your pep talks, and your criticisms have made me into the researcher and person I am today. I would also like to thank Dr. Patrizia Pasini and Dr. Mark Ensor. You have both taken the time to help me grow in the scientific process and much of my successes in the lab I owe to you. I also thank Dr. Zach Hilt and Dr. Yinan Wei for your guidance with my research.

I truly believe you are as good as the people you surround yourself with. There have been many great labmates throughout my career that have been instrumental in shaping me both intellectually and personally. First I thank Laura Rowe, my first graduate student mentor. Watching her adventurous spirit, listening to her unbiased advice, and learning from her intelligent conversations have definitely made me better than before we met. Second, I thank Krystal Teasley Hamorsky, Kendrick Turner, and Megan Gillespie for the fun and for the science. I thank Trajen Head for making my science beautiful through his figures. I thank Emre Dikici for putting up with me and challenging me daily to be a better scientist. I thank Gregory O'Connor for your belief in me as a scientist and your eagerness to be part of the big and little stuff. Finally, I thank Dr. Rahul Mittal for his

unending enthusiasm and support teaching me how to handle mice and to look at my science from a different viewpoint.

It has been said that sticking with your family is what makes them a family. That is why I am so grateful to Darryl and Freda Smith for being there when they didn't have to be and loving me no matter what. Your support has been and will always be more appreciated than I can convey. I thank my mom, Patricia Doane, for always believing in me and reminding me to always be strong and to always be kind. Finally, I thank the two men in my life-my husband Marc Knecht and my son Tobin Knecht. I owe much of what I am and have achieved to you.

TABLE OF CONTENTS

## LIST OF FIGURES

CHAPTER 1

CHAPTER 2



CHAPTER 3



CHAPTER 4

## LIST OF TABLES

List of Publications

1. L.D. Knecht, P. Pasini, S.K. Deo, and S. Daunert. “The Janus Nature of Serotonin: Neurotransmitter and Bacterial Quorum Sensing Molecule”, in preparation.

2. L.D. Knecht, H. Anderson, B.V. Sharma, M. Daftarian, S.K. Deo, and S. Daunert. “Paper Strips for Arsenic Detection Based on Engineered Sensing Spores”, in preparation.

3. L.D. Knecht, H. Anderson, G. O’Conner, B.V. Sharma, S.K. Deo, and S. Daunert. “Genetically Encoded Biosensors in Diverse Organisms for Remote and *In situ* Detection”, in preparation.

4. L.D. Knecht, P. Pasini, and S. Daunert. “Luminescent Biosensing Systems Based on Genetically Engineered Spore-Forming Bacteria” in Luminescent Microbial Biosensor: Design, Construction and Implementation, **2014,** G. Thouand, Ed., Pan Stanford: Singapore.

5. L. D. Knecht, Nur Ali, Y. Wei, J. Z. Hilt, and S. Daunert. “Nanopartcile-Mediated Control of Enzymatic Activity,” *ACS Nano* **2012**, *6*, 9079-9086. This work was highlighted on the Nanowerk website http://www.nanowerk.com/spotlight/spotid=26973.php

6. L.D. Knecht, P. Pasini, and S. Daunert. “Bacterial Spores as Platforms for Bioanalytical and Biomedical Applications,” Special Issue *Microorganisms for Analysis*, *Anal Bioanal Chem* **2011**, *400*, 977-989.

7. L. A. Doleman, L. L. Davies, L. A. Rowe, E. A. Moschou, S. K. Deo, and S. Daunert “Bioluminescence DNA Hybridization Assay for *Plasmodium falciparum* Based on the Photoprotein Aequorin,” *Anal Chem* **2007**, *79*, 4149-4153.

8. L. A. Doleman, S. Bachas-Daunert, L. L. Davies, S. K. Deo, and S. Daunert “Photoproteins and Instrumentation: Availability and their Applications" in Photoproteins in Bioanalysis, **2006**, S. K. Deo and S. Daunert, Eds., Wiley-VCH: New York, NY.

# CHAPTER 1. INTRODUCTION

Environmental and biomedical research has a need for selective, sensitive tools for detection and analysis. In past years, many different technologies have been exploited to detect analytes, understand biochemical reactions, and for remediation purposes. One example is the emergence of nanotechnology as a powerful tool for detection. For example, quantum dots are ideal for the analytical purposes due to their unique properties such as a broad absorption, size tunable emission, and high quantum yields. For this reason, they have been employed for various applications such as drug discovery, imaging, and biosensing (1-4). Exploiting nanomaterials for biotechnology, however, has some shortcomings such as the lack of sensitivity and/or specificity for an analyte of interest. Nature has endowed us with rationally designed tools to overcome these limitations. Specifically, bacteria and proteins isolated from bacteria have been employed in numerous aspects of scientific research. For example, researchers have used bacterial inclusion bodies as a therapeutic vessel to target pathogens (5). Many proteins which are important to human health and development, such as bone morphogenic protein, have been expressed and isolated from bacteria (6). Beyond the aforementioned applications of bacteria in research, bacteria and their isolated proteins have also been exploited for the development of powerful analytical detection systems.

## 1.1 Bacterial Protein-Based Sensors

Advances in biotechnology for identifying and isolating bacterial proteins have stimulated their use in analytical applications. Molecular biology has evolved through the years to allow for more simplistic methods to manipulate bacteria and bacterial components and isolate proteins to make “designer” proteins for a plethora of

applications. These advancements have been at the level of novel enzymes for polymerase chain reactions to ligation free cloning kits. Further, site-directed mutagenesis and random mutagenesis of a particular gene of interest no longer take weeks or months but can be completed in days. Another example is the numerous purification tags which can be genetically fused to a protein of interest for purification such as the His-tag, Glutathione-S-transferase, Maltose Binding Protein, Halo-tag and many more. These tags allow for the purification of proteins using affinity chromatography which allows for cleaner purifications in less time than previous methods. Further, proteins with innate functional abilities such as fluorescence, bioluminescence, remediation, analyte binding, etc… are continuously being discovered. With each discovery, the toolbox for analytical applications is ever expanding.

### 1.1.1 Green Fluorescent Protein

The advancement of genetic techniques has allowed for proteins to be synthesized *in vivo*, thus making it more feasible to integrate fluorescent detection methods in biological systems. Arguably, the most significant fluorescent protein to date has been green fluorescent protein. GFP was first discovered by Shimomura in 1962 (7). Later, Chalfie *et al*. were able to clone GFP and Ormö *et al*. crystallized the protein in 1996, making it available to researchers for a plethora of biotechnology applications (Figure 1.1) (8-9). Since its discovery and the availability made possible through molecular cloning techniques, GFP has been employed in a variety of applications, from sensing to imaging. Rajendran *et al*. imaged protein-protein interactions *in vivo* using a lanthanide (Tb(III)) as a donor and GFP as a receptor protein (10). The long lifetime of the

lanthanide allowed for time-gated spectroscopy and the authors were able to eliminate nonspecific background fluorescence. This method has also been employed for caspase-3 detection (11).

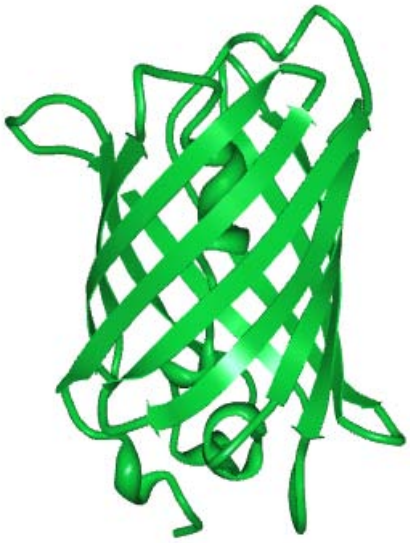

**Figure 1.1.** Crystal structure of Green Fluorescent Protein (PDB 1GFL).

Further, the applications for GFP have expanded due to the manipulations of its amino acid sequence to expand the optical properties of GFP (12). This has been particularly useful in the application of GFP and its variants for Förster re sonance energy transfer (FRET), specifically to understand the interaction of proteins or molecules *in vivo*. Biskup *et al*. employed the GFP variants YFP and CFP to study the interactions of the α and $\beta_1$ subunits of the human cardiac sodium channel (13). The authors use a mode-locked laser and confocal microscopy to determine that the subunits were associated with the endoplasmic reticulum before reaching the plasma membrane. The benefits of using

two mutants of GFP allows for resolvable fluorescence spectra and lifetimes of both the donor and acceptor, allowing both to be measured simultaneously. This is advantageous because it allows the FRET and emission-quenching processes to be differentiated. The FRET pair, CFP and YFP, have also been employed in flow cytometry to allow for cell-sorting assays (14).

Beyond FRET-based applications, the modification of GFP to produce proteins with various fluorescence characteristics has also been employed for multianalyte detection. For example, Lewis *et al*. employed a red-shifted GFP (rsGFP) and a blue fluorescent protein (BFP) which were each conjugated to a different model peptide (15). Each GFP derivative fluoresced at a different wavelength, allowing for dual-analyte detection in a single well. The peptides were incubated in the same well with antibodies specific to each peptide. The authors were able to detect $1 \times 10^{-6}$ M and $1 \times 10^{-7}$ M peptides in a mixed solution, demonstrating the feasibility of their system for multi-analyte detection.

Furthermore, a genetic fusion of GFP to proteins of interest has found numerous applications in biotechnology. For example, GFP was genetically fused to streptavidin and employed for the identification of biotinylated antibodies in living or fixed cells by fluorescence microscopy (16). However, although the GFP fusion proved efficient for histochemical applications, it did not have as good of a detection limit in the microtiter plate format as compared to the luciferase-streptavidin fusion. GFP has also been fused to single-chain antibody variable fragments. Casey *et al*. fused a red shifted enhanced GFP (eGFP) to the antibody specific for hepatitis B antigen (17). The fusion protein was able to retain the specificity of the antibody and the fluorescence properties of eGFP with

either N- or C-terminus fusion of the antibody. In addition to genetically fusing GFP to whole-proteins of interest, the structure of the GFP molecule makes it a candidate for altering its amino acid sequence to genetically engineer a mutant of GFP that has novel binding characteristics. Goh *et al*. engineered eGFP to contain binding sites for the bacterial endotoxin lipopolysaccharide (LPS) (18). The mutant was expressed in COS-1 cells and the fluorescence of the protein was quenched in the presence of LPS binding to the eGFP mutant proteins. Not only was the modified eGFP applicable for the detection of the bacterial endotoxins, further studies demonstrated that the protein could be employed to specifically tag gram-negative bacteria in contaminated water samples (19).

### 1.1.2 Bioluminescent Proteins

Bioluminescence is the production and emission of light from living organisms such as fish, insects, bacteria, fungi, etc…(Figure 1.2) Due to their efficient quantum yield, the absence of a need for an excitation source, and low background, bioluminescent proteins have been exploited in numerous detection and imaging applications (20). These attributes have allowed bioluminescent proteins to be successful in applications which require high sensitivity and low limits of detection, specifically in physiologically relevant matrices. There are two subgroups of bioluminescent proteins: photoproteins and luciferases. Photoproteins are able to emit light that is proportional to the concentration of protein present. Luciferases rely on an enzymatic reaction in which, in the presence of oxygen, the luciferase oxidizes the luciferin forming an electronically excited state and the resultant relaxation causes the emission of light. Therefore, the concentration of the luciferin is proportional to the amount of light produced.

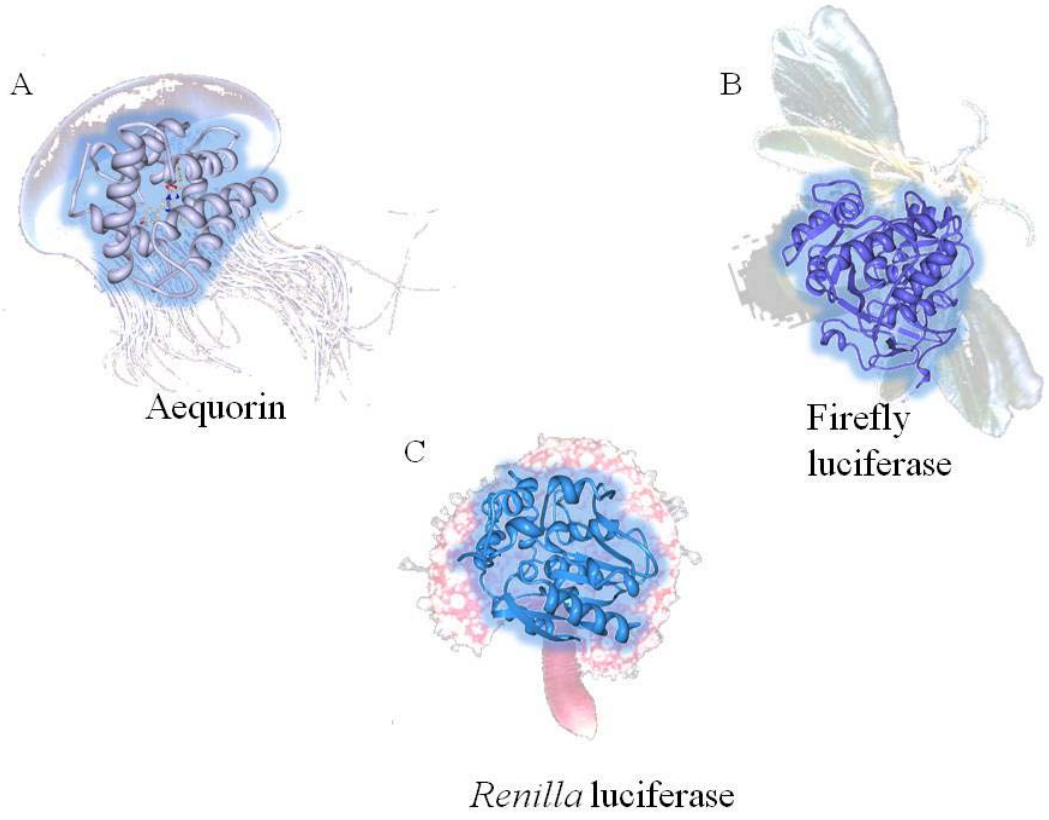


**Figure 1.2.** Select bioluminescent proteins which have been used as reporters in bioassays. A) The photoprotein aequorin (PDB 1EJ3) was first isolated from the jellyfish *Aequoria victoria*. B) The firefly luciferase (PDB 3IEP) and C) *Renilla* luciferase (PDB 2PSE).

Firefly luciferases and its derivatives rely on ATP to catalyze the oxidation reaction of the luciferin substrate (Figure 1.3). This characteristic has been exploited for the development of highly specific assays for the detection of ATP. One such assay was developed by exploiting the ATP dependency of firefly luciferase to screen for the levels of ATP produced through contaminating fungi, bacteria, and yeast in food and feeds (21). The authors found that the amount of bioluminescence was directly proportional to the number of contaminating organisms.

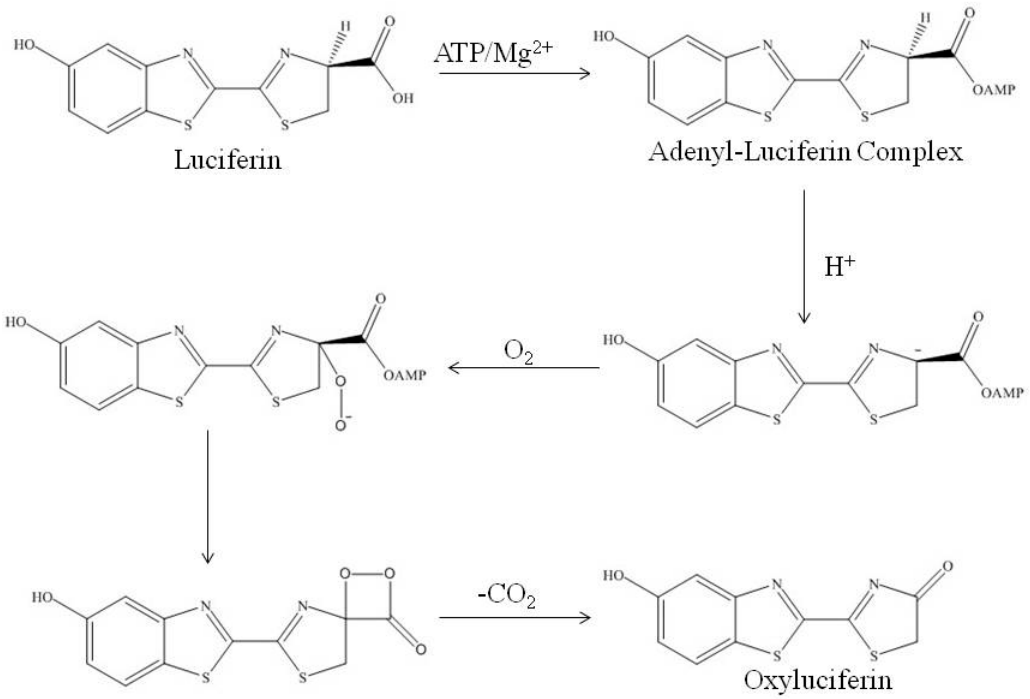


**Figure 1.3.** The mechanism by which the luciferin reacts with ATP to produce an oxyluciferin and light.

Just as firefly luciferases are ATP dependent, another bioluminescent protein, aequorin from *Aequoria victoria*, is $Ca^{2+}$ dependent which has allowed aequorin to be utilized for the determination of $Ca^{2+}$ ions *in vivo*. The release of $Ca^{2+}$ is triggered by the activation of G protein receptors and ion channels through the initiation of signal transduction mechanisms in the cell. The role of $Ca^{2+}$ in such cell signaling events makes it an important ion to study to help elucidate signaling pathways and develop new drug targets (22). To this end, Menon *et al*. expressed apoaequorin intercellularly alongside a chimeric G protein and a G protein-coupled dopamine receptor (23). The cells were then used to screen over 8,000 compounds for potential drugs to target G protein-coupled

receptors and ion channels. Further, the method was implemented alongside a fluorescence-based system demonstrating that both techniques performed similarly to identify positive compounds although the bioluminescence-based system had several advantages one of which was reduced number of false positives.

Luminescent proteins have also been employed as reporters for DNA hybridization assays. One such study employed the photoprotein aequorin for detection of the malaria parasite *Plasmodium falciparum* (24). A biotinylated DNA oligo specific to *P. falciparum* was immobilized via the biotin-streptavidin interaction on a neutravidin coated microtiter plate (Figure 1.4). Aequorin was genetically engineered to have only one cysteine and was conjugated to streptavidin and subsequently incubated in the presence of a biotinylated target DNA which was complementary to the DNA immobilized on the plate. The labeled DNA was incubated with varying concentrations of unlabeled target. The assay was able to detect 3 pg/μL of *P. falciparum* DNA in human serum, which was within the required concentration range for malaria diagnosis. Additionally, unlike other malaria detection methods, there was no need for PCR amplification prior to testing.

Luminescent proteins are ideal for biomedical analysis because of the aforementioned relatively low background in biological matrices, which have allowed for these proteins to be exploited for immunoassays. In order to employ these luminescent proteins in such assays, the protein is modified either chemically or genetically to be fused to an antigen or an antibody of interest. One example of chemical conjugation is the conjugation of biotin to the *Cypridina* luciferase (25). The conjugate was incubated with streptavidin and then used in a sandwich immunoassay by adding the conjugate to wells

of a microtiter plate where the primary antibody, antigen (α-interferon), and biotinylated secondary antibody were previously immobilized. Using this method, the authors were able to achieve a linear range of detection of 7.8 to 500 pg/mL of α-interferon. A genetic modification is typically preferred to ensure reproducible batch-to-batch production of the labeled probes. This method also provides a one-to-one conjugation of the reporter protein to the recognition moiety. For example, angiotensin II was genetically fused to aequorin (26) and the resulting fusion protein was employed in the detection of angiotensin II in human serum. The assay yielded a detection limit of 1 pg/mL of angiotensin II.

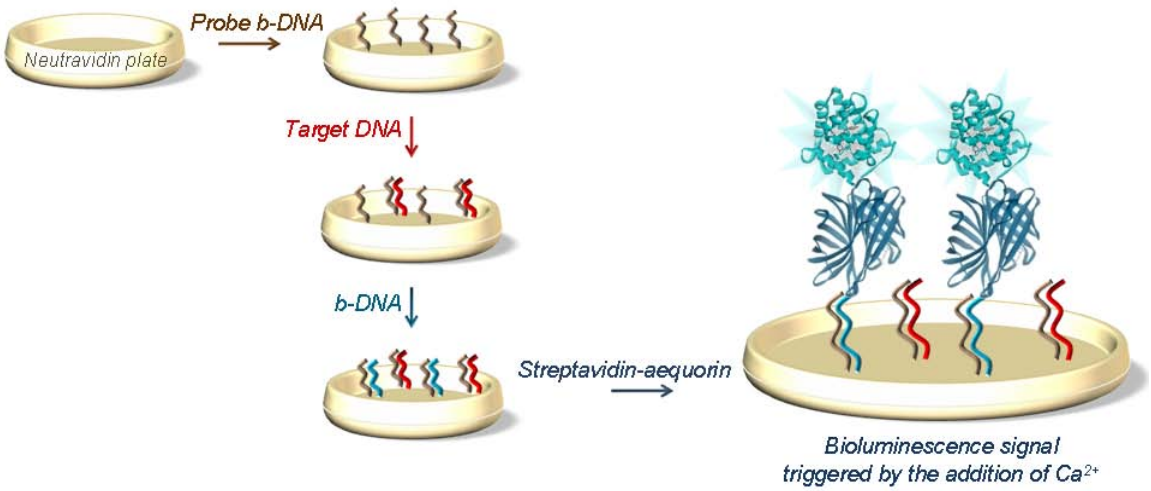


**Figure 1.4.** Schematic demonstrating the DNA hybridization assay employing aequorin as the reporter. Image used with copyright permission from reference (24).

### 1.1.3 Hinge-Motion Binding Proteins

As stated previously, nature has designed highly selective tools, such as bacterial proteins, which can be exploited for analytical purposes. One such class of proteins is hinge-motion binding proteins (HMBP). These proteins typically have two domains

which bend around a 'hinge' region of the protein upon binding to the ligand, such as glucose binding protein (Figure 1.5). This conformational change can be exploited to detect analyte binding in several ways.

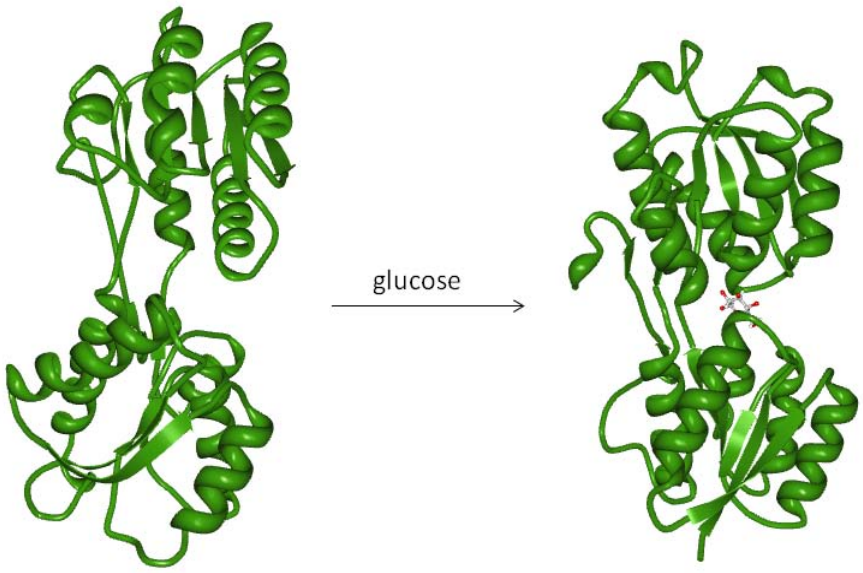


**Figure 1.5.** An example of the conformational change of a hinge-motion binding protein. The crystal structure of *E. coli* glucose/galactose binding protein in the absence (PDB 2FW0) and presence (PDB 2FVY) of glucose. The conformational change upon binding of glucose can be exploited for sensing applications.

First, a reporter group, such as an environmentally sensitive fluorescent probe, can be chemically conjugated to the protein in a strategic manner such that, upon binding and the conformational change, it experiences a change in its microenvironment. Since the fluorophore is sensitive to its environment, the intensity of the fluorescence emission is affected. This change in the intensity is proportional to the bound/unbound ratio of the ligand to the hinge motion binding protein. This method has been applied for the detection of various environmental and medically relevant analytes. For example, an environmentally relevant analyte, sulfate ion, can be detected by employing sulfate

binding protein (SBP), an *E. coli* periplasmic protein (27). Sulfate is known to influence the quality of drinking water. SBP was found to have three amino acids Ser90, Ser171, and Val181, which undergo significant changes in their microenvironment upon analyte binding. Wild-type SBP lacks cysteine residues that can be used as a convenient attachment locations in its structure. Therefore, site-directed mutagenesis was used to introduce cysteine residues at each of these sites. Environmentally sensitive fluorophores, such as 5-({2-[(iodoacetyl)amino]ethyl}amino)naphthalene-1-sulfonic acid (1,5-IAEDANS) and 7-Diethylamino-3-((((2-Maleimidyl)ethyl)amino)carbonyl)coumarin (MDCC), were conjugated to the cysteine residues and tested for sulfate binding. The sensor had a detection limit of $1 \times 10^{-6}$ M for sulfate ions and a detection can be performed within 5 min. Further, selectivity studies were performed with various tetrahedral, oxydianions. Of the molecules tested, only selenate was shown to interfere with the sensor. The sensor was stable and could be stored at 4 °C for 6 months without the loss of sensitivity. Additionally, several other HMBPs have also been conjugated to various fluorescent probes and exploited to detect environmental analytes such as nickel and phosphate (28-31).

Due to the overwhelming number of diabetic patients worldwide, glucose has become an important clinical analyte. Glucose sensors are typically based on glucose oxidase; however, previous studies have demonstrated the feasibility of using the *E. coli* periplasmic protein, glucose binding protein (GBP), for the development of protein-based sensors (32). As described previously, cysteine residues were incorporated into the GBP at rationally selected locations which were around the hinge region of the protein. Then these cysteine residues were used to chemically conjugate MDCC to the protein. In the

presence of glucose, the fluorescence was altered in a dose-dependent manner. The sensor had a dynamic range of $5 \times 10^{-8}$ to $1 \times 10^{-5}$ M for glucose. Further, selectivity studies were performed and no other sugars interfered with the signal except for galactose. Since the dissociation constant for galactose/GBP pair was higher than that of glucose/GBP pair, galactose should not interfere when detecting glucose *in vivo*. Other HMBP have been employed for the detection of biomedically relevant analytes, such as phenothiazines (33).

The second method to use a HMBP as a sensor is to genetically fuse a reporter protein to the hinge-motion binding protein. There are two methods to achieve this. In the first, a reporter protein can be genetically fused to either the N- or C-terminus of the HMBP. When the protein undergoes a conformational change, the environment of the reporter is changed, thus altering the fluorescence intensity of the reporter protein. This approach was taken when Dikici *et al*. fused enhanced green fluorescent protein (EGFP) to CaM to develop a sensor to detect phenothiazines and calcium (34). CaM is a $Ca^{2+}$-binding protein which has four calcium binding sites arranged in two globular domains. Upon binding of calcium, it undergoes a significant conformational change and adopts a dumbbell shape. The change exposes a hydrophobic region at each end of the protein which allows for various phenothiazines to interact with the protein. EGFP was fused to the C-terminus of CaM. The pH sensitivity was found to be similar to that of EGFP alone and calcium was shown to dose-dependently decrease the fluorescence of the EGFP. Further, several phenothiazine derivatives were shown to interact with CaM, which was indicated by a further change in fluorescence upon addition of the phenothiazine.

Proteins can also be genetically fused as chimeras. In this scenario, a reporter protein is truncated and one section is fused to the N-terminus of a HMBP and the other is fused to the C-terminus of the HMBP. Upon the conformational change of the HMBP, the two pieces of the truncated protein either comes into closer proximity to increase signal intensity or is forced away from one another, which decreases signal intensity. One of the first examples of this was the fusion of GFP to truncated CaM to design a sensor for $Ca^{2+}$ for use in imaging applications (35). Teasley *et al*. truncated the bioluminescent protein aequorin and fused it to the termini of glucose binding protein (GBP) (36). Upon addition of glucose, the GBP undergoes a conformational change which moves the truncated pieces in proximity of one another to allow for luminescence. The switch was "on" and "off" from a range of $1 \times 10^{-7}$ M to $1 \times 10^{-2}$ M glucose. The same strategy was also applied to develop molecular switches for sulfate and cyclic AMP as well (37-38).

### 1.1.4 Bacterial-Proteins Encapsulated in Hydrogels

The applications of bacterial proteins have expanded by the implementation of proteins into a polymer network for the construction of stimuli-sensitive hydrogels. A hydrogel is a crosslinked polymer chain network which readily absorbs water (39). By incorporating proteins into hydrogel networks, materials can be fabricated which respond selectively to an analyte of interest and have the sensitivity of the hydrogel to pH, ion concentration, temperature, or electric potential, depending on the polymer chosen. Miyata *et al*. employed a modified acrylamide hydrogel into which immunoglobulin G (IgG) and a goat anti-rabbit IgG antibody were chemically linked (40). The antigen-responsiveness of the resultant hydrogel was then quantified. In the absence of antigen, the hydrogel maintained a shrunken state due to the interactions of the antibody to IgG,

both of which were immobilized in the hydrogel network. Upon addition of free IgG, the swelling ratio of increased abruptly. Further, the selectivity of the hydrogel was studied by the addition of both rabbit IgG and goat IgG. Only rabbit IgG elicited a swelling response in the hydrogel. It was found that the swelling was reversible when the hydrogel was placed in a solution that is IgG deficient. The authors also examined the permeability of drugs through the hydrogel by using a model protein, namely hemoglobin, and examining the permeation profile. The protein was able to permeate the hydrogel network following the step-wise addition of free antigen. Importantly, the drug was unable to permeate the hydrogel in the absence of antigen.

As described earlier, many proteins undergo significant conformational change upon a given stimulus. One such protein is CaM, a previously described hinge-motion calcium-binding protein. CaM can undergo a further conformational change in the presence of certain peptides and the phenothiazine class of drugs. Ehrick *et al*. genetically engineered CaM to contain a unique cysteine at the C-terminus and reacted to an allylamine moiety to immobilize CaM within the polymer network (41). A polymerizable phenothiazine was prepared to contain the acrylamide moiety and the hydrogel was fabricated by free radical polymerization of the allylamine moiety on the CaM, the acrylamide on the phenothiazine as well as free acrylamide and *N*, *N*, -methylenebis(acrylamide). It was found that the hydrogel exhibited reversible swelling as a function of $Ca^{2+}$ concentration. Upon $Ca^{2+}$ binding, the phenothiazine was able to bind to the CaM. Addition of EGTA caused the release of the phenothiazine and a conformational change of CaM, causing swelling of the hydrogel. The authors also fabricated a control hydrogel which did not contain protein to determine if the swelling

response was because of the interaction of the ion with the protein or a change in ionic strength of the environment. It was found that the hydrogel swelled in the presence of $Ca^{2+}$, which is opposite of the trend seen in the hydrogels which had CaM present, indicating that the shrinking and swelling behavior was due to CaM and not the change in the microenvironment. Further, another phenothiazine, chloropromazine (CPZ), was added to the hydrogel. The immobilized phenothiazine derivative was displaced by CPZ and caused the hydrogel to swell. Complete swelling in the presence of CPZ was achieved in 3.5 min and 50% of swelling was observed in less than one minute. The authors also employed the hydrogel as a gate controlling flow of dextran, a blue dye, in a test tube. It was found that the blue dye was unable to penetrate the hydrogel in the swollen state and, upon addition of $Ca^{2+}$, was able to penetrate the hydrogel. This study demonstrated the feasibility of employing the hydrogels as microfluidic valves. Further studies performed by the same group evaluated the use of these hydrogels as microdomes (42). The microdomes were fabricated by a "microspotting" technique and a "UK" pattern was projected on the microdome to allow for it to be brought into focus and quantify the extent of shrinking and swelling. The lensing behavior could then be quantified by using a photomultiplier tube interfaced with a microscope. The authors found that the microlenses were able to detect $3 \times 10^{-8}$ M concentrations of CPZ. The authors suggest that these microlenses could also be used in arrays to screen for molecules that can bind to CaM.

There are a variety of hinge-motion binding proteins which would be ideal for incorporation into a bioactive hydrogel network. Glucose/galactose binding protein (GBP) is one such protein. Ehrick *et al*. employed GBP as the hinge-motion binding

protein in a hydrogel to quantify glucose in solution and to serve as a method for gated control of molecules through the hydrogel network (43). Upon the addition of glucose, the protein responded in an according-like conformational change and shrank. The response was reversible and the hydrogel was able to revert back to its normal swollen state when glucose was removed from the solution. The hydrogels were then tested for their ability to allow for diffusion of molecules in the presence and absence of glucose. It was found that in the presence of glucose, very little transport of molecules were observed; however, when glucose was not present, the molecules were able to pass in a size-dependant manner with the smallest having faster diffusion than the largest.

Beyond exploiting protein conformational changes due to analyte recognition, hydrogels have also been fabricated which contain enzymes and undergo macroscopic changes due to enzymatic activity. Upon addition of the appropriate substrate, the microenvironment of the hydrogel is altered and this allows for shrinking or swelling of the hydrogel in response to the stimulus. For example, Peppas *et al*. prepared glucose-sensitive poly(methacrylic acid-***g***-ethylene glycol) (poly(MAAc-***g***-EG)) hydrogels in the presence of activated glucose oxidase (44). At a low pH, the carboxy groups of MAAc formed a complex with etheric groups of ethylene glycol. At higher pH's, the carboxyl groups were ionized which caused the complex to dissociate. As the glucose oxidase in the hydrogels catalyzed glucose oxidation, gluconic acid was released which caused the microenvironment pH of the hydrogel to decrease, causing the hydrogel network to collapse, thus invoking the release of insulin. Other hydrogels have also been fabricated which contain glucose oxidase and are reviewed here (45).

### 1.1.5 Surface Display of Bacterial Proteins on the Surface of Bacterial Spores

In 1986, it was first demonstrated that heterologous proteins could be biologically functionalized onto the surface of bacterial cells (46-47). These systems typically take advantage of outer-membrane proteins such as OmpA, LamB, and PhoE (46-48); however, they are limited by the size of fusion protein that they are able to express as the heterologous protein is usually inserted into extracellular loop regions (49). To address this issue, spores have been utilized for surface display systems. The spore coat is decorated with surface proteins that can be conjugated to heterologous proteins via the C- or N- terminus and function as carrier proteins to display the passenger protein on the surface of the spore. Advancements in spore surface display techniques have led to the expression of proteins in their bioactive form and allowed for proteins such as reporters, enzymes, and recognition elements (e.g., antibodies) to be incorporated on this rugged platform for bioanalytical applications (Figure 1.6).

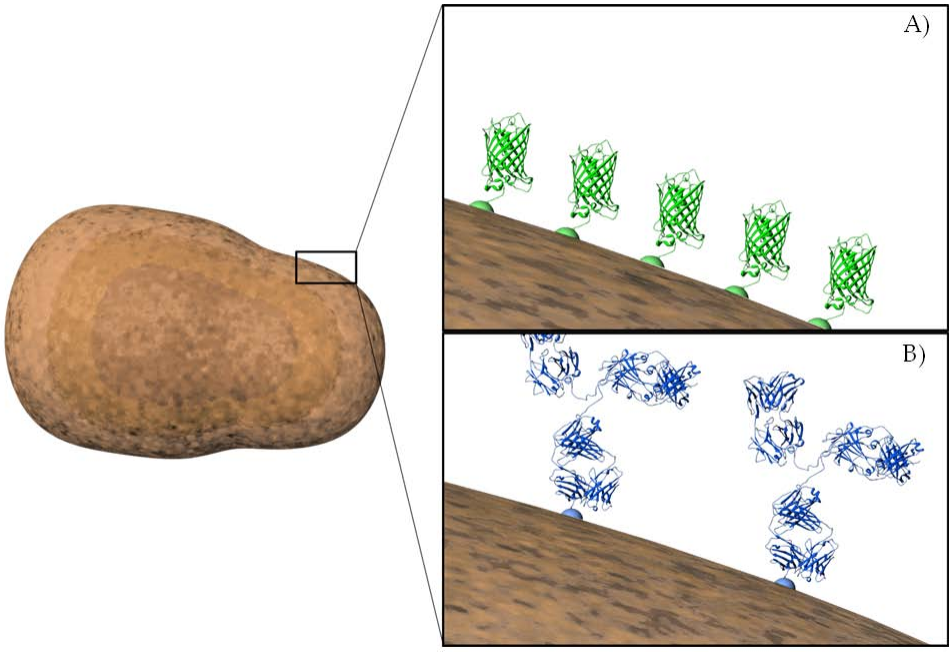


**Figure 1.6.** Schematic showing various classes of proteins displayed on the spore surface, including a) reporters, enzymes and b) recognition elements.

One of the most studied spore surface display systems is that of *B. subtilis*, due to the detailed knowledge of its spore structure. In particular, the CotB protein, which is expressed on the surface of *B. subtilis* spores, was one of the first spore coat proteins used to demonstrate the ability to display heterologous proteins on the surface of the spores (50). In this work, the authors fused the tetanus toxin fragment C (TTFC) to the CotB protein, thus exposing the non-natural protein structure on the spore surface. To confirm the presence of both CotB and TTFC on the surface of the spores, Western blot analyses were performed. Although this proved the expression of TTFC on the spore surface, it did not confirm that TTFC was in its active form. To evaluate the bioactivity of the toxin, mice were immunized with the surface modified spores to elicit a detectable immune response. Approximately four weeks into the study, TTFC specific IgG antibodies were present in the mouse serum at levels significantly above that of mice immunized with native spores, confirming the bioactivity of the TTFC. Not only did this study demonstrate the ability to effectively express bioactive proteins on the surface of the spore coat, but it was also one of the first studies to surface display a protein of such large molecular mass (51.8 kDa) without disrupting the bioactivity of the protein. Importantly, this work showed that proteins displayed on the surface of spores under varying temperatures retained similar activity to that of proteins expressed on fresh spores for up to 12 weeks, indicating the ruggedness of the spore as a platform for expressing heterologous proteins (50).

The importance of the biotin-streptavidin interaction in analytical applications has made it attractive for spore surface display. Streptavidin is a protein with four binding sites for its ligand, biotin (vitamin B2), and has one of the lowest known $K_d$ values ($10^{-15}$

M). One of the attractive features of this interaction is that biotin can be easily chemically conjugated to many biomolecules such as proteins, carbohydrates, and nucleic acids. Due to this strong, specific interaction and the ease of conjugation of the ligand to many biomolecules of interest, the biotin-streptavidin system has been exploited in numerous bioanalytical applications through the years for immobilization and detection in DNA hybridization assays, immunoassays, purification, and biomarker detection to name a few (24, 51-53). Kim *et al.* fused streptavidin to the spore surface protein CotG of *B. subtilis* (54). Successful display on the spore surface was confirmed by immunostaining the spores with an anti-streptavidin antibody and a fluorescein isothiocyanate (FITC)-labeled secondary antibody. Next, the streptavidin displaying spores were incubated with biotin-FITC to ensure that the streptavidin expressed on the spore surface was still in its bioactive form. From the fluorescence observed via confocal microscopy, it was found that the biotin-FITC bound with higher affinity to the outermost portion of the spore indicating that the streptavidin was functional with available biotin binding sites. To further prove the activity of the streptavidin displayed on the spore surface, the spores were analyzed with fluorescence activated cell sorting (FACS). From this data, it was concluded that there was a difference in fluorescence when spores with streptavidin expressed on the surface were incubated with biotin-FITC as compared to native spores. In addition to demonstrating one of the first examples of spore surface display of a tetrameric protein, this study showed the ability of the spores to overcome toxicity issues due to biotin sequestering, which are found when using vegetative cells for streptavidin surface display, once again demonstrating the ruggedness of spores as platforms for bioanalytical sensing systems.

Due to the innate stability of the spore, certain biological moieties can be expressed on the surface to allow the spores to be applied as bioremediation tools. Specifically, a system was developed where eighteen histidine residues were surface expressed via a fusion to the *B. subtilis* spore surface protein CotB (55). The spores were then analyzed for their ability to bind nickel ions. It was found that both, native and recombinant spores, were able to bind nickel; however, the spores displaying the histidine residues on their surface adsorbed significantly more nickel than their native counterparts. Additionally, it was found that neither pH nor temperature affected the ability of spores to bind nickel. The only factor that influenced the nickel adsorption was the amount of spores present in the suspension. Furthermore, the spores were subjected to desorption experiments to evaluate whether the nickel could be released from the spores. It was shown that approximately 40% of adsorbed nickel ions could be recovered from the native and histidine surface-displaying spores. Although this work demonstrated the feasibility of using spores as bioremediation agents, it should be noted that the histidine tag could only be imaged on the forespore and not on fully mature spores. The authors speculate that this could be due to the presence of a recently discovered spore crust in *B. subtilis* covering the histidine tag and making it inaccessible to the anti-histidine antibody employed in the imaging studies (56). This could indicate that biomolecules displayed with fusion partners on the spore coat of *B. subtilis* may not be accessible to an analyte of interest if the analyte is unable to penetrate this crust layer.

In addition to recognition elements such as the histidine tag and streptavidin, enzymes have also been displayed on the surface of spores. Specifically, work by Kwon *et al.* demonstrated the fusion of the enzyme ß-galactosidase to a surface protein of *B.*

*subtilis*, CotB, to develop a spore-immobilized biocatalyst for transgalactosylation in a water-solvent biphasic reaction system (57). After sporulation of the *B. subtilis* cells, the spores were tested under varying conditions such as ultrasonic vibration, vigorous shaking, and detergent treatment, to determine the extent of anchoring of the ß-galactosidase-CotB fusion to the spore surface. Interestingly, the enzyme remained conjugated to the spore surface, demonstrating a high degree of stability. It was found that the only treatment that was able to extract the enzyme from the spore was hot alkaline sodium dodecyl sulfate solution. Additionally, the activity of the enzyme displayed on the spore surface was evaluated in varying organic solvents. It was found that the immobilized ß-galactosidase was more active in the organic solvents than the free enzyme in solution. The thermal stability of the surface displayed enzyme was also increased as compared to the free enzyme, maintaining over 45% of activity after two hours of incubation at 40 ºC as compared to a complete loss of activity of the free enzyme at this temperature. Furthermore, this work described a higher enzyme activity at the interface between a polar and nonpolar phase, probably due to the mobility of spores at the interface, resulting in a higher availability of the enzyme. This increase in enzymatic activity at water/organic solvent interfaces had been previously noted when ß-galactosidase was conjugated with polystyrene (58). Although the chemical conjugation of ß-galactosidase to a polymer showed similar activities, the spore surface display has many advantages over polymer conjugation. First, through regular biofermentation processes at relatively low temperatures and pressure, the spores can be made available with properly folded enzyme. This is also a benefit because it requires no additional purification of the enzyme as it is genetically encoded on the spore DNA and displayed

on the spore surface. Additionally, the spores can be easily removed from the reaction by centrifugation and reused for further biocatalytic processes. The authors found that the spore surface displayed enzyme retained over 80% of the activity after being centrifuged, isolated, and reused.

Certain *Bacillus* spores have been utilized as natural probiotics in humans and animals or as feed supplements that improve the digestive health of the host (59-60). In fact, certain *Bacillus* species are known to act as probiotics. Their administration in the form of spores allows survival across the highly acidic environment of the stomach, meanwhile the ability of the spore to germinate and the bacterial probiotic activity are still maintained in the intestine. Although these microorganisms have innate probiotic properties, these properties can be enhanced by the addition of proteins, such as feed enzymes, to the surface of spores. Feed enzymes are typically incorporated into animal nutritients to increase the ability for the animal to digest and/or assimilate the feed, which minimizes the environmental impact of increased animal production. One obstacle for the use of these enzymes as probiotics is the ability to deliver them to the gut of animals while maintaining the activity of the enzyme in the harsh environment of the stomach. To overcome this obstacle, spores have been employed as carriers of such enzymes due to their innate resistance to harsh environments. Potot *et al.* displayed the feed enzyme phytase on the surface of *B. subtilis* spores using the inner coat protein OxdD as the carrier protein (61). Phytase increases the nutritional value of feed by freeing phytate-bound phosphorous, thus decreasing the need for supplementation of feed with free phosphorous. Previous studies, in which the reporter protein, GFP, was conjugated to OxdD, have shown that OxdD is a protein expressed in the inner layers of the spore coat

of *B. subtilis* spores (62). Due to its position on the interior of the spore coat, the authors hypothesized that using OxdD as a fusion partner to passenger proteins could offer protection from the surrounding environment as well as minimize the effect of the fusion on the formation of the spore coat. To further test their hypothesis, the authors fused phytase to both OxdD and CotB independently, and expressed both fusions on the surface of the spores. It was found that OxdD fusion showed a two-fold decrease in enzymatic activity as compared to fusion to CotB, which is positioned in the outermost layer of the coat. The authors suggested that although the location of OxdD may protect the enzyme from the environment, it could also hinder enzyme substrate accessibility.

The spore surface display of selected bioanalytically relevant species is possible for the development of spore-surface-based assays. For this, it is important to be able to express reporter molecules and other proteins of interest on the spore surface. Reporter proteins can help characterize the anchoring motifs of the various spore coat proteins without immunostaining, as well as be used for the signal production in bioanalytical assays. Green fluorescent protein (GFP) was one of the first reporter proteins to be expressed on the surface of the *B. subtilis* spores (63). In this study, $GFP_{UV}$ was fused to the C–terminus of the *B. subtilis* spore coat protein CotG. Additionally, *B. subtilis* cells were transformed with a plasmid that would allow for expression of the $GFP_{UV}$ without the fusion to CotG, to determine if GFP expressed in the cell without CotG as its fusion partner would be incorporated into the coat of the spore. Next, the native cells, the spores with the plasmid encoding for only GFP, and the spores encoding for the GFP-CotG fusion were analyzed via flow cytometry. With the wild type cells that do not have the plasmid encoding for GFP, no fluorescence was observed. However, the cells that

express GFP in the cytosol showed a combination of the non-fluorescent spores and the fluorescence of the mother cell, which contains cytosolic GFP. When the spores had fully formed, however, there was no fluorescence visualized on the resultant spores. The study concerning only the spores containing the GFP-CotG fusion showed a marked increase in fluorescence, indicating that the GFP was expressed on the surface of the spores. Additionally, the results from the flow cytometry experiments were confirmed by confocal microscopy. The display of GFP on the surface of spores has been further exploited by the fusion of GFP to other spore coat proteins to probe the interactions of these *B. subtilis* coat proteins during and after sporulation (62, 64). By using the GFP in a fusion for spore surface display, fluorescence microscopy can be a powerful tool to help elucidate the formation and structure of the intricate spore coat as well as the optimum termini for protein fusion to many of the surface display proteins, such as CotC, which form dimers in the spore coat (65-66). Additionally, fusion of EGFP to surface proteins in other *Bacillus* species, such as BclA and BclB in *Bacillus anthracis*, has led to the identification and characterization of other host proteins to be exploited in surface display (67).

Phage display has been a major tool in the discovery of novel peptides, antibodies, and proteins with high affinities for receptors or haptens; however, the toxicity of some proteins displayed on the surface of the phage leads to only the selection of mutants with stop codons or deletions in the protein sequence (68). Additionally, the high level of display may affect the infectivity of the phage while a low level may be discarded at the affinity chromatrography phase, during the phage selection. Spore surface display offers an advantage for the creation of mutagenesis libraries because the

surface of the spore is durable and the amount of displayed protein can be controlled based on the protein used to anchor the mutant. Many proteins are incorporated into the spore coat of *B. subtilis*, including enzymes. Gupta *et al.* exploited the surface display to perform directed evolution of an enzyme on the spore coat, CotA (69). CotA is a laccase which catalyzes the oxidation of a broad range of substrates, including diammonium 2,2-azino-bis(3-ethylbenzothiazoline-6-sulfonate) (ABTS) and 4-hydroxy-3,5-dimethoxybenzaldehyde azine (SGZ). The endogenous function of CotA in the spore is unknown, although it is responsible for the brown pigment of the spore which helps protect the spore from UV light (70). A mutagenesis library was constructed and the mutant as well as native CotA genes were ligated into a plasmid that was transformed into a *B. subtilis* CotA knockout strain. Upon cell growth and spore formation, both the control spores (with native CotA) and the mutant spores obtained from the mutagenesis library were assayed for CotA activity by measuring changes in absorbance of the ABTS and SGZ substrates. The authors found that one mutant of CotA, termed CotA-ABTS-SD1, was 120 times more specific for ABTS than the native enzyme. To ensure this increase in activity was not due to different levels of expression of each protein on the surface of the spore, the proteins were extracted and analyzed via SDS-PAGE, which showed that the levels of expression were similar for each protein. The sequence of the mutant CotA-ABTS-SD1 was then analyzed to determine the specific nucleotide mutations. This work was one of the first to demonstrate that the display of proteins on the surface of spores could be exploited to create and analyze mutagenesis libraries.

Although *B. subtilis* has been extensively used for the display of proteins on the surface of the spore, there are some shortfalls with this surface display system. Perhaps

the most pressing issue is the competition between expression of native spore surface coat proteins versus the expression of fusion proteins incorporating the coat proteins as carriers (71). Additionally, it has been shown that CotB$^-$ strains, not expressing the native CotB, cannot be used to express heterologous proteins (50). To overcome these problems, *Bacillus thuringiensis* spores have been explored for surface display. Specifically, $\partial$-endotoxins expressed on the surface of *B. thuringiensis* spores have been exploited as fusion carrier partners for spore surface display. These endotoxins, such as the crystal (Cry) and cytosolic (Cys) proteins, have biocidal activities that contribute to the use of *B. thuringiensis* spores as an insecticide in many agricultural applications (72).

Du *et al.* have constructed a plasmid that fuses a protein of choice to a 415 nucleotide sequence of a protoxin, Cry1Ac, which, in turn, acts as a fusion partner for the display of the chosen protein on the surface of the spore (73). It is important to note that this work was carried out using Cry$^-$ mutant strains of *B. thuringiensis*. This allows for expression of the fusion protein on the surface of the spore without competition from the native protoxin. Since this was one of the first studies utilizing the *B. thuringiensis* surface display system, the authors first had to optimize the length of the fragment of the protoxin needed for adequate surface display on the spore and yet minimize protease cleavage of the protoxin. In order to identify which fragments of the protoxin were large enough to have the anchoring site enabling adequate display of fusion proteins on the surface, but small enough to avoid degradation by proteases, the well-studied fluorescent reporter GFP was employed as the fusion protein to be displayed. Varying fragment lengths of the protoxin were evaluated to display the GFP on the surface of the spore. This was accomplished via fluorescence microscopy. The degree of fluorescence

intensity was dependent on protoxin length, ranging from spores with no protoxin and only the gene for GFP showing no fluorescence to spores with the longest construct (Bt10) exhibiting the highest fluorescence on the surface. After evaluating the display efficiency of several fragments of the protoxin, it was determined that the most efficient construct was a 415 nucleotide sequence termed Bt6. To further characterize their optimized system, the authors surface diplayed a single-chain antibody (scFv), which recognizes the hapten 4-ethoyxlmethylene-2-phenyl-2-oxazolin-5-one (phOx), as a fusion with Bt6. Upon treating the spores with bovine serum albumin (BSA) to block nonspecific binding and incubating them with either FITC-BSA-phOx or FITC-BSA as a control, it was noted that the spores treated with FITC-BSA–phOx had visible surface fluorescence and those spores treated with the control had no observable fluorescence, thus showing the ability of the surface displayed scFv to bind its ligand. This work was significant for two reasons: 1) it optimized the fragment size of the protoxin needed for spore surface display and 2) it demonstrated that functional biomolecules could be displayed on the surface of the *B. thuringiensis* spores.

Surface display has been employed to assist in the micropatterning of spores on a surface (74). Specifically, EGFP was displayed on the surface of *B. thuringiensis* spores by fusion to the spore surface protein InhA (Figure 1.7). This reporter protein was chosen due to the ease of detecting the fluorescence to image the position of the spores on the target surface. Glass surfaces were patterned with streptavidin conjugated to a fluorophore and poly(ethyleneglycol) (PEG) for surface passivation. An anti-GFP antibody was incubated with the spore to selectively bind to the EGFP on its surface. Next, a biotin-protein A complex was incubated with the spores for binding to the anti-

GFP antibody. The spore complex was then incubated on the streptavidin-patterned glass and was imaged with confocal microscopy. It was found that the spores would only bind to areas on the glass where streptavidin was patterned (Figure 1.7). The micropatterned spores were subsequently germinated in the presence of appropriate nutrients. Importantly, the obtained unattached vegetative cells were mostly spatially confined to where the spores were present, even though some cells could migrate to the PEG-patterned regions. This work demonstrates the feasibility of using surface displayed

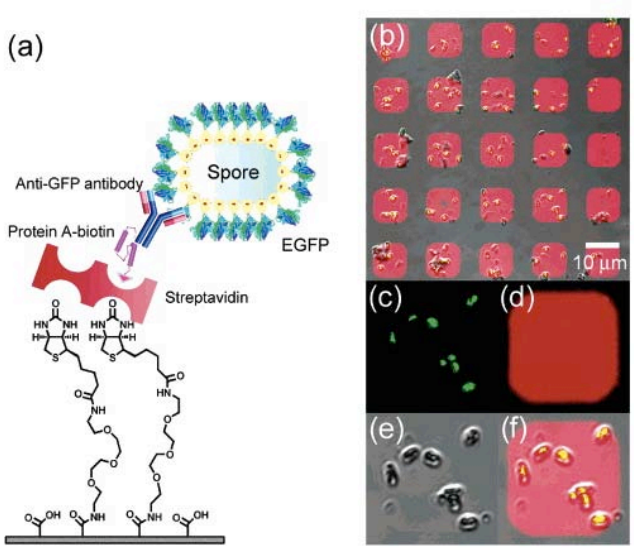


**Figure 1.7.** Micropatterning of spores with streptavidin displayed on the surface. a) Schematic showing the display of EGFP on the suface of *B. thuringiensis* spores and the method used for immobilization of the spores to the micropatterned surface. b) Fluorescent image of the micropatterned surface. Streptavidin was conjugated with tetramethylrhodamine isothiocyanate (TRITC), indicating that the streptavidin is only present in the red areas, as further shown by d). c) Fluorescence micrograph of spores displaying EGFP on the surface. e) Bright field image of the spores. f) Image showing that the spores are patterned only in areas where streptavidin is immobilized. Figure reproduced with permission from reference (74).

proteins on spores for micropatterning and proposes a general strategy for the micropatterning of any spore-forming microbial cells. However; due to the ability for the vegetative cells to migrate, the authors conducted another study in which they functionalized the spore surface with biotin and coated three-dimensional PEG microwells with streptavidin (75). As previously observed, the biotinylated spores were able to selectively bind to microwells with streptavidin and the vegetative cells remained consistently in place after spore germination due to the three-dimensional well structure. The ability to restrict spores to specific areas on the surface where also vegetative cells are confined could lead to future development of spore microarrays for multianalyte detection.

**1.2 Bacterial Whole-Cell Biosensors**

Genetically engineered living cells have found numerous applications as whole-cell biosensing systems (76-79). Inducible bacterial whole-cell biosensors are comprised of genetically engineered bacterial cells harboring a plasmid that bears a reporter element under the control of a specific operator/promoter (O/P). It is necessary to also have a regulatory/recognition element coding for a protein that will bind to an analyte of interest and, thus, either bind to (positive regulation) or release (negative regulation) the O/P region to begin transcription of the reporter element. Within a certain concentration range, this interaction results in an analyte dose-dependent response that is detectable by a color change, light emission, or other quantifiable signal, depending on the nature of the reporter and detection method employed (Figure 1.8). Non-inducible bacterial whole-cell biosensors rely on the toxicity of the molecule or sample of interest. These either naturally produce a signal, usually bioluminescence, or contain a plasmid with a reporter

protein that is constitutively expressed. When a toxic compound that is lethal to the cells is introduced to the system, the cells die, which results in a dose-dependent decrease in signal of the reporter protein. Inducible whole-cell biosensors have been used for detection of a variety of analytes (80-82). These biosensing systems have proven to be valuable analytical tools due to their selectivity, sensitivity, rapidity, ease of use, and cost-effectiveness.

### 1.2.1 Environmental Detection

Whole-cell biosensors are efficient tools for the detection of environmentally relevant molecules. Specifically, one benefit is the sensor detects only the bioavailable amount of analyte, which helps to predict the fate of molecules in toxicological studies. Unlike non-biological sensors, whole-cell biosensors are highly selective due to the need for a regulatory protein, which has high specificity and selectivity, for signal development. For these reasons, whole-cell biosensors have been employed for the detection of environmentally relevant molecules.

An important analyte that has been detected by whole-cell biosensors is hydroxylated polychlorobiphenyls (OH-PCBs), which are metabolites of PCBs. These molecules are extremely persistent in nature and have numerous negative health effects on humans such as inhibiting intercellular communication and forming DNA adducts which lead to the damage of DNA (83-84). Turner *et al*. developed a whole-cell biosensor based on the HbpR protein for the detection of OH-PCBs (85). The authors screened approximately 30 OH-PCBs to determine the sensitivity and selectivity of the

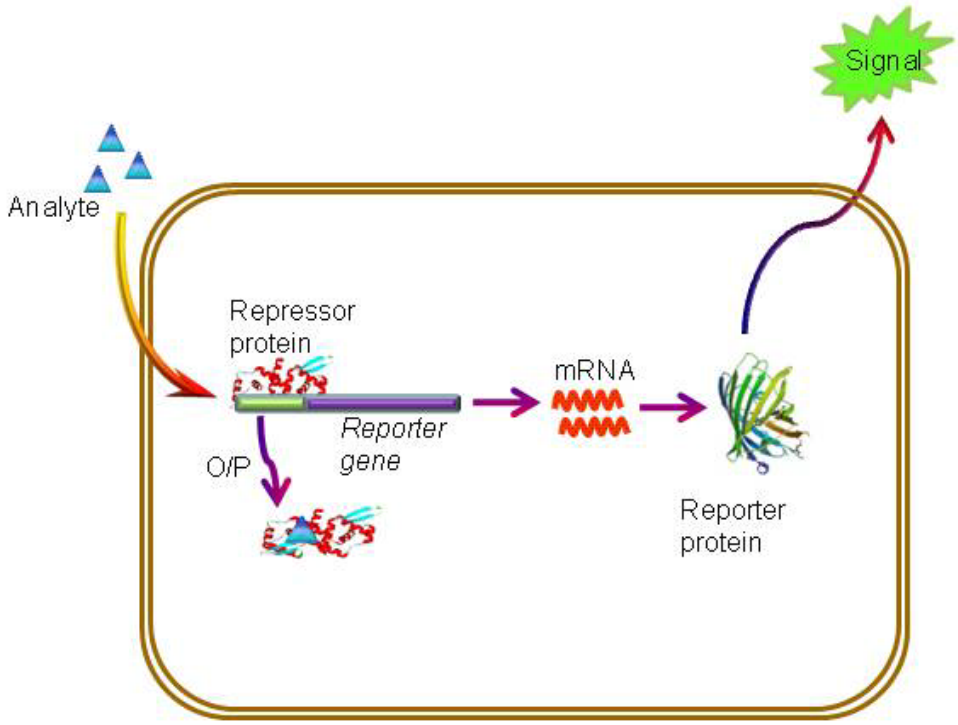


**Figure 1.8.** Inducible whole-cell biosensors harbor plasmids carrying reporter elements under the control of an O/P region. Upon analyte binding to a recognition/regulatory protein, the protein either releases the O/P region (negative regulation), as shown in the schematic, or binds to the O/P region (positive regulation) to begin transcription of downstream reporter genes. The result is a dose-dependent expression of the reporter protein, accompanied by a dose-dependent signal production based on analyte concentration.

sensor for a range of OH-PCBs with various hydrophobicities and chlorine substitutions. The sensor had a detection limits ranging from $1 \times 10^{-5}$ M to $1 \times 10^{-7}$ M, depending on which OH-PCB was being detected. Further, the authors demonstrated the feasibility of employing the sensor in human serum. OH-PCBs have also been detected using a whole-cell biosensor which employed ClcR, a chlorocatechol binding protein, although this sensor was only able to detect *para*- substituted OH-PCBs (86).

Whole-cell biosensors have also been employed for the detection of arsenic. In a study by Stocker *et al*., three separate whole-cell biosensors were developed which utilize

the *E. coli ars* operon (87). In the first sensor, *luxA* and *luxB* were fused upstream of the *arsR* gene and promoter region. The sensor was able to detect arsenite within 30 min and had a detection limit of 0.05 μM. In the second sensor, GFP was used as the reporter molecule. This sensor obtained a detection limit of 0.1 μM within 1 h. Finally, the third whole-cell sensor developed in the study employed β-galactosidase as the reporter. Due to the ability to use a chromagenic substrate with β-galactosidase, the authors utilized paper strips to develop a semi-quantitative method for the detection of arsenic. The strips, which had the whole-cell biosensors harboring *arsR* and *lacZ*, were incubated 30 min in the presence of analyte before the addition of X-gal. The blue color intensity that appeared correlated in a dose-dependent manner to the amount of arsenic present in solution. The authors could not differentiate between the color production from a strip exposed to 0.4 μM arsenic or higher, although this is well within the EPA limits for arsenic in drinking water. Further, water samples were tested from Bangledesh and all samples tested above the EPA limits. Rosen *et al*. genetically engineered a whole-cell biosensor to respond selectively to organoarsenicals over inorganic arsenic (88). Organoarsenicals are commonly found in livestock feed and as herbicides. Other whole-cell biosensors have been developed for the detection of chromate, copper, lead, cadmium, mercury, and other environmental compounds (89-92).

### 1.2.2 Detection of Quorum Sensing Molecules

Quorum sensing bacteria are responsible for diseases such as cystic fibrosis and irritable bowel disease (IBD) (93-94). IBD includes diseases such as ulcerative colitis and Crohn's Disease and is thought to be caused in genetically predisposed individuals by an

overly aggressive immune response to commensal bacteria (95). These diseases are characterized by an increase in inflammatory activity against chronic inflammation.

Raut *et al*. hypothesized that monitoring the quorum sensing molecules over time can give an idea of the amount of bacteria present, inflammation, and the progress of the disease (96). Specifically, a universal quorum sensing molecule which encompasses both Gram-negative and Gram-positive bacteria would be an ideal non-invasive biomarker for gastrointestinal disease. In recent years, a group of molecules referred to as autoinducer-2 (AI-2) have been found in both Gram-positive and Gram-negative bacteria (97). These molecules are used for interspecies communication. The production of these molecules from their common precursor, 4,5-dihydroxy-2,3-pentanedione (DPD), is catalyzed by the LuxS enzyme. In the organism *Vibrio harveyi*, the AI-2 diffuses out of the cell and binds to a periplasmic binding protein, LuxP. This binding event starts a cascade of phosphorylation/dephosphorylation events and leads to the expression of luciferase for the production of light (98). Raut *et al*. developed a biosensing system based on a *V. harveyi* strain BB170 developed by Bassler *et al*. (99). Native *V. harveyi* has a complex quorum sensing network which responds to both AHLs and AI-2; however, strain BB170 has been genetically modified to only respond to AI-2. Previously, this system has only been used as a bioassay to screen cell cultures to identify bacteria able to produce AI-2. Raut *et al*. optimized strain BB170 for use as a whole-cell biosensor and applied it for the quantitative detection of AI-2 in saliva, stool, and intestinal samples from IBD patients and control subjects (96). When AI-2 is present, it binds to the periplasmic binding protein LuxP, which undergoes a conformational change and initiates the transcription of the *luxCDABE* cassette. This cassette codes for bacterial luciferase and the enzymes that

catalyze the synthesis of the substrate for the luciferase. The amount of light generated by the cells is directly proportional to the amount of AI-2 present, which allows the sensor to be used to monitor the concentration of AI-2 in physiological samples. Specifically, the authors are monitoring the AI-2 levels in saliva, stool, and intestinal washing samples. The concentration of the biomolecule in saliva is indicative of systematic concentration while the concentration in stool and intestinal washing samples are representative of the bowel environment (100-101).

Initially, the authors optimized the protocol for the assay and established a dose-response curve for AI-2 with a detection limit of $2.5 \times 10^{-8}$ M and a dynamic range between $2.5 \times 10^{-8}$ M to $1 \times 10^{-5}$ M. It is important to note that the detection limit of the whole-cell biosensor is below the level of AI-2 previously found in human saliva. The AI-2 levels were reported to be between 244-965 nM by using LC-MS/MS, indicating the feasibility of use of this whole cell biosensor in biological samples (102). Additionally, the sensing system was found to be reproducible, having an intra- and inter-assay percent relative standard deviation of less than 8%. The entire assay took only 2.5 h, which was a 40% reduction in time as compared to the conventional assay.

Next, the authors detected AI-2 in stool samples. It was found that when the stool was not diluted, significant quenching of the bioluminescence was observed. Therefore, the authors optimized the stool dilution to remove any matrix effects and found that a 1:750 (w/v) dilution of stool in reverse osmosis (RO) filtered water was necessary. Due to the change of the matrix, the authors generated a new dose-response curve in 1:750 diluted pooled stool samples. This curve was compared to the standard dose-response curve and it was shown that the curves overlapped and had similar analytical

characteristics. The authors then tested stool samples from IBD patients and control patients. It was found that in the IBD patients, the levels of AI-2 varied considerably. The authors hypothesized that these variations may reflect perturbations in the microflora of the inflamed intestines (103-104).

Similar to the stool samples, when AI-2 was detected in saliva, matrix effects were noted. The authors determined that a 1:100 (v/v) dilution of the saliva eliminated the matrix effects and allowed for a dose-response curve with analytical characteristics similar to the standard dose-response curve. This confirmed that the whole-cell biosensor could be used in the detection of AI-2 in saliva.

When developing sensors which may have relevance for diagnostics or environmental detection, it is important to utilize a sensor and detection method which can be amenable to a portable bedside or field kit. Whole-cell biosensors are ideal candidates for such sensors due to their ability to withstand a range of environmental conditions, requirement of minimal or no sample pretreatment, easy and rapid detection, and cost-effectiveness, to name a few (105-106). Due to the prevalence of quorum sensing in the pathogenesis of bacteria-related disorders, developing a fast, reliable visual detection method for bacterial signaling molecules are of great interest. Previous work has been done to sense AHLs visually without instrumentation; however, these methods have shortcomings such as being time-consuming and not allowing detection in a dose-dependent manner (107). To overcome these shortcomings, Struss *et al*. designed a whole-cell biosensor that was amenable to paper strips for the semi-quantitative detection of bacterial quorum signaling molecules (108). This whole-cell sensor was based on plasmid pSD908, which contains the *lasR* gene and the *lacZ* gene under the

transcriptional control of $P_{lasI}$, transformed into *E. coli* DH5α cells. When long-chain AHLs are present (C8 and above), they bind to the LasR regulatory protein which, in turn, binds to its promoter sequence, $P_{lasI}$. This binding event begins the translation of the *lacZ* gene which produces β-galactosidase and is directly proportional to the amount of AHL present in the environment of the sensing cells. B-galactosidase has a variety of substrates to determine signal intensity and, depending on the chosen substrate, detection of the signal can be fluorescent, chemiluminescent, electrochemical, or colorimetric (109).

Initially, the whole-cell biosensor was incubated with *N*-dodecanoyl homoserine lactone (C12-HSL) to develop a dose-response curve. C12-HSL was chosen because it had previously been shown to induce a higher response in a whole-cell sensing system based on *lasR*/$P_{lasI}$ as the sensing element than shorter chain quorum sensing molecules(110). A chemiluminescence-based detection was used in solution to ensure the assay worked properly in solution before applying it to the filter paper. The limit of detection for the dose-response curve for C12-HSL was found to be $1 \times 10^{-9}$ M. To investigate matrix affects on the system, C12-HSL was also detected in pooled saliva previously determined to not contain C12-HSL. The dose-response curve generated was compared to the curve that was generated in the assay buffer, in the absence of saliva, and in the same analytical run and showed almost no matrix affects.

Next, the *E. coli* cells harboring plasmid pSD908 were immobilized on the filter-paper-based strips. This was accomplished by suspending the cells in a drying protectant solution and applying the solution directly to filter-paper strips to allow them to dry via a liquid-drying method. This method was used to help in the long-term preservation of

cells. After the cells were dried on the filter-paper strips, they were immersed in a test solution containing Luria-Betrani broth at 37 °C for 1.5 h. To detect, X-gal was added onto the bacterial cells to develop a blue color. The intensity of the blue color was directly proportional to the concentration of C12-HSL (Figure 1.9). The pixel intensities were measured using the software ImageJ. After 1.5 h, the detection limit for the paper strip biosensor was $1 \times 10^{-8}$ M; however, in only 60 min a detection limit of $1 \times 10^{-7}$ M AHL was obtained, demonstrating that the higher concentrations of AHLs can be detected at an earlier time. The assay was performed again incubating at room temperature (RT) and the dose-response curve had the same limit of detection as the one

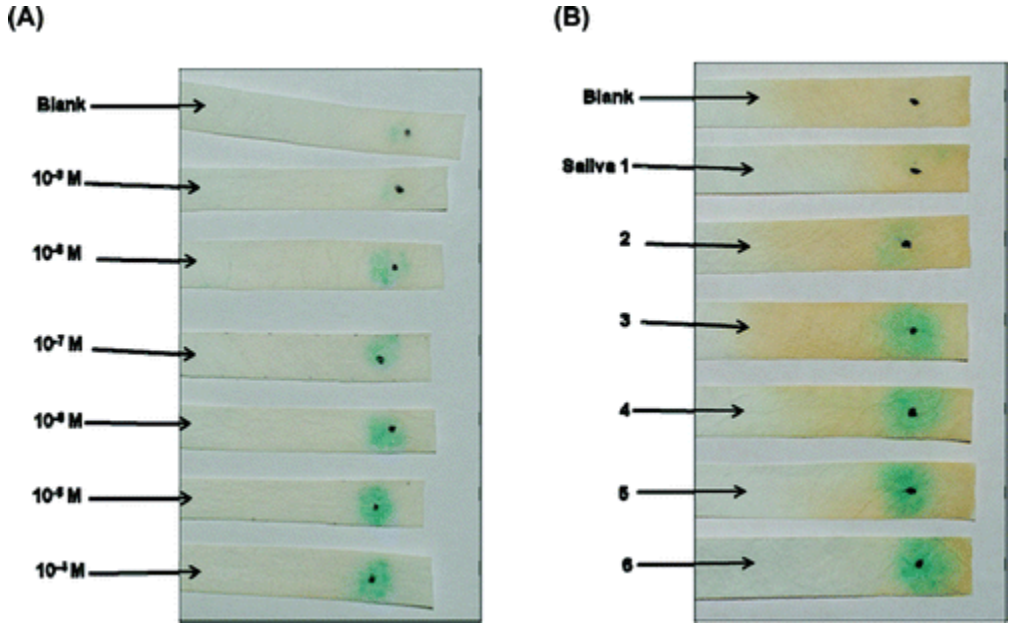


**Figure 1.9.** Paper strips for the detection of QSMs. Paper strips for the detection of QSMs. A) Dose-response data in buffer using filter-paper-based strips. The color intensity increases with increasing concentration of AHL. B) Detection of AHLs in healthy patients (1-5) and a patient with Crohn's Disease (6). Reproduced with copyright permission from reference (108).

at 37 °C. This demonstrates the applicability of the system for point-of-care diagnostics and field applications. Additionally, the paper strip sensors were found to be stable for 3

months at 4 °C without loss of analytical characteristics of the sensor. Finally, the paper strip sensor was employed for detection of AHLs in saliva and distinct AHL levels were found in both healthy patients and diseased individuals, showing that the use of paper strip sensors in physiological samples for the detection of AHLs is feasible.

Previous studies have shown that the gut bacterial flora may play a role in pathogenesis of inflammatory bowel disease (IBD) (111). Additionally, because antibiotics have been shown to successfully treat IBD patients, bacteria have been further implicated in the development of the disease (112). Previous reports demonstrate that the antibiotic azithromycin was able to interfere with the regulation of the quorum sensing network of *P. aeruginosa* by inhibiting virulence factors and biofilm formation (113-114). These studies, however, only investigated the behavior changes of the native cells, such as motility and biofilm formation, but did little to investigate the mechanism of action of the antibiotic on the quorum sensing system. To better understand how antibiotics are able to interact with the quorum sensing network and screen for antibiotics that are able to interfere with quorum sensing, Struss *et. al.* employed whole-cell biosensors with regulatory elements of *P. aeruginosa*, RhlR and LasR, that control the expression of *luxCDABE* which is under control of the promoter, $P_{rhlI}$ or $P_{lasI}$ in plasmids pSB406 and pSB1075, respectively (115-116). The plasmids were harbored by *E. coli* cells. Briefly, when AHLs are present in proximity of the whole-cell biosensor, they are able to form an AHL-regulatory protein complex which, in turn, is able to bind to its specific promoter and activate the transcription of *luxCDABE*. The production of light from the bioluminescent protein from *luxCDABE* is directly proportional to the amount of AHL present in the environment around the whole-cell biosensor. By utilizing the whole-

cell biosensor in an organism other than *P. aeruginosa*, it is possible to determine if the antibiotic inhibits quorum sensing regulation on the level of the regulatory proteins or if it interacts via a different mechanism. The authors investigated three antibiotics that were commonly used in the treatment of IBD: ciprofloxacin, metronidazole, and tinidazole. Azithromycin was used as a control because it has previously been shown to act as a quorum sensing agonist/antagonist (117). Additionally, to test the efficacy of the assays, the native compounds for RhlR and LasR were used, C6-HSL and C12-HSL, respectively.

Azithromycin was able to induce a dose-dependent response in both the pSB406 and pSB1075 based whole-cell sensors. Furthermore, it was able to induce light production both in the presence and absence of the cognate AHL. The other compounds tested were also able to induce the production of light in both whole-cell sensors both in the presence and absence of the cognate AHL; however, the similarly structured tinidazole and metronidazole activated the pSB1075 sensor to a greater extent than the pSB406 system. It is important to note that when the authors performed the studies with the whole-cell biosensor, they normalized all of the results to cell viability. This is to ensure that the changes observed are due to the interaction of the compound with the regulatory protein and not other interactions with the other components in the cells or due to a decrease in signal is due to a decrease in the number of live cells. Another important thing to note is that the concentrations of antibiotic that initiated an agonistic response were clinically relevant and included the peak plasma concentrations of the antibiotics.

The authors point out that their results are in contrast to previous studies reported for ciprofloxacin (118). However, the previous studies were performed in *P. aeruginosa*

PAO1 cells while the current study was performed using *E. coli* cells. This is an important demonstration of how whole-cell biosensors can allow studying the effects of molecules on a specific protein/promoter system, while in the native cells the effect could be due to other cell components. This was proven by a study showing that azithromycin did not directly affect the expression of QS-related genes, but decreased AHL production by lowering expression of genes upstream to the synthase ones (119).

Whole-cell biosensors are powerful tools, specifically for quorum sensing regulatory proteins which are difficult to purify and elucidate the structure. The ligand binding domain (LBD) of LasR was isolated and a crystal structure was solved (120). A study was performed to screen antibiotics for inhibitory quorum sensing activity. Specifically, azithromycin and ciproflaxicin were docked against the LBD of LasR. It was shown that these antibiotics do not bind to the AHL binding site of LasR but rather to a different site (118). By using a whole-cell biosensor, it was shown that although these molecules may not be binding to the LBD, they still bind in such a way that they can cause a conformational change and allow for LasR binding to its promoter region.

Beyond the molecules described above, whole-cell biosensors have been employed for the detection of numerous quorum sensing molecules which are noted in Table 1.1.

### 1.2.3 Packaging of Whole-Cell Biosensors

Although whole-cell biosensing systems are now well established, they are still limited due to the lack of stability of the cells for in-field analysis. Several cell storage methods have been employed to address these limitations such as, but not limited to, freeze-drying(121), sol-gel entrapment(122-124) and cryogel immobilization(125-126).

**Table 1.1.** Organisms and their autoinducers* that have been utilized in whole-cell biosensors.

| Organism | Autoinducer | Synthetase | Receptor | Reference |
|---|---|---|---|---|
| ***Psuedomonas aeruginosa*** | C4-HSL | RhlI | RhlR | (110, 127) |
| | 3-OXO-C12-HSL | LasI | LasR, QscR | (110),(116, 128-130) |
| | HHQ, PQS | PqsA | PqsR | (129) |
| ***Vibrio fischeri*** | 3-oxo-C6-HSL | LuxI | LuxR | (116, 131) |
| | AI-2 | LuxS | LuxP | (96) |
| ***Agrobacterium tumefaciens*** | 3-oxo-C8-HSL | TraI | TraR | (132-133) |

*For a complete list of quorum sensing organisms and their autoinducers, please see reference (97).

Although these methods are able to extend the shelf-life of whole-cell biosensors to a few weeks or months, they often are cumbersome, need additives to enhance the preservation method or require storage at low temperatures, which are not available in the field. Further methods to enhance long-term storage of whole-cell biosensors have been recently reviewed and critically discussed (134); An emerging method with promising initial results to improve the stability of whole-cell biosensors is to package them in spores. Particularly, these spores are simple and inexpensive to obtain, can endure extreme environmental conditions, have no need for nutrients, and can be stored and easily regenerated to active cells with little to no loss of analytical characteristics when implemented as whole-cell biosensing systems (135). These bacteria, such as those from the species *Clostridium* and *Bacillus*, have the ability to form spores in environments where nutrients are depleted. Bacterial sporulation is a process that results in the protection of DNA within a hard, dry coating. Spores can survive years in this dormant

state, with some reports of spore dormancy spanning longer than 25 million years (136-137). Although spores from different bacteria have similar structure, they vary in shape and size, and are specific to the organism from which they developed.

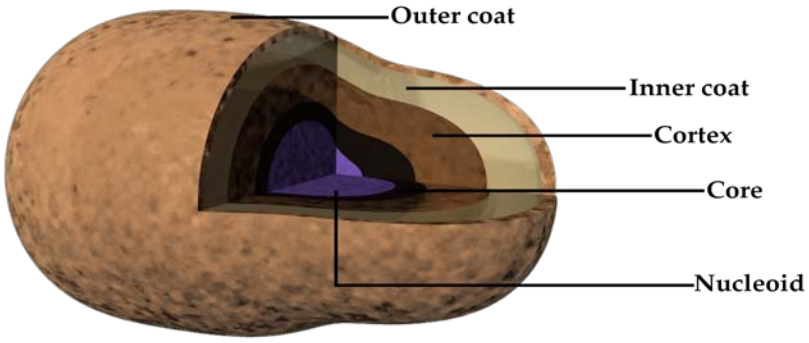


**Figure 1.10.** A schematic showing the layers of the spore coat.

A thick layer of modified peptidoglycan called the cortex surrounds the forespore (the section of the mother cells that is committed to sporulation after DNA replication and unequal division of the mother cell), and is coated by a multilayered protein shell comprised of an inner and outer coat (Figure 1.10). At the center of the spore is the core, in which the DNA is housed and protected by complexation with small acid-soluble proteins (SASP's), which make up more than 20% of the spore (138). These SASP's, along with the spore multiple layers, function to protect the spores from environmental damage and enhance their stability in extreme temperatures, pHs, humidity levels, and allow them to not be affected by UV, gamma radiation as well as the presence of toxic chemicals (136, 139-141). The *Clostridium* and some *Bacillus* species have an exosporium, a further outer layer that is composed of proteins, lipids, and carbohydrates. The exosporium serves as a site for spore surface antigens that may further help protect the spore from macrophages. This is important for the pathological species of

Clostridium and Bacillus where they need to escape the immune system of humans or animals of which they routinely infect (142). Despite the dormancy of the spores, receptor proteins on the surface of the spore are sensitive to small amounts of nutrients in

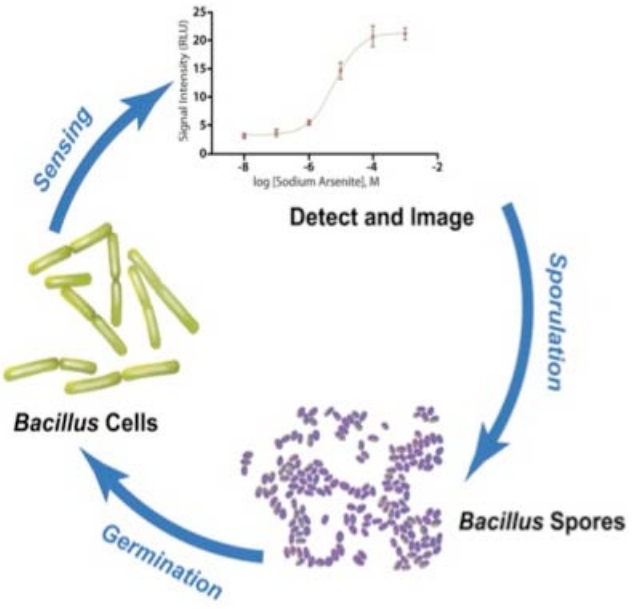


**Figure 1.11**. The germination and sensing of whole-cell biosensing systems preserved by sporulation. It has been shown that the sensing cells maintain similar analytical characteristics through numerous germination and sporulation cycles. Figure reproduced with permission from reference (143).

the environment and, upon binding these nutrients, they trigger the process of germination, which leads to metabolically active vegetative cells (144). Other organisms, such as bacteriophages, exploit the stability of the spore by entering a carrier state and allowing the spore to trap their DNA into the developing endospore for preservation (140). The properties of spores have also led to a stable vehicle for biosensing, drug delivery, and other state-of-the-art bioanalytical applications (143).

To use spores as a storage method for biosensing systems, the plasmid with a recognition element and reporter element must be transformed into a sporulating

organism. Once this is achieved, sporulation is carried out to form the highly stable long-term spore-based storage system; following spore germination, the revived cells can readily be used for analytical sensing (Figure 1.11).

Rather recently, our laboratory reported the first use of spores to enhance the long-term stability of whole-cell biosensors (145). Specifically, *Bacillus subtilis* cells harboring a plasmid that contained three genes *arsR, arsB,* and *arsC,* which confer bacterial resistance to arsenic, and *lac-Z* reporter gene, encoding β-galactosidase, under the control of the ArsR regulatory protein and *ars* operon O/P were employed for arsenic sensing. The cells were then sporulated and initially evaluated over 6 months for their detection limit, dynamic range and reproducibility. Detection limits in the submicromolar range were determined that were maintained during storage. Additionally, the analytical parameters did not vary significantly over the time period studied where the biosensing system was exposed to multiple sporulation-germination cycles. Follow-up studies demonstrated the stability of the spore-based sensing system when stored at room temperature for up to 24 months (134). To confirm the viability and broad applicability of this spore-based storage approach, *Bacillus megaterium* cells were employed to develop a whole-cell sensing system for zinc detection (145). For that, a plasmid containing the *smtB* gene, which encodes for the zinc binding protein, SmtB, and the *egfp* reporter gene, encoding the enhanced green fluorescent protein (EGFP), placed under the control of the *smt* operon O/P, was constructed and transformed into *B. megaterium* cells. Again, the analytical characteristics were unchanged through many germination and sporulation cycles as well as after storage of the spores for 8 months at room temperature. This work was the first demonstration of whole-cell biosensor stability when encapsulated in a spore

over long periods of time. Furthermore, work by Date *et al.* showed the feasibility of using these spore-based sensors in the determination of arsenic and zinc in environmental and biological samples, such as, freshwater and blood serum (Figure 1.12). The assay was performed in a microtiter plate format and results were obtained in 2.5 h or less upon direct incubation of the sensing spores with the samples. Importantly, the detection limit for arsenic was below the accepted levels of arsenic in drinking water as set by US Environmental Protection Agency (EPA), and the detection range for zinc was within the physiological and pathological levels in human serum (135). While this demonstration of using spores as whole-cell biosensors was completed in a laboratory setting, it represents an initial step towards the development of rugged biosensing systems for in field applications.

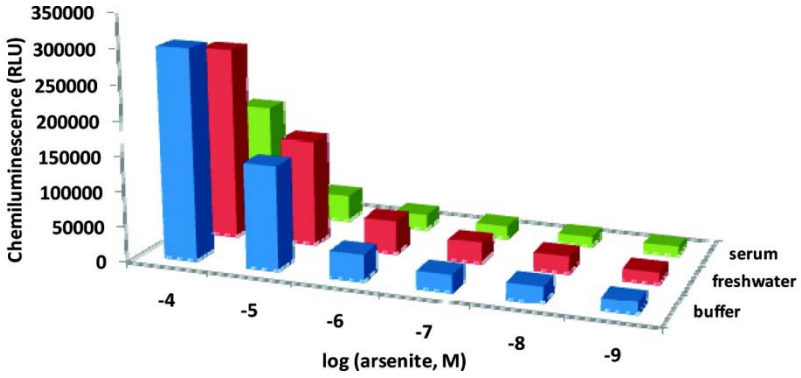


**Figure 1.12.** The dose-dependent responses of the B. subtilis arsenic sensing system in various matrixes, such as human blood serum, freshwater and buffer. *B. subtilis* cells harboring a plasmid with the *lacZ* reporter gene, encoding β-galactosidase, under the control of the ArsR regulatory protein and *ars* operon operator/promoter were employed for arsenic sensing. β-galactosidase was expressed dose-dependently on the basis of the addition of various concentrations of arsenic. *RLU* relative luminescence units. Figure reproduced with permission from reference (146).

Recent work by Fantino *et al.* demonstrated the use of spores for colorimetric sensors for zinc and the antibiotic bacitracin, terming these systems sposensors (147). This sposensor works by spotting the spores on filter paper and uses β-galactosidase as a reporter whose activity is detected by a colorimetric method, which allows for facile transport and reading of the sensor. *B. subtilis* cells incorporating a gene fusion of the *czcD* gene (a gene induced by the presence of $Zn^{2+}$) with *lacZ* reporter gene were sporulated. The spores were then spotted on filter paper and were incubated with a range of zinc concentrations. The sensor was found to be sensitive enough to detect zinc concentrations (10 μM) approximately eight times lower than the EPA approved levels in drinking water. Additionally, *B. subtilis* cells containing a gene fusion between *bceA* (a bacitracin-inducible gene of the *bceRSAB* operon that causes resistance of *B. subtilis* to bacitracin) and *lacZ* were turned into spores. Upon being spotted on paper in the sposensor format, the spores were exposed to varying bacitracin concentrations and showed a minimal detected concentration of 0.035 μM of antibiotic. This work utilizes a colorimetric sensor that can be easily operated and evaluated even by untrained personnel; however, it is still limited by the incubation time needed (at least 16 h) and controlled temperatures (37 or 30 °C) required for optimal results; furthermore, the system as presented can only provide semi-quantitative information, although the use of proper imaging software for color intensity measurements could produce quantitative data. Therefore, there is still a need for a system to incorporate rapid germination and quantitative detection all on a single platform at room temperature. Additionally, the authors did not test the viability of the sensor in real samples, which is necessary for laboratory and on-site applications.

To address the need for a portable system where spore germination, incubation with samples, and signal detection are all integrated, Date *et al.* have developed a miniaturized device where the sensing spores are incorporated into a centrifugal microfluidics compact disc (CD) platform (148). This system has multiple reagent loading chambers with valves that burst at varying angular frequencies, known as burst frequencies, upon spinning of the CD. This allows the nutrient rich media containing the spores and the analyte/sample to be released from their respective reservoirs to the mixing channel and, subsequently, the detection chamber. When a substrate is needed to detect the activity of the reporter enzyme, additional reservoirs are added to the design of the microfluidics structures. This system was evaluated using the previously described zinc and arsenic spore-based sensing systems and the luminescent signals were detected by employing a fiber optic based detection system (145). It was found that 150 and 180 min, respectively, were the minimum amounts of incubation time to detect the lowest concentration of zinc (1 μM) and arsenic (0.1 μM). This is a marked decrease in time as compared to the previously discussed sposensor, which requires 16 h for germination and signal development. Additionally, all experiments were carried out at room temperature, which facilitates on-site analysis. Furthermore, the detection limits in the microfluidics platform were comparable to those obtained on a microtiter plate format with coefficients of variation below 10%. The miniaturized system was also evaluated in real samples, such as, freshwater and serum, demonstrating similar detection limits and the feasibility of using the centrifugal microfluidics spore-based system in real world samples. These

results pave the way to the use of this miniaturized sensing system for on-site applications where a portable photodiode-based detector could be employed to measure the luminescent signals.

The natural hardiness and resistance of spores could also enable the use of whole-cell biosensors in locations with harsh environmental conditions as well as without easy access to a laboratory, e.g., remote areas and developing countries, which often lack adequate commercial distribution and storage facilities. To that end, a year-long study to investigate the effect of extreme climatic conditions on the stability of spores-based whole-cell biosensing systems has been accomplished in our laboratory (149). The spores were stored in laboratory conditions that simulated those found in real harsh environments, including, cold (arctic/polar areas), wet heat (tropical areas), dry heat (hot deserts), and desiccation. Aliquots of the stored spores were germinated at one-month intervals and the obtained sensing cells were assessed for their ability to respond to target analytes. The achieved results proved that the intrinsic resistance of spores to harsh environmental conditions helped maintain the integrity of the encapsulated sensor bacteria, thus allowing the revived active cells to retain their analytical performance during the course of the twelve-month storage period. This study supports the effective use of spore-based sensing systems for monitoring human health and the environment in the field, in extreme conditions.

**1.3 Statement of Research**

The goal of this dissertation is to exploit bacteria and their proteins for the development of tools for biotechnology applications. Specifically, we exploit these tools for the development of novel materials, to demonstrate the growing applications of

bacteria in the field of analytical chemistry, and to aid in the understanding of complex relationship between bacteria and their human host.

Chapter 2 focuses on the use of a bacterial whole-cell sensing system to understand the impact of mammalian neurotransmitters, specifically serotonin, on bacterial quorum sensing. This chapter delves into the concept of interkingdom communication where a species in one kingdom is able to respond to and react to a species of another kingdom. In this chapter, the effect of a common neurotransmitter, serotonin, on the quorum sensing system of a known pathogen, *Pseudomonas aeruginosa*, is evaluated using both a whole-cell sensing system and known processes native to the organism.

In chapter 3, the evolution of a whole-cell biosensor is demonstrated. We show how a bacterial whole-cell biosensor, which was originally created to detect inorganic arsenic, can be amended to various platforms and exploited for use in different applications than solely the detection of inorganic arsenic. This chapter includes data from a variety of experiments ranging from bacterial whole-cell biosensor data in solution to bacterial whole-cell biosensor data in nematodes. Chapter 4 expands on this concept and explores the use of packaging whole-cell biosensors in bacterial spores and immobilizing them on paper strips for the development of a facile, colorimetric sensor for the detection of arsenic. The paper-based system was one of the first to employ immobilized spores for enhanced stability and long-term storage of a whole-cell biosensor on paper and achieve detection in less than 4 h.

In chapter 5, a novel remotely controlled biohybrid material was developed. The thermophilic enzyme L-2-$HAD_{ST}$ was chemically conjugated to an

acrylamide hydrogel network and encapsulated with $Fe_3O_4$ nanoparticles. The activity of the thermophilic enzyme could be controlled by exposing the material to an alternating magnetic field (AMF) which, in turn, heated the nanoparticles and, thus, enhanced the activity of the enzyme. This chapter includes data optimizing the field strength of the AMF for enzyme activity and long-term stability data of the biohybrid material.

# Chapter 2. The Janus Nature of Serotonin: Neurotransmitter and Bacterial Quorum Sensing Molecule

## 2.1 Overview

Bacterial cells represent ~90% of the cells in a human body, with an estimated 500 to 1000 bacterial species present in the gastrointestinal (GI) tract, constituting part of our microbiome (150). The diverse and large population of bacteria in our microbiome prompted research aimed at understanding the bacterial influence on the host's physiology. It was found that incubation of *Pseudomonas aeruginosa* with norepinephrine causes increased expression of PA-I lectin, an adhesion protein, indicating that bacteria are able to sense the host's stress and alter their virulence phenotype accordingly (151). Sperandio et al. showed that the mammalian neurotransmitters epinephrine and norepinephrine activate the transcription of Lee1, a gene under control of the quorum sensing regulator QscA in enterohemorrhagic *Escherichia coli* (EHEC) as well as to activate flagella genes (152). The Lee genes express genes involved in attaching and effacing of EHEC cells for colonization in the large bowel. Epinephrine and norepinephrine are in high levels in the human GI tract, where EHEC cells colonize and cause outbreaks of diarrhea and hemolytic uremic syndrome (153).

Serotonin is an important neurotransmitter with more than 90% of serotonin in humans located in the enterochromaffin cells of the GI tract and regulating intestinal movements (154). It has been reported that bacterial flora in the intestines of the parasite nematode *Ascaris suum* alter serotonin levels in the host's intestinal tissue when they

become pathogenic (155). Research on the physiological effects of selective bacterial colonization of germ-free mice revealed in vivo elevated concentrations of serotonin and its main metabolite, 5-hydroxyindoleacetic acid, indicating that gut microbiota influence production of mammalian compounds (156-157). Further, plasma serotonin levels are reported to be 2.8 times higher in conventional mice compared to germ-free mice (158). These observations demonstrate the influence of the microbiome on the host production of neurotransmitters such as serotonin, an interaction which has been termed microbial endocrinology (159). This interaction is of upmost importance because certain bacteria endogenously produce serotonin, including *Rhodospirillum rubrum*, *Streptococcus faecabalis*, and *E. coli* (160). To date, it is not well understood why these organisms produce serotonin, although serotonin has also been shown to stimulate culture growth and cellular aggregation in a variety of microorganisms (160-162). Previous reports speculated that serotonin acts as an intercellular communication agent to accelerate and synchronize microbial populations (163). In bacteria, when populations reach a specific threshold, they communicate with organisms in their surroundings by releasing small diffusible molecules, autoinducers, in a process known as quorum sensing, QS (164). As previously hypothesized for serotonin's role in microbial populations, QS molecules (QSMs) are involved in the synchronization of the behavior of microbial systems and are responsible for many phenotypes of bacteria such as biofilm formation, expression of virulence factors, and light production, to name a few (165). These studies combined led us to hypothesize that serotonin may have a Janus-type behavior, acting both as a host's endogenous neurotransmitter and bacterial signaling molecule. To evaluate our hypothesis we performed a series of studies that demonstrate serotonin's participation in

bacterial quorum sensing and its ability to modulate quorum sensing behaviors, leading to well established bacterial quorum sensing phenotypes such as elastase production and biofilm formation (Figure 2.1).

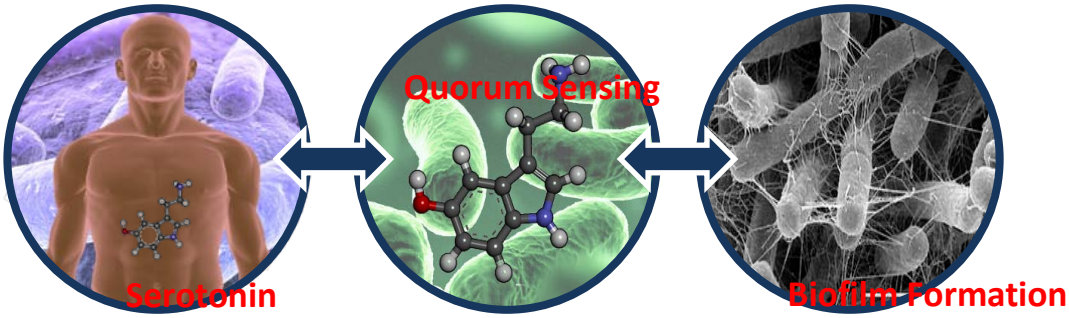


**Figure 2.1.** Over 90% of serotonin is produced in the gastrointestinal tract by enterochromaffin cells. Serotonin is able to dose-dependently bind to and activate regulatory proteins involved in bacterial quorum sensing and initiate the transcription of genes involved in the pathogenic response such as biofilm formation. This finding has implications in human disease and may lead to novel strategies for treatments of bacteria-related disease.

## 2.2 Materials and Methods

### 2.2.1 Plasmids and Bacterial Strains

For the whole-cell bioassays, *E. coli* DH5α cells harboring pSB1075 and pSB904, for LasR and RhlR production, respectively, and the expression vectors for QscR, pJN105Q, and PA1897-*lacZ*, pJL101(166) were used. Native *P. aeruginosa* strain PAO-1 and the *lasI* and *rhlI* double mutant, JP2, were supplied by Dr. Johanna Schwingel.

### 2.2.2 Reagents

Serotonin, Luria-Bertani (LB) Broth, gentamycin, tris base, dimethyl sulfoxide (DMSO), Costar white 96 well plates, and *N*-3-oxo-acylhomoserine lactone, *N*-butyryl-homoserine lactone, 1% crystal violet solution, and elastase were purchased from Sigma Aldrich (St Louis, MO). FilmTracer FM 1-43 biofilm stain was purchased from Life

Technologies (Grand Island, NY). Petri dishes and poly-L-lysine coated slides were purchased from VWR (Radnor, PA). The chemiluminescent substrate for β-galactosidase, the Beta-Glo kit, was obtained from Promega (Madison, WI) and used as suggested by the manufacturer. All solutions were made with Milli-Q purified water.

### 2.2.3 Apparatus

Chemiluminescence measurements were made on a BMG Labtech PolarStar Optima microplate luminometer (Ortenberg, Germany). All experiments were conducted at room temperature unless otherwise specified. All luminescent intensities are reported as the average of a minimum of three replicates that are blank subtracted and are expressed in relative light units (RLU). Fluorescent images were obtained using a FluoView FV10i Olympus Confocal microscope using a 63x oil immersion lens (Center Valley, PA). All data were graphed using GraphPad Prism 5.0 (La Jolla, CA).

### 2.2.4 Dose-response Curve for LasR

Glycerol stocks of *E. coli* DH5α cells harboring the pSB1075 plasmid for LasR were used to inoculate 5 mL LB broth containing 100 μg/mL ampicillin overnight at 37 °C with shaking at 250 rpm. This overnight culture was transferred to a 250 mL flask containing 50 mL of LB broth containing 100 μg/mL ampicillin and grown at 37 °C until the $OD_{600}$ reached between 0.4-0.6. Then, an aliquot of 90 μL of the culture was added to wells of a 96-well microtiter plate. A standard curve for *N*-3-oxo-C12-HSL, ranging from from $10^{-3}$ to $10^{-9}$ M, was prepared in DMSO by serial dilutions of a freshly prepared 1 x $10^{-2}$ M of *N*-3-oxo-C12-HSL stock solution. From these dilutions, standard solutions of concentrations ranging from 1 x $10^{-3}$ to 1 x $10^{-10}$ M were obtained by serial dilutions in distilled, deionized water. A 1% solution of DMSO in distilled, deionized water was

used as a blank. This percentage of DMSO was not found to be toxic for the sensing cells. This was also the method used to prepare serial dilutions of melatonin. A 1 x $10^{-2}$ M stock solution of the compounds from the tryptophan metabolic pathway was also prepared in 50 mM Tris, pH 7.5 for tryptophan, serotonin, and 5-hydroxytryptophan. To each well containing 90 µL of the sensing cells, 10 µL of each standard was added in triplicate. The microtiter plates were then incubated on an orbital shaker at 175 rpm, 37 °C for 2 h. After the incubation period, 100 µL of the β-Glo reagent was added to each well and incubated at room temperature for 30 min. The induced luminescence intensity was then measured using the microplate reader. The results were plotted using the software GraphPad Prism 5. The assay for determining the effect of serotonin on the RhlR system was performed as described above but with *E. coli* DH5α cells harboring plasmid pSB409.

**2.2.5 Dose-Response Curve for QscR**

Glycerol stocks of *E. coli* DH5α cells harboring plasmids pJN105Q and pJL101 were used to inoculate 5 mL LB broth containing 20 µg/mL gentamycin overnight at 37 °C with shaking at 250 rpm. This overnight culture was transferred to a 250 mL flask containing 50 mL of LB broth containing 20 µg/mL gentamycin and grown at 37 °C until the $OD_{600}$ reached 0.4. For QscR expression, an aliquot of 100 µL of a 20% arabinose solution was added to the culture. Then, an aliquot of 90 µL of the culture was added to wells of a 96-well microtiter plate. A standard curve for *N*-3-oxo-C12-HSL, ranging from from $10^{-3}$ to $10^{-9}$ M, was prepared in DMSO by serial dilutions of a freshly prepared 1 x $10^{-2}$ M of *N*-3-oxo-C12-HSL stock solution. From these dilutions, standard solutions of concentrations ranging from 1 x $10^{-3}$ to 1 x $10^{-10}$ M were obtained by serial dilutions in

distilled, deionized water. A 1% solution of DMSO in distilled, deionized water was used as a blank. This percentage of DMSO was not found to be toxic for the sensing cells. A 1 x $10^{-2}$ M stock solution of serotonin was also prepared in 50 mM Tris, pH 7.5. To each well containing 90 µL of the sensing cells, 10 µL of each standard was added in triplicate. The microtiter plates were then incubated on an orbital shaker at 175 rpm, 37 °C for 2 h. After the incubation period, 100 µL of the β-Glo reagent was added to each well and incubated at room temperature for 30 min. The induced luminescence intensity was then measured using the microplate reader. The results were plotted using the software GraphPad Prism 5.

**2.2.6 Effect of Serotonin on *N*-3-oxo-C12-HSL Response**

Studies were performed to determine the competitive nature of serotonin binding to the LasR protein. The cells were grown to an $OD_{600}$ of 0.4 and aliquots of 90 µL of the cells were transferred into the wells of a 96-well microtiter plate. Standard solutions of *N*-3-oxo-C12-HSL, ranging from 1 x $10^{-4}$ to 1 x $10^{-10}$ M, were prepared in 10% DMSO either in the absence of or containing $1 \times 10^{-3}$ M, $1 \times 10^{-4}$ M, or $1 \times 10^{-5}$ M serotonin Ten microliters of the standard solutions were added to the cells in triplicate. The assay was performed as described above and a dose-response curve was generated using GraphPad Prism 5.0.

**2.2.7 Effect of N-3-oxo-C12-HSL Response on Serotonin**

After identifying the concentration of *N*-3-oxo-C12-HSL which serotonin can compete, studies were performed to determine the effects of the QSM on LasR response to serotonin. The cells were grown to an $OD_{600}$ of 0.4-0.6 and 90 µL of these cells were aliquoted into the wells of a 96-well microtiter plate. Standard solutions of serotonin,

ranging from $1 \times 10^{-4}$ M to $1 \times 10^{-6}$ M, were made in the absence or presence of 0.1 nM *N*-3-oxo-C12-HSL in 10% (v/v) DMSO. Ten microliters of each standard solution were added to the wells in triplicate. Measurements were performed as described above and a dose-response curve was generated using GraphPad Prims 5.0.

**2.2.8 Elastase Studies**

Elastase production was measured using a previously established protocol with minor adjustments (167). *P. aeruginosa* PAO-1 cells and JP2 cells were grown overnight in LB broth at 37 °C and 250 rpm. The cells were then diluted to an $OD_{600}$ of 0.05 in fresh LB broth and incubated in the presence of either *N*-3-oxo-C12-HSL or serotonin for 16 h at 37 °C and 250 rpm. After incubation, the $OD_{600}$ of the cells was measured and they were centrifuged to separate the cells from the supernatant. The supernatant was then added to tubes containing 5 mg of elastin Congo Red and 1 mM $CaCl_2$ and incubated overnight at 37 °C and 250 rpm. The reaction was then quenched with EDTA and the tubes were then centrifuged to remove unreacted Congo red-elastin and the absorbance of the supernatant was measured at 495 nm. All absorbance values were normalized to the $OD_{600}$ values in order to correct for the variations of cell growth.

**2.2.9 Biofilm Formation**

*P. aeruginosa* strain PAO-1 and JP2 were grown overnight in LB broth at 37 °C and 250 rpm. The culture was then diluted 100-fold in M9 minimal media supplemented with 0.5% (w/v) casamino acids, 11.1 mM glucose, and 1 mM $MgSO_4$. Next, 1.0 mL solutions of cells containing either the analytes or the appropriate blanks were prepared according to table 2.1.

**Table 2.1.** Combinations of analytes for biofilm and elastase studies.

| ***N*-butyryl HSL** | ***N*-3-oxo-C12-HSL** | **serotonin** | **1% DMSO** | **50 mM Tris, pH 7.5** |
|---|---|---|---|---|
| **100 µL** | 100 µL | 100 µL | none | none |
| **100 µL** | 100 µL | none | none | 100 µL |
| **100 µL** | none | none | 100 µL | 100 µL |
| **none** | 100 µL | 100 µL | 100 µL | none |
| **none** | 100 µL | none | 100 µL | 100 µL |
| **none** | none | none | 200 µL | 100 µL |
| **none** | none | 100 µL | 200 µL | none |

Then, 200 µL of each solution was placed on poly-L-lysine coated microscope slides which was then placed in 100 mm petri dishes. A humidity chamber was created by placing a 35 mm petri dish filled with 5 mL of water in the larger dish and sealing with parafilm. The dishes were then incubated at 37 °C for 16 h without shaking. After incubation, the slides were gently washed with Milli-Q purified water and 200 µL of FilmTracer FM 1-43 stain was added to each slide and incubated in the dark for 30 min. The slides were then washed with Milli-Q purified water and covered with a cover slip. Fluorescent images of the formed biolfilms were captured on a FluoView FV10i confocal microscope using an FITC filter and a 63x oil immersion lens.

### 2.2.10 Crystal Violet Biofilm Studies

*P. aeruginosa* strain PAO-1 and JP2 were grown overnight in LB broth at 37 °C and 250 rpm. The culture was then diluted 100-fold in M9 minimal media supplemented with 0.5% (w/v) casamino acids, 11.1 mM glucose, and 1 mM $MgSO_4$. The solutions were prepared as described in Table S1. Next, 125 µL of each dilution was added in triplicate to the wells of a 96-well flat bottomed, white microtiter plate. The plate was then covered and incubated overnight at 37 °C in a humidity chamber. After incubation, the plates were inverted to remove any non-adhering cells. The plate was then washed three times by submerging the whole plate into container filled with double distilled, deionized water and inverting after each wash. Then, a 0.1% (w/v) aqueous solution of crystal violet was added to each well and incubated for 15 min at room temperature. The plates were then washed three times, as described above, to remove any excess crystal violet. After drying overnight in open air at room temperature, 125 µL of a 30% acetic acid solution was added to each well and incubated 15 min to dissolve the crystal violet. The resultant solution was transferred to a clear, flat bottomed microtiter plate and the absorbance was measured at 550 nm using an absorbance reader. (PolarStar Optima). All values were blank subtracted using 30% acetic acid as the blank.

## 2.3 Results and Discussion

To examine the effects of serotonin on bacterial communication, we employed a cellular system that, upon action by bacterial QSMs, elicits a response that can be measured by production of bioluminescence by the cells. Specifically, we employed *E. coli* JM109 cells harboring plasmid pSB1075, which encodes for the *P. aeruginosa* QS

regulatory protein LasR and contains the *luxCDABE* reporter gene cassette under the control of the promoter $P_{lasI}$ (110). Only when a signaling molecule is present, it binds to the ligand-binding domain of LasR, causes a conformational change in the protein, and initiates transcription of the *lux* cassette encoding for luciferase. The bioluminescence generated is related to the amount of signaling molecule present and capable to bind to LasR. Based on this principle, a dose-response curve was generated using the *P. aeruginosa*'s *las* system cognate QSM, *N*-3-oxo-C12-HSL, which helped validate the use of our cellular system in determining dose-response effects of molecules on the bacterial communications circuitry (Figure 2.2A). We then investigated our hypothesis that serotonin interferes with bacterial signaling by employing LasR regulatory system described above. It was found that serotonin reproducibly elicited a response from the bacterial cells starting at μM levels (Figure 2.2B). It is important to note that physiological concentrations of serotonin in the digestive tract, 10 μM (168), are able to activate the LasR quorum sensing network. Further, it has been reported that serotonin levels in the GI tract of patients with IBS, a condition in which bacteria are implicated (169), are ~ 100 μM (170), which corresponds to the serotonin levels eliciting a response mirroring that of the bacterial QSM *N*-3-oxo-C12-HSL.

Although the aforementioned experiments demonstrated that serotonin was able to trigger a response and, thus, presumably bind to and activate LasR, the nature of their interaction was still unclear. Further, in the gut serotonin co-exists with bacterial QSMs and therefore, it is important to determine how the presence of both molecules affects activation of LasR. To better understand the interaction between serotonin and the bacterial communication circuitry in the presence of the native QSM ligand, we

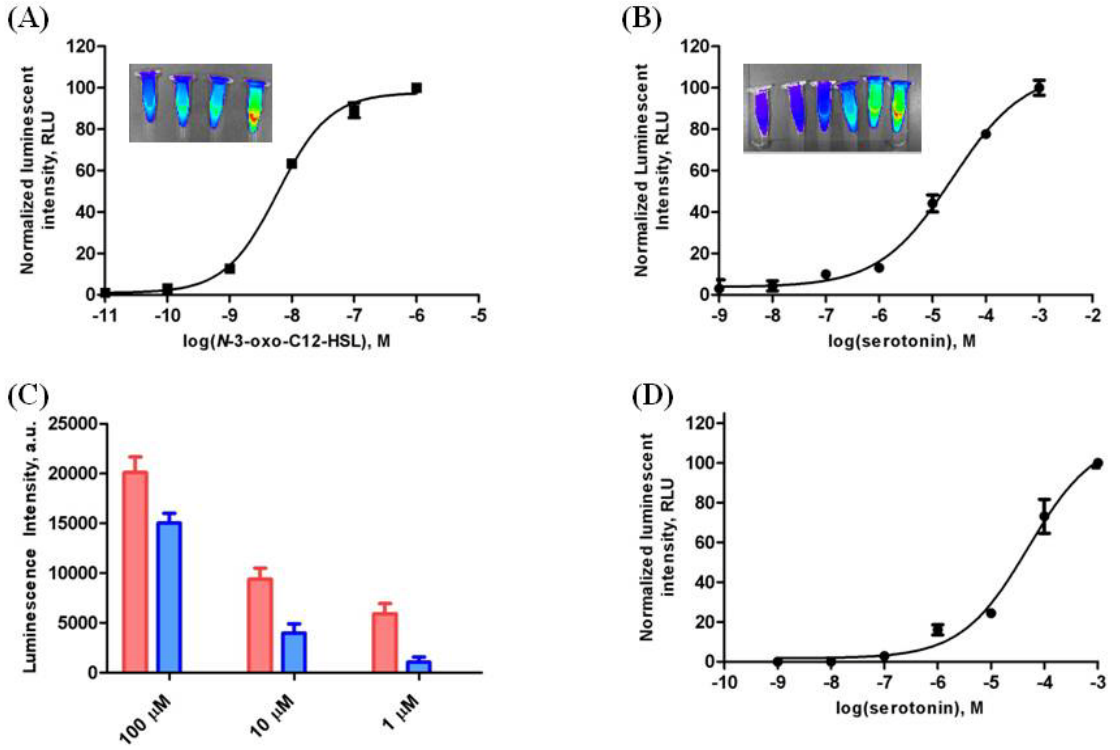


**Figure 2.2.** Activation of the LasR QS pathway by (A) Dose-response curve for *N*-3-oxo-C12-HSL of *E. coli* cells harboring pSD202. Subset is the luminescence of 1 µM, 0.01 µM, 0.1 nM, and a blank (left to right) taken using an IVIS instrument. The insert shows bioluminescence obtained from IVIS in eppendorf tubes containing 1 mL of sensing cells incubated for 2 h in the presence of varying concentrations of QSM. The concentration of analyte in the tubes are, left to right, blank, 0.1 nM, 0.01 µM, and 1 µM *N*-3-oxo-C12-HSL. (B) Dose-response curve for serotonin. Serotonin is able to activate the LasR regulatory protein down to µM concentrations. Subset shows the luminescence obtained using an IVIS instrument from the blank (far left) to 100 µM (far right), using the same concentrations shown in the graph. (C) The concentration of QSM was kept constant at 0.1 nM and incubated in the presence of various serotonin concentrations. The red bars represent the signal generated from serotonin in the presence of 0.1 nM QSM. The blue bars represent signal generated from serotonin in the absence of the QSM. The signal is enhanced in each concentration when serotonin is in the presence of 0.1 nM QSM as compared to serotonin alone. (D) Serotonin is able to elicit a response in *E. coli* cells which employ QscR as the regulatory protein. Data shown are an average of triplicates ± one standard deviation.

conducted studies where the concentration of QSM was varied and a constant concentration of 100 µM serotonin was added to the cells. This concentration was chosen because it is within the physiological concentration of serotonin in the gut. At this

serotonin concentration and in the presence of 0.1 nM QSM, the signal intensity generated by the bacteria was higher than that emitted by the sensing bacteria with 0.1 nM QSM alone. This suggests that serotonin may be an agonist for LasR induction, albeit with a lower affinity than that of the cognate QSM. Based on the previous study, we tested our system by keeping the concentration of QSM constant (0.1 nM) and varying the serotonin concentration. The signal intensity increased for each concentration tested in the presence of the QSM as compared to serotonin alone (Figure 2.2C). Interestingly, at levels below 1 μM serotonin, the signal intensity was higher than that normally found when only serotonin was present and equivalent to the signal generated by 0.1 nM QSM alone. These results indicate that when serotonin and QSM co-exist, they bind to and activate the bacterial LasR circuitry in an additive manner.

Due to the difficulty expressing and purifying soluble LasR, to date only the crystal structure of the ligand binding domain in the presence of the cognate ligand has been solved (120). In addition, removal of the cognate ligand after expression is difficult, making it challenging to perform binding studies with other molecules. Therefore, we employed another quorum sensing regulatory system based on QscR, which is known to bind to LasR's QSM, *N*-3-oxo-C12-HSL (171). Since these regulatory proteins bind the same QSM, we investigated the specificity of the binding of serotonin to QscR by employing cells harboring an expression vector for QscR and β-galactosidase under control of the QscR promoter DNA sequence. Figure 2.2D shows that serotonin was able to elicit a response as in the LasR system from the QscR-based system down to μM levels. The *P. aeruginosa* quorum sensing network also consists of the *rhl* pathway which

is not regulated by *N*-3-oxo-C12-HSL, but regulated by short chain QSMs and is responsible for rhamnolipid biosynthesis (172). Serotonin did not elicit a response with a

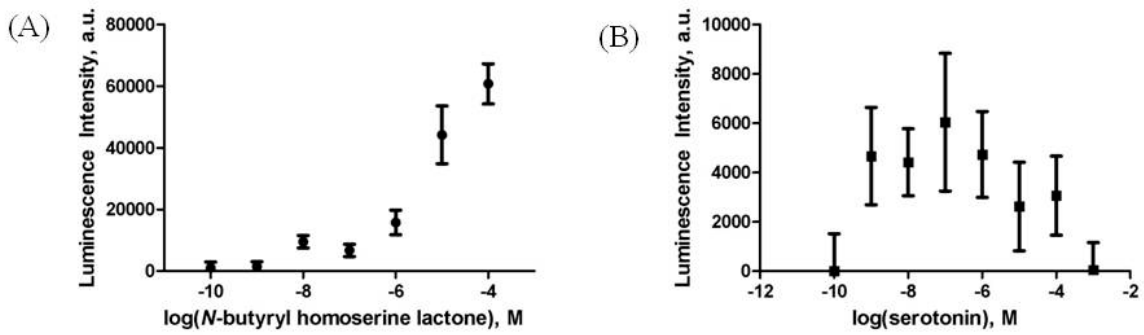


**Figure 2.3.** Serotonin does not activate RhlR. The *P. aeruginosa* quorum sensing network also consists of the *rhl* pathway which is regulated by short-chain QSMs and is responsible for rhamnolipid biosynthesis (172). To probe if serotonin had any effects on this pathway, a second set of cells were used that contained pSB406, a plasmid encoding for the QS regulatory protein RhlR and the *luxCDABE* reporter gene cassette under the control of $P_{rhlI}$ (110). When the cells were incubated with various concentrations of serotonin, no signal above the background was observed, indicating that serotonin is selective for the *las* QS pathway.

RhlR-based system based on *rhl* pathway (Figure 2.3). Further, other molecules in the tryptophan metabolic pathway were unable to reproducibly elicit a response in the *las*-based whole-cell sensing system, demonstrating the selectivity of the Las system for serotonin (Figure 2.4).

Whole-cell based sensing systems are ideal to demonstrate selectivity of a protein for a specific molecule, but involve over-expression of the regulatory protein and, therefore, may not accurately depict the concentration of protein in the native organism, potentially overestimating the real *in vivo* interaction. To elucidate the phenotype effects of serotonin on the *las* quorum sensing pathway in the native organism we employed the JP2 strain of *P. aeruginosa* lacking the synthase for the cognate compound of this circuit

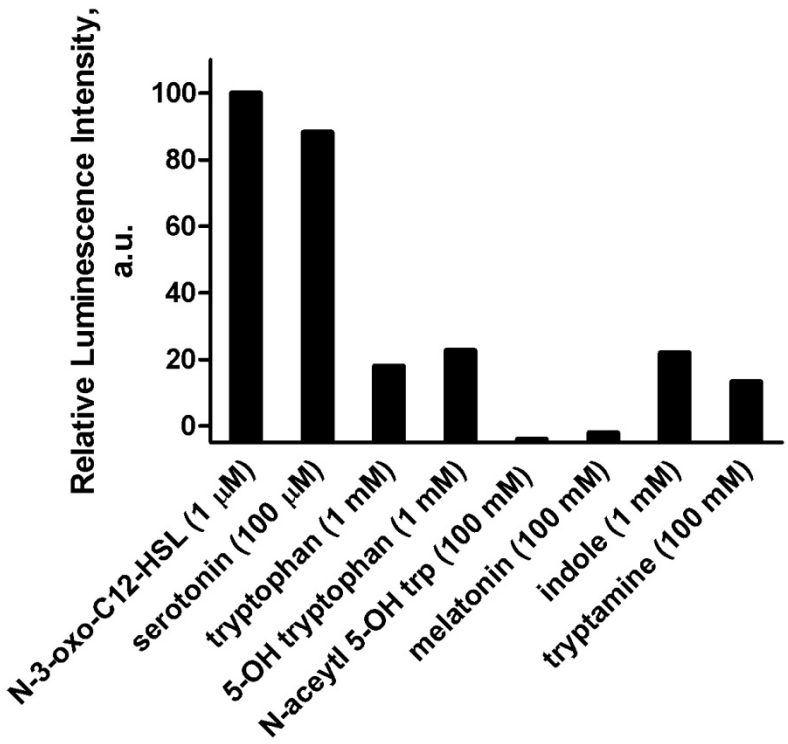


**Figure 2.4.** Selectivity of the las QS system for serotonin. We examined the selectivity of our QS system for serotonin over a number of structurally similar molecules found in physiological samples. Given that serotonin is one of the products of the tryptophan metabolism as are *N*-acetyl-5-OH tryptophan, tryptamine, and melatonin, we decided to investigate the potential interaction of all of these compounds with the QS circuitry (156). None of these compounds elicited a response from our sensing cells in a reproducible manner. This finding, however, is not surprising as previous studies have demonstrated that very small structural changes in synthetic quorum sensing agonists, such as changing a hydroxyl group to a keto group, can drastically reduce agonistic activity of molecules in the *P. aerugniosa las* quorum sensing system (173).

(174) and evaluated elastase synthesis and biofilm formation, two functions depended on the *las* QS circuit and facilitated by the $Zn^{2+}$ metalloprotease, LasB (172, 175). Elastase has been implicated in *P. aerugionsa*-related keratitis, pneumonia, and burn infections in humans (176) and linked to biofilm formation. Elastase synthesis was examined by

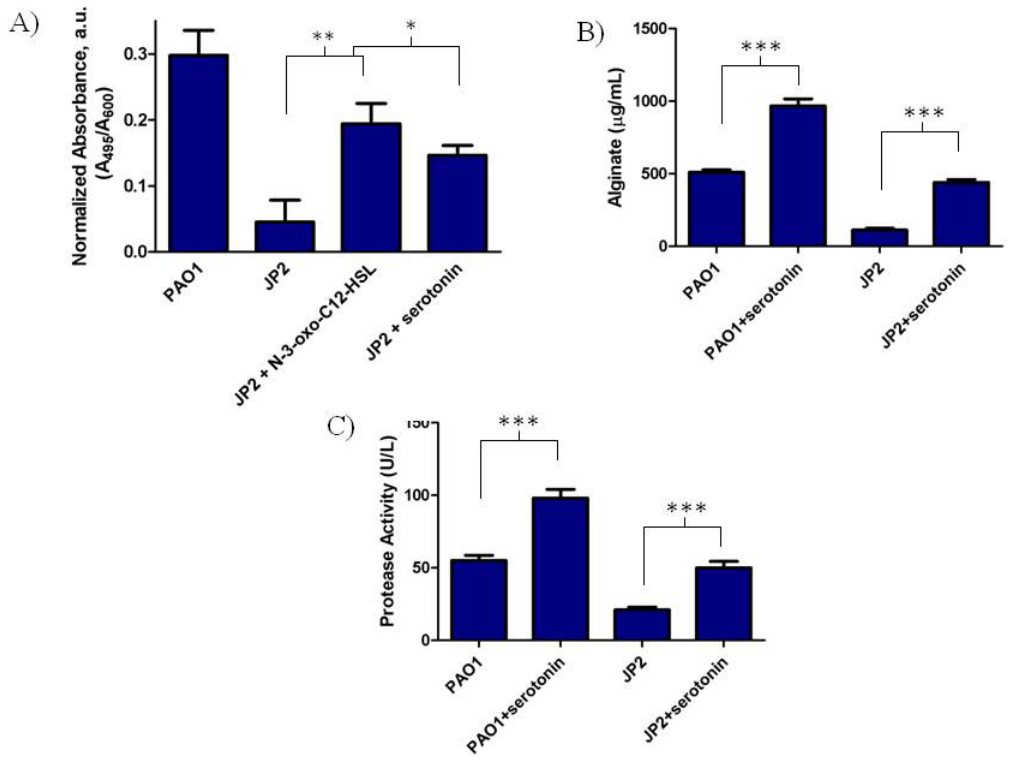


**Figure 2.5.** *P. aeruginosa* JP2 cells, which lack the synthases for the cognate QSMs, were employed to determine if serotonin is able to activate QS gene regulation in the native organism. (A) Cells were incubated in buffer, 1 μM *N*-3-oxo-C12-HSL, or 100 μM serotonin overnight. The elastase activity was determined by measuring the absorbance at 495 nm upon addition of elastin-Congo red to the culture supernatant. All data were normalized according to the $OD_{600}$ of the culture. Both serotonin and *N*-3-oxo-C12-HSL were able to activate elastase synthesis in *P. aeruginosa* JP2 cells. Data shown are an average of triplicates ± one standard deviation. Virulence factor assays were performed for (B) alginate and (C) proteases in the absence and presence of serotonin.

incubating cells overnight in the absence of any compound (control), and in the presence of QSM or serotonin. The elastase activity was then quantified by following established methods (172). As shown in Figure 2.5A, it was found that control cells had negligible activity, while 1 μM exogenous QSM and 100 μM serotonin showed a significant increase in elastase activity, thus indicating the ability of serotonin to activate the *las*

quorum sensing pathway and facilitate elastase production. Wild-type PAO1 cells, which are able to produce QSMs endogenously, were used as a positive control for the assay. Alginate synthesis, an important extracellular component of *P. aeruginosa* biofilms (177), also increased in the presence of serotonin in both JP2 and PAO1 cells (Figure 2.5B). Protease synthesis, which has been shown to enhance the long-term association of *P. aeruginosa* to cystic fibrosis lungs (178), also increased in the presence of serotonin (Figure 2.5C).

Bacterial biofilms are the cause of on-set of pathogenicity in the hosts. The formation of bacterial biofilms is controlled by quorum sensing, and therefore, we investigated the effect of serotonin on this process. Given that biofilm formation is dependent on the *las* quorum sensing pathway (175) and our demonstration of the activation the *las* circuitry by serotonin, we hypothesized that serotonin could trigger biofilm formation. To examine our hypothesis, we employed the JP2 cell strain that lacks the ability to produce its own *las* QSM. Biofilm formation was evaluated in the absence of any compound (control), and in the presence of QSM or serotonin (Figure 2.6A). As demonstrated in panel 1 (top), the JP2 cells were unable to form complete biofilms in the absence of external QSMs. Panel 1 (bottom) shows that in the presence of serotonin, the biofilm formation increases. Panel 2 (top) shows the biofilm growth in the presence of *N*-butyl-homoserine lactone, which is more dense than JP2 alone but not as dense as the biofilm in the presence of *N*-3-oxo-C12-homoserine lactone (Panel 3, top). Upon the addition of serotonin in each case, however, the biofilm formation increases as shown by the bottom panel in each pair. SEM imaging was also performed and similar results were found (Figure 2.6B). Further, we employed a crystal violet biofilm assay to quantify our

data. Figure 2.7 shows that the biofilm formation of the JP2 strain in the presence of serotonin is significantly greater than that of JP2 alone. Our results demonstrated that, indeed, exogenous QSM and serotonin were able to trigger the formation of biofilms that resemble those of natural pathogenic bacterial processes. We also examined two phenotypes of *P. aerugionsa*, swarming and lipopolysachharide (LPS) production, which are not dependent on the *las* pathway and thus, quorum sensing independent in this particular communication circuit (174, 179). As expected, upon addition of serotonin we did not observe any changes in either of both phenotypes (data not shown).

**2.4 Conclusions**

The abundance and diversity of our microbiome necessitates an in-depth understanding of the effect that chemical signaling molecules native to their human host, such as serotonin, cause on the normal microbiome behaviors. To the best of our knowledge, this is the first study demonstrating that the mammalian neurotransmitter serotonin can activate bacterial quorum sensing. Serotonin in the absence of QSMs is able to activate LasR when present at micromolar levels. Previous studies have shown that serotonin is present at micromolar levels in the urine and plasma of individuals (180) and even at higher levels in the GI tract (168), indicating that, at physiological concentrations, serotonin may be able to impact the quorum sensing circuitry. Further, our studies point out at cooperativity between serotonin and the cognate quorum sensing molecule to enhance quorum sensing behavior. Serotonin recognition by the QSM regulatory circuit appears to be selective since other molecules involved in the tryptophan metabolic pathway, the pathway in which serotonin is synthesized *in vivo*, are unable to elicit a quorum sensing response. Serotonin is also able to induce the production of

elastase and biofilm formation, two quorum-dependent phenomena. These data suggest that serotonin can potentially impact the human microbiome through interactions with the bacterial quorum sensing circuitry. To date, studies have only demonstrated a link between serotonin and the microbiota and have not taken the next step to understand the mechanism by which serotonin may be able to affect the microbiota. Our work demonstrates that serotonin interacts with the quorum sensing circuitry of bacteria and, thus, it has a Janus-type behavior and acting both as a neurotransmitter in the host and serving as a signaling molecule in bacterial communications. The newly found Janus nature of serotonin points out at a complex behavior that may shift the signaling of serotonin from to the host to the bacterial population and vice versa. To shed light into the mystery of the host-microbiome interactions, further studies are needed to elucidate the conditions that trigger for serotonin to choose to behave as a signaling molecule for the host or bacteria. Such knowledge will help in better understanding the equilibrium between the host and the microbiome. Consideration of the Janus role of serotonin along with the pathogenicity of bacteria to the host could lead to paradigm shifting therapeutic implications in the treatment of bacterial-related diseases or diseases that have a heavy bacterial component.

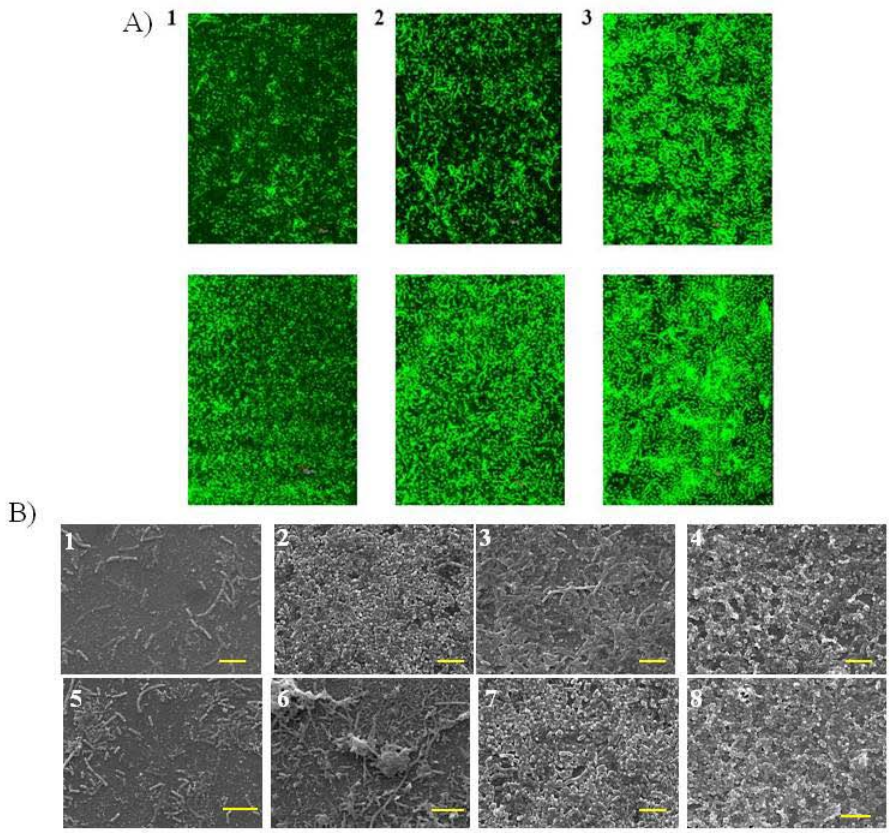


**Figure 2.6.** Serotonin effect on biofilm formation. (A) *P. aeruginosa* JP2 cells were used to grow static biofilms on poly-L-lysine coated glass slides in the absence or presence of QSMs and serotonin. JP2 cells (1, top panel) are unable to form biofilms without the addition of exogenous QSMs. Biofilm formation increases upon the addition of 50 µM *N*-butyryl-homoserine lactone (2, top panel) or 1µM *N*-3-oxo-dodecanoyl-homoserine lactone (3, top panel). Further, in all three cases, the addition of 1 mM serotonin increases biofilm formation when compared to the JP2 cells in the absence or presence of each individual QSM. (B) SEM images were also taken of poly-L-lysine coated glass slides in the presence or absence of serotonin. Panel 1 shows the incomplete biofilms formed by JP2 cells. Panel 2 shows the production of biofilms by JP2 in the presence of serotonin. Panels 3 and 4 show the biofilm formation of PAO1 in the absence and presence of serotonin, respectively. Panels 5 shows biofilm formation of JP2 in the presence of *N*-butryl-HSL. Panels 6 and 7 show biofilm development of JP2 in the presence of *N*-3-oxo-C12-HSL in the absence and presence of serotonin, respectively. Panel 8 shows the biofilm development of JP2 in the presence of both QSMs and serotonin.

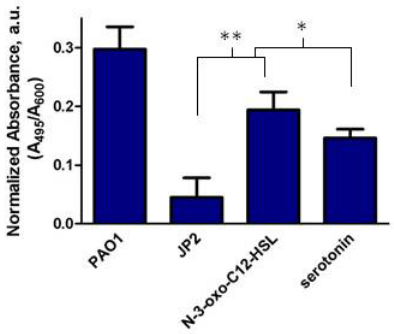


**Figure 2.7.** Crystal violet biofilm assay of JP2.. A crystal violet assay was also performed to determine biofilm formation. Cells were incubated overnight in a 96-well flat bottom microtiter plate at 37 °C. After washing and incubation with a 0.1% crystal violet solution, the adhered crystal violet was quantified at 550 nm. Results are an average ± one standard deviation (n=5).

# Chapter 3. Genetically Encoded Biosensors in Diverse Organisms for Remote and *in situ* Detection

## 3.1. Overview

Nature has endowed us with biological recognition systems, specifically proteins, which are able to bind to their respective ligands with exquisite selectivity and sensitivity. One such class of proteins is bacterial regulatory proteins. These proteins have allowed bacteria to evolve and respond to environmental stressors by bestowing the bacteria the ability to initiate transcription in response to a specific stimuli and modify their metabolic pathways (181). An example of bacterial adaptation to survive in toxic environments, specifically in the presence of arsenic, is the emergence of the *ars* operon that forms a pump enabling bacteria to survive in arsenic environments (105). Advances in technology have allowed scientist to exploit these natural bacterial adaptations to create designer analytical detection systems for arsenic. One such example is the development of genetically encoded biosensing systems which are comprised of genetically engineered bacteria that harbor the *ars* operon. When the cells are in the presence of arsenic, the analyte permeates the cellular membrane and binds to ArsR causing a conformational change that allows for the release of ArsR from the promoter region, and hence the expression of genes that confer arsenic resistance as well as the expression of a protein capable of emitting a dose-response signal in the presence of arsenate. Genetically encoded biosensing systems have been exploited as analytical detection systems due to their unique advantages such as selectivity, ease of use, specificity, and batch-to-batch

reproducibility (106). However, they have other inherent concerns based upon the conditions required to develop a robust, reusable, on-site detection approach using a living system. By evolving these highly specific bioanalytical sensing systems, methods to address these limitations and advance their detection capabilities beyond point locations may be possible. In recent years, research has focused on evolving genetically encoded biosensing systems' technology to meet above mentioned challenges by enhancing adhesion to platforms (182), adapting the systems to portable platforms (108, 183), enhancing reusability of the sensors (184), and using genetically encoded biosensing systems as detection elements in higher organisms such as plants and rat intestines (185-186).

While the versatility of genetically encoded biosensing systems has lent this technology as a tool for numerous applications, multiple stages of technological evolution focused on a single system have not yet been demonstrated. This is critically important in demonstrating the broad applicability of such technology to various platforms based upon a range of intended use, including point-of-care diagnostics and in-field applications. Herein, we demonstrate the technological evolution of a genetically encoded biosensing system based on the above described *ars* operon for the target species arsenic, a highly toxic compound, as recognized by the United States Environmental Protection Agency (187). Specifically, this study investigates the progression of a genetically encoded biosensing system from its intended use for analyte detection, portability, and long term storage *in vitro* to the incorporation of the sensor into a living organism. The system was initially validated using a genetically encoded biosensing system in bacterial cells containing the *ars* operon in a standard platform. After validation, the system was

employed for the detection of arsenic in soil and to detect organoarsenicals. To demonstrate the incorporation of genetically encoded biosensing systems to more economical and stable platforms, a paper-based system was designed for the sensing system. The genetically encoded biosensing system was sporulated to enhance its long-term storage, stability, and allow for transport of the biosensing cells. The spores were then immobilized onto paper strips to demonstrate the ability of a sensor to be deployed on-site to detect environmental samples. To demonstrate the next level in the technological evolution of the genetically encoded biosensing system, it was integrated into a more complex organism, *Caenorhabditis elegans,* either via ingestion or through genetic modification, which was able to display a phenotype, fluorescence, in response to arsenic in real time. Taken together, this work demonstrates the directed evolution of a genetically encoded biosensing system technology from single-cell bacteria to a multi-cellular organism for advanced and enhanced analytical detection on-site or in a laboratory.

## 3.2. Materials and Methods

### 3.2.1 Reagents

The β-glo kit was purchased from Promega (Madison, WI). The paper-based platform was made from Whatman brand chromatography paper purchased from GE Healthcare (Piscataway, NJ). Arsenic compounds, X-gal (5-bromo-4-chloro-3-indolyl-β-D-galactopyranoside), lysozyme, potassium phosphate, bacto nutrient broth, potassium chloride, magnesium sulfate heptahydrate, sodium hydroxide, malachite green, safranin, and agar were purchased from Sigma Aldrich (St. Louis, MO). Sodium arsenite was purchased from Ricca Chemical (Arlington, TX). The 96-well microtiter plates were

purchased from Costar (Corning, NY). LB Broth was purchased from EMD Chemicals (San Diego, CA). The PolarStar Optima used for microtiter plate assays was from BMG Labtech (Durham, NC).

### 3.2.2 Plasmids and Bacterial Strains

For the experiments utilizing the microtiter plate, spores, or paper we employed *Bacillus subtilis* cells harboring plasmid p-MUTin-23. The plasmid p-MUTin-23 carried three genes (*ars*R, *ars*B, and *ars*C) that provide arsenic resistance and the β-galactosidase encoding reporter gene *lac*-Z under the control of the ArsR regulatory protein. This plasmid is contained in the *B. subtilis* bacteria strain ars-23 (188).

### 3.2.3 Detection of Arsenic and Organoarsenicals in Microtiter Plates

*B. subtilis* cells were grown overnight at 37 °C and 250 rpm in a cell culture tube containing 5 mL of autoclaved LB broth and 5 μL of erythromycin (25 mg/mL). The overnight culture was used to inoculate 50 mL of LB broth at a 1:10 volume ratio and also 50 μL of erythromycin. The culture was grown to an $OD_{600}$ of 0.6-0.8. Analyte standard solutions were prepared at various concentrations ranging from $10^{-2}$ to $10^{-9}$ M in Milli-Q purified water. Aliquots of 90 μL of LB cell suspension were transferred to the wells of a 96-well microtiter plate. A volume of 10 μL of arsenic solutions at various concentrations and Milli-Q purified water as a blank was added in triplicate to the cells. The microtiter plate was then incubated in an orbital shaker/incubator at 37 °C and 175 rpm for 1 h. The plate was then removed and 50 μL of β-glo reagent was added. After incubating for 30 min at room temperature, luminescence signal was measured on the microplate luminometer.

### 3.2.4 Soil Extraction and Spiked Soil

A 0.5 g sample of soil was weighed and suspended in 20 mL of 50 mM phosphate buffer in Milli-Q purified water. Solutions were shaken at room temperature and 300 rpm for 3 hours and then syringe filtered through 0.45 μm nylon filters. Soil samples of 0.5 g were spiked with 100 μL of a known concentration of sodium arsenite followed by shaking at room temperature and 300 rpm for 24 hours prior to extraction.

### 3.2.5 Bacterial Spores

Bacterial spores were prepared using standard protocols (189). Briefly, 5 mL cultures of the cells were used to inoculate 500 mL cultures of sporulation media (8 g/L bacto nutrient broth, 10% (w/v) KCl, 1.2% (w/v) $MgSO_4 \cdot 7H_2O$, adjust pH to 7.6 with NaOH) and incubated in an orbital shaker at 37 °C, 250 rpm for 48 h. The spores were then washed once with Milli-Q purified water and twice with a 1 M NaCl solution before a final wash in Milli-Q purified water. After washing, sporulation was confirmed using the Schaeffer-Fulton method for staining endospores and visualizing under a microscope. The spores were then diluted to an $OD_{600}$ of 2.0 and stored in Milli-Q purified water until use. To perform the assay in the microtiter plate format, 90 μL of the spore suspension was added to each well of a 96-well microtiter plate. To each well, 10 μL of standard solutions of arsenite ranging from $1 \times 10^{-3}$ M to $1 \times 10^{-9}$ M prepared in Milli-Q purified water by serial dilution of a stock solution of $1 \times 10^{-2}$ M sodium arsenite were added in triplicate to the plate. Milli-Q purified water was used a blank. The spores and analyte were incubated on an orbital shaker at 37 °C, 250 rpm for 2.5 h. Then, 50 μL of luminescent substrate was added to each well and allowed to incubate at RT for 30 min. The luminescence signal was measured on the microplate luminometer.

### 3.2.6 Detection on Paper with Vegetative Cells

Paper-based platforms were designed on Adobe Photoshop CS6 in the dimensions of a standard 96-well microtiter plate. They were then printed onto sheets of cellulose filter paper using a wax-based printer. The printed designs were incubated at 110 °C for 30 s, then flipped and left to cure for 30 s more. This step was to allow the wax to melt through the paper and create a hydrophobic barrier to prevent diffusion of liquids from the detection chamber. For the microtiter plate paper-based assay, 45 µL of cells and 5 µL of analyte or the appropriate blank solutions were added to each well. After incubating at room temperature for 1 h, 10 µL of 20 mg/mL lysozyme and 10 µL of 50 mg/mL X-gal was added to each well. The lysozyme served to lyse the cells and release all the β-galactosidase for sensing while also providing a means for safe disposal of the paper-based platform by killing the cells. A color change was apparent in approximately 30 min. After drying, a picture was taken of the paper-based assay. All images were quantitated by ImageJ software. The image was changed to an 8-bit type and was then inverted. Each well was encircled and analyzed according to the color inside.

### 3.2.7 Detection on Paper Strips with Spores

Spores diluted to an $OD_{600}$ of 2.0 were mixed in a 1:1 volume ratio with a warmed 4% agar solution prepared in a 10 mM Tris-HCl pH 8.0 solution. Before cooling, 20 µL of the suspension was spotted on strips cut from Whatman filter paper (0.6 x 4 cm) and cooled to solidify the agar and maintain the position of the spores on the paper strips. The strips were left at room temperature until use. Arsenite standards ranging from 1 x $10^{-2}$ M to 1 x $10^{-9}$ M were prepared in Milli-Q purified water. A volume of 100 µL each of these standards was added to 900 µL of LB broth containing 12 mM $Ca^{2+}$-dipicolonic

acid (DPA) in culture tubes. Milli-Q purified water was used as the blank. Paper strips which were previously prepared were added to the tubes and incubated at 37 °C and 250 rpm for 3 h. The strips were then taken out of the tubes and 10 µL of lysozyme (20 mg/mL) in double-distilled DI water and 10 µL of X-gal (50 mg/mL) in DMF were added to the spot on which the sensing cells were immobilized. Color development was carried out for 30 min. In addition to observing the development of the blue coloration, color intensities were measured using ImageJ software (NIH, Bethesda, MD) upon digital acquisition as previously described (108). The final color intensity signals were corrected with respect to the blank.

### 3.2.8 *Caenorhabditis elegans* Assays

#### *3.2.8.1 Caenorhabditis elegans* Strains and Culture Conditions

The N2 (wild type) and SJ4001 (zcIs1 [aip-1::GFP] )strains were acquired from the *Caenorhabditis* Genetics Center (St. Paul, Minnesota). Nematodes were maintained on NGM agar (United States Biological Corporation, Swampscott, MA) plates seeded with *E. coli* OP50, which grows slowly on NGM media, as food at 20 °C (190). Synchronization of nematode cultures was achieved by bleaching gravid hermaphrodites in a 20% sodium hypochlorite solution and overnight hatching in sterile liquid NGM media, then adding OP50 the next day (191). Prior to assay, *C. elegans* were washed off of NGM/OP50 plates with M9 medium, collected by mild centrifugation and rinsed three times in M9 to remove OP50.

### 3.2.8.2 Ingestion of aArsenite-Responsive Bacteria by Nematodes

*E. coli* AW10 cells containing the plasmid pSD10 include the ArsR gene upstream of the GFPuv gene. Majority L4 adult nematodes were washed from NGM/OP50 plates, settled on ice to collect and washed twice with M9. They were then transferred to 10 cm NGM plates containing an 8 hr at RT (to allow the surface to dry) culture of pSD10/AW10 *E. coli*, which grew at a normal rate on NGM media. The pSD10/AW10 cells have been shown to be selectively responsive to arsenite and antimonite (192) and fluoresce at 507 nm when exposed to either of the metal salt solutions for 30 min at 37 °C at sub-millimolar concentrations.

### 3.2.8.3 Preparation of Arsenite Standards

A 0.1 M solution of sodium arsenite was purchased from Ricca Chemical Co. (Arlington, TX). Arsenite solutions were prepared as serial dilutions ranging from 1 x $10^{-3}$ M to 1 x $10^{-10}$ M in sterile M9 medium, plus a control sample of M9 medium only.

### 3.2.8.4 Arsenite Exposure

Nematodes that were fed pSD10/AW10 overnight were collected by washing plates with M9, allowing worms to settle on ice, and briefly centrifuging at 1,000 rpm to wash away bacteria. For imaging: a 50 uL “bubble” of arsenite in M9 or M9 only (control) was placed into each well of 2, 12-well plates for 3 replicates of each concentration. Five microliters of nematodes in M9 were added to each arsenite bubble, such that each sample had between 10- 30 worms available for imaging after a 2 h incubation at RT. For microtiter plate assay: 50 uL of the nematodes in M9 solution and

50 uL of arsenite in M9 or M9 only were added to each well of a 96-well black, clear-bottom plate. Each well contained approximately 100 nematodes. Plates were shaken at 50 rpm for 2 h prior to fluorescence measurement.

**3.2.8.5 Fluorescence Measurements**

Worms were imaged in the 12-well plates using a Nikon Eclipse T10 Epifluorescent Microscope (Melville, NY) and using an iPhone 4.0 with a Magnifi adapter from Arctus Labs (Palo Alto, CA) for image collection. Images were acquired using identical settings and exposure times to allow direct comparisons. The 96-well plate was shaken at 100 RPM at RT for 2 h before reading the fluorescence signal on a FluoStar Optima spectrofluorimter (BMG Labs) using an exciation wavelength of 410 nm and an emission wavelength of 510 nm.

**3.3 Results and Discussion**

Genetically encoded biosensing systems have proven to be versatile tools for the detection of a variety of analytes which are environmentally or biologically relevant. The innate stability, ability of the sensor to give information about bioavailability, and the amenability of genetically encoded biosensing systems to a variety of platforms makes them an ideal tool for analysis. To date, there has been no study presenting the versatility of a single genetically encoded biosensing system. To this end, we have employed a genetically encoded biosensing system for arsenic based on the Ars operon from *B. subtilis* cells to demonstrate the applicability of these systems for versatile sensing, starting with the bacterial whole-cell biosensor and advancing to a multi-cellular organism. The Ars operon consists of four genes: *arsA*, *arsB*, *arsC*, and *arsR*. The *arsA* gene encodes for ArsA, which is a membrane-linked protein that exhibits

arsenite(antimonite)-stimulated ATPase activity and is responsible for providing energy for the protein pump via ATP hydrolysis (193). ArsB, encoded by the *arsB* gene, is a hydrophobic membrane protein that pumps As(III) out of the cells using an electrochemical gradient (194). However, ArsB is only able to efflux As(III) out of the cells, thus another gene, *arsC*, encodes for a small cytoplasmic reductase protein, ArsC, responsible for the reduction of As(V) to As(III) so it can be removed by the ArsB pump (195). ArsR is the regulatory protein which binds to the operator/promoter region of the *ars* operon. When oxanions are present in the cell, they bind to ArsR causing a conformational change and subsequent dissociation of ArsR from the promoter region to begin the transcription of the genes necessary for arsenic resistance (105).

Initially, the genetically encoded biosensing system was incorporated into *B. subtilis* cells and incubated with sodium arsenite in a traditional 96-well microtiter plate format to establish the analytical characteristics of the sensor for comparison after implementation onto different platforms. The cells were incubated in the presence of varying concentrations of analyte for 1 h at 37 °C. The limit of detection was determined to be $3.2 \times 10^{-8}$ M (Figure 3.1). This limit of detection was then used as a baseline to determine the effects that changing the platform has on the characteristics of the sensor. The first step in the technological evolution of the biosensor was to test it on environmental samples. Date *et al*. have shown previously that the sensor can be used to detect arsenic in complex matrices such as human blood serum and fresh water (146). To date, however, this sensor has not been employed for the detection of arsenic in soil, which is a common site of environmental arsenic contamination (88). While the EPA has set guidelines for arsenic in drinking water (196), such standards do not exist for arsenic

in soil. Multiple methods for arsenic extraction from soil have been established, though many depend upon high performance liquid chromatography (HPLC) as their method of detection (197-199). These HPLC-based methods focus on preserving arsenic species

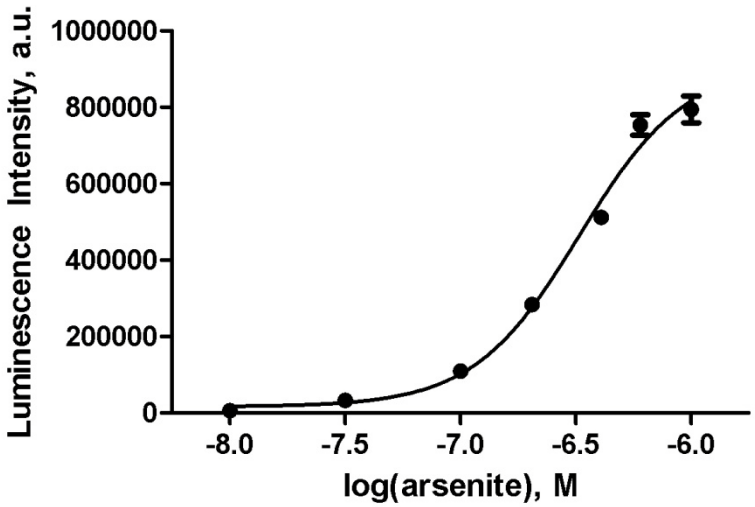


**Figure 3.1.** Detection of arsenite using *Bacillus subtilis* vegetative cells in a microtiter plate format.

(arsenate, As[V] and arsenite, As[III]), which can complicate extraction procedures. HPLC detection requires expensive equipment, highly trained personnel, and lacks portability. To avoid these issues, we have employed our bacterial whole-cell based biosensor for arsenic detection in soil samples. Additionally, because the ArsC protein reduces inorganic As(V) to As(III), which can then bind the ArsR protein and generate a dose-dependent response, there is no need to preserve the arsenic species in our samples, eliminating time-consuming sample preparation steps. This bacterial whole-cell based biosensing system has the potential for on-site detection, which is paramount to people living in regions where arsenic contamination occurs.

In order to employ ArsR for soil samples, a method for arsenic extraction was developed and optimized based upon work by Georgiadis *et al*. (199). Various concentrations of phosphate buffer and extraction times were tested, leading to an optimized extraction buffer of 50 mM phosphate with a 3 h extraction at room temperature. To validate these parameters, soil samples were spiked with known concentrations of arsenite, extracted, assayed using ArsR, and then compared to standards (Figure 3.2A.). Four soil samples were collected from Guánica Bay, Puerto Rico to assay for arsenic. Guánica Bay, located on the southwest coast of the island, is a major watershed that has been greatly contaminated (200) and is under the watch of the EPA and other organizations (201-202). The watershed is a major source of nutrients to the bay and offshore waters, including a large offshore coral reef area. Amongst other sources of contamination, there are two large factories, one of which produces fertilizer, as well as agricultural fields, with runoff into the bay. These pollutants have caused harm to the coral reefs, as well as posing a potential hazard to inhabitants of this region (200). Of the four soil samples collected, one sample (#3) tested positive for arsenic (Figure 3.2B) and the concentration was found to be $6.33 \times 10^{-8}$ M for the 20 mL extraction solution or approximately $1.26 \times 10^{-9}$ moles of arsenic for every 0.5 g of soil. This sample was then sent out for ICP-MS and it was found to contain 0.800 mg/kg, indicating a 40% yield. Although this yield is low, it is important to note that ICP-MS detects all arsenic species present in the sample while the sensor only detects arsenic (III) or (V) species.

Previous work in our laboratory has demonstrated that the sensor is able to selectively detect arsenate, arsenite, and antimonite (188); however, the sensor has never

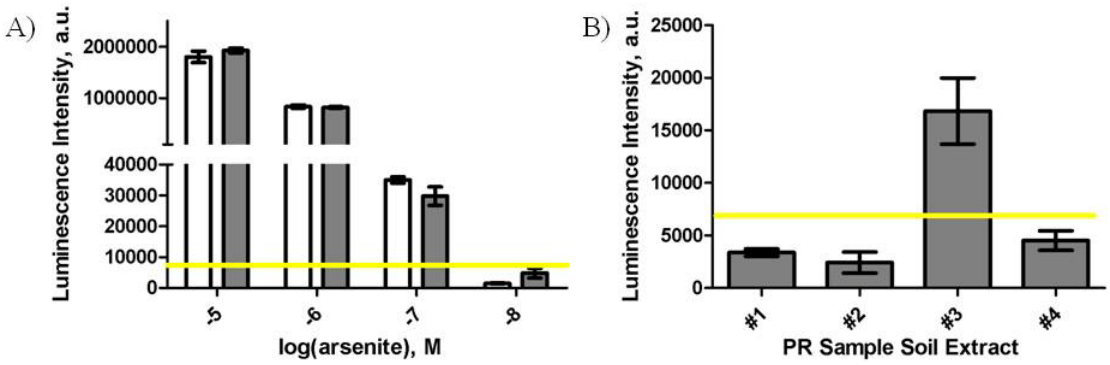


**Figure 3.2.** Detecting arsenic in soil samples. A) Spiked soil samples (gray) were extracted and compared to standards (white). B) Soil samples from Guanica Bay, Puerto Rico were extracted and assayed with the genetically encoded biosensing system. Sample #3 has an interpolated value of 6.33 x $10^{-8}$ M. In both captions, the yellow line indicates the limit of detection which is defined by the average of the blank plus three standard deviations. Data are blank subtracted and the average ± 1 SD.

been employed to test other arsenic containing molecules such as organoarsenicals. Organoarsenicals are employed in various industries and due to the widespread use of the compounds and their persistence in nature, their detection is important. To this end, we employed our sensor for the detection of various organoarsenicals or the degradation products of these compounds. For example, in Figure 3.3A we demonstrate the detection of a phenylarsenite, *p*-arsenilic acid, which is used to promote growth in animal husbandry. Additionally, we are able to detect the byproducts for the degradation of roxarsone, a second phenylarsenite. It is first degraded to 4-OH-3-aminophyenyl arsonic acid and eventually to As(III) (203-205), which is detectable by our sensor (Figure 3.3B). As(III) is also a product of the hydrolysis of a chemical warfare agent, 2-chlorovinyldichloroarsine (Lewisite) and the degradation product of a pesticide, methylarsenate (205-206). Disodium methyl arsenate (DSMA) is an herbicide and was able to be detected by our whole-cell biosensor (Figure 3.3B). Although each of these compounds have differing detection limits and elicit different signal intensities, each

species or a by-product of these species are able to induce a response in our sensor. The range of concentrations which elicited a response from the sensor for each organoarsenical or by-product of organoarsenicals is shown in Figure 3B. Previous studies have shown that a system employing the ArsR protein has demonstrated the ability to tune a genetically encoded biosensing system to be selective for one class of arsenic containing analytes over another (88). Additionally, studies have been ongoing to isolate bacterial enzymes responsible for the oxidation and reduction of organoarsenicals, which can be implemented in genetically encoded biosensing systems for the detection of both inorganic and organic arsenic species (207).

The portability of a genetically encoded biosensing system can be enhanced by amending it to fit on a platform which is miniaturized, portable, and allows for high throughput analysis for the low-cost detection of analytes on-site. Previously, the genetically encoded biosensing system mentioned herein has been employed on a portable centrifugal microfluidic platform for the detection of arsenite in both serum and freshwater samples (183). However, there is still a need to successfully perform analysis on-site in areas which lack resources for expensive equipment. In recent years, paper-based platforms have evolved as ideal tools for on-site detection of analytes which are relevant to environmental and biomedical applications (208). Paper has many benefits as compared to other materials for portable devices in that it is inexpensive, easily disposable, and different designs can be created and applied to the paper. The design on paper platforms can be printed using many different methods such as PDMS printing, photolithography, and inkjet etching, to name a few (209-213). One of the most promising methods is the use of wax patterning in which hydrophobic barriers are

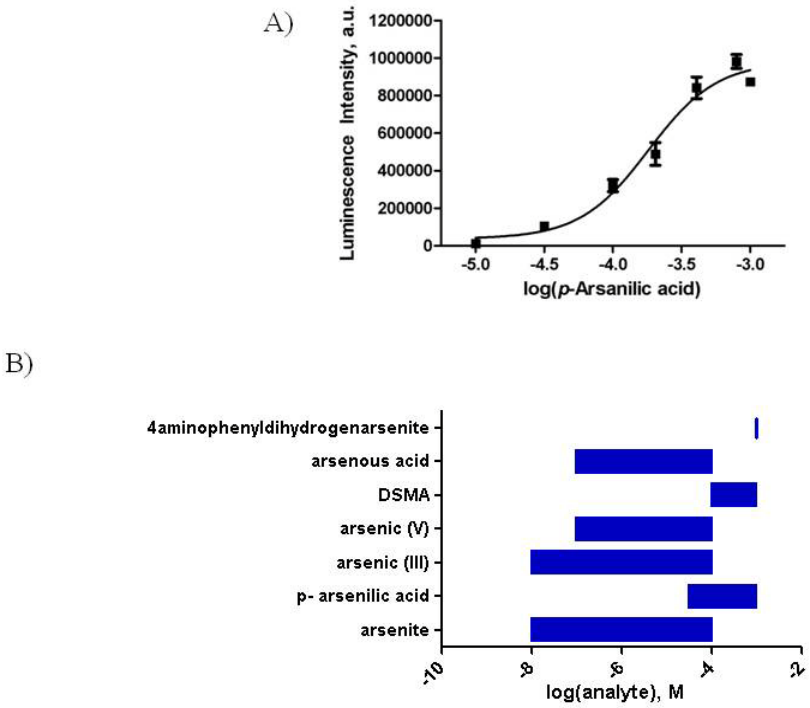


**Figure 3.3.** Detection of organoarsenicals using B. subtilis cells harboring plasmid pMUTin-23. A) Detection of *p*-arsanilic acid. B) A selection of organoarsenicals tested with the sensor and the range each compound elicited a signal from the sensor.

patterned onto a paper matrix to prevent the mixing of reagents and allowing for multiplexed assays. Wax patterning can be achieved by multiple methods, but perhaps the most reproducible method is wax printing (214). In this method, a design is created using a computer program of choice and a sheet of paper is fed into a wax printer and then heated on a hot plate or in an oven to form a hydrophobic barrier through the paper. This process is fast, efficient, and allows for hundreds of devices to be reproducibly manufactured at once (215). To demonstrate the feasibility of using genetically encoded biosensing systems on wax printed paper platforms, we designed a 96-well microtiter plate pattern which was printed using a wax printer. The paper-based microtiter plate was

then heated to form a hydrophobic wax barrier throughout the paper. Sensing cells were then spotted onto the wells of the printed plate in ten replicates and incubated in the presence of arsenite for 1 h at RT without shaking. After incubation, X-gal and lysozyme were added to the cells for color development for visual confirmation of arsenic contamination. Figure 3.4A show the color change as the concentration of arsenic (III) decreases. Further, the assay can be semi-quantitative by determining the values for the color intensity using ImageJ software (108) and the results are shown in Figure 3.4B. The detection limit for arsenic (III) was found to be $3.2 \times 10^{-8}$ M, which is comparable to the detection limits found on a standard microtiter plate.

Although the aforementioned studies demonstrate the feasibility of using genetically encoded biosensing systems on paper-based platforms, there are inherent concerns such as the immobilization and stability of the biological system under various conditions. To overcome these concerns, various immobilization techniques have been employed to incorporate genetically encoded biosensing systems into transportable devices such as immobilization onto fiber optic tips, sol-gel encapsulation, and immobilization on electrodes (216-218). Further, various techniques to store and maintain the viability of the sensing systems have also been explored such as freeze-drying, vacuum-drying, continuous culturing, and immobilization in organic and inorganic polymers (219). Recently, a new approach has been undertaken to allow for the long-term storage of whole-cell biosensors. Certain bacteria, such as those of *Bacilli* and *Clostridia*, are able to form a hard coat around the cell, called a spore, when exposed to adverse environmental conditions such as the absence of nutrients or extreme temperatures (143). When sporulated, the bacteria are in a dormant, non-growing phase but are able to

actively sense their surroundings. The ruggedness and environmental resistance of spores of B. *subtilis* and *B*. *megatarium*has previously been exploited to serve as a stable packaging for whole-cell biosensors (188). Further, previous studies have shown that the natural hardiness of spores allows whole-cell biosensors to withstand various environmental conditions such as heat, cold, dessication, and humidity for at least a year without losing analytical sensitivity or selectivity (149). Additionally, spores have proven to be stable vehicles for genetically encoded sensing systems and can go through numerous germination/sporulation cycles and still maintain the analytical characteristics of the sensor (183, 188). Therefore, the ability to employ organisms which are able to sporulate allows for the application of genetically encoded sensing systems for field applications. To this end, the arsenic sensing cells were sporulated and the assay was performed in a microtiter plate at 37 °C and RT. Initially, a study was performed at both temperatures to determine the time it took to germinate the cells because to successfully employ spores as a sensor, they must first be germinated by the introduction of nutrients. For both temperatures, 2.5 h was determined to be an optimal time for the germination and sensing of the analyte which was consistent with previous results with this sensor (188). The assay was performed with a 2.5 h incubation time and the results are shown in Table 3.1. Although at both temperatures a dose-response curve was generated, it is important to note that the absolute signal intensity was higher when the cells were incubated at 37 °C as compared to RT. This is likely due to higher germination efficiency at higher temperatures. Additionally, although the absolute signal intensity differed between the spores germinated at 37 °C and RT, the limit of detection was the same for each condition.

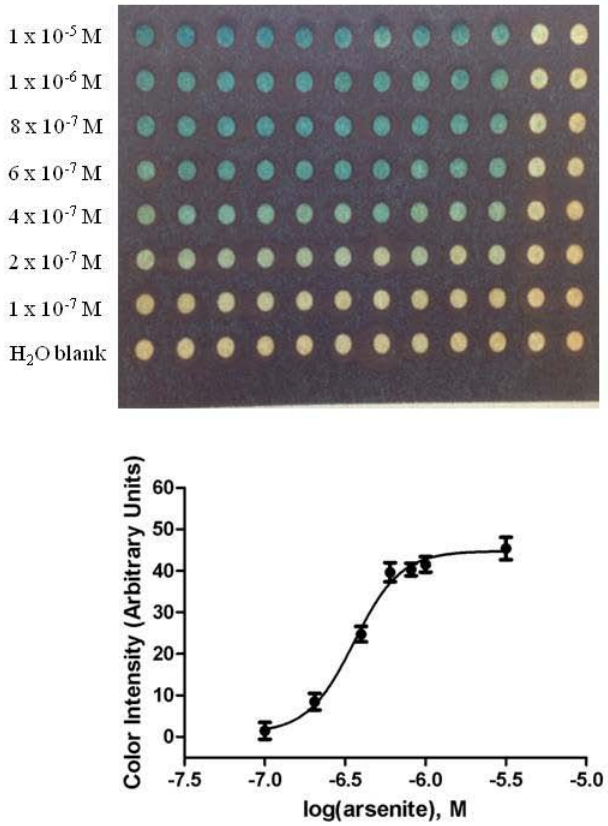


**Figure 3.4.** Detection of analytes using a wax-based printed design. A) Microtiter plate design printed on cellulose paper and heated in an oven for 30 sec on each side to create a hydrophobic barrier. The assay was performed on the paper microtiter plate by placing 45 µL of cells and 5 µL of analyte into each "well" and incubating for 1 h at RT. After incubation, lanes 1-10 were treated with X-gal and lysozyme while lanes 11 and 12 were only treated with X-gal. B) The data were analyzed using ImageJ software and a dose-response curve was generated. All data are triplicates ± one standard error of the mean.

Although the spores allow for a stable packaging material for genetically encoded biosensing systems, a portable device would still be necessary to evolve the system for use in remote areas. As previously mentioned, paper is an ideal inexpensive substrate for the sensing applications. Just as vegetative cells were immobilized on the paper, the spores can also be immobilized on paper-based platforms as well. This pairing of the

durable spore and the stability of the paper makes for a robust, portable sensor that would be ideal for on-site detection of arsenic. Previously, it has been demonstrated that spores

**Table 3.1.** Detection of arsenite after germinating spores in a microtiter plate format. The spores were germinated in LB broth for 2.5 h and 250 rpm at RT or 37 °C.

| | Maximum signal intensity | Limit of detection |
|---|---|---|
| Germination at RT | 5890 ± 190 | $2 \times 10^{-7}$ M |
| Germination at 37 °C | 18750 ± 4172 | $2 \times 10^{-7}$ M |

can be immobilized on paper and used to detect analytes of environmental or biomedical interest (220). In this work, the spores were immobilized on paper strips cut from Whatman filter paper by mixing spores of an $OD_{600}$ of 2.0 with a 4% agar solution in 20 mM Tris-KCl, pH 8.0 (220). The strips were then incubated in the presence of LB broth containing 12 mM $Ca^{2+}$-DPA and varying concentrations of arsenite at 37 °C and 250 rpm for 3 h. After incubation, the strips were removed and a solution of X-gal and lysozyme were added to release the β-galactosidase. As previously mentioned, β-galactosidase is produced in a dose-dependent manner in response to the analyte concentration. Figure 3.5A shows the visual change of color intensity on the strips as the concentration of analyte decreases. The color change was quantified using the ImageJ software and the signals were subtracted from the blank signal and corrected for any variations in light intensity due to the camera (Figure 3.5B). The spores on paper strips based sensor had a detection limit of 1 x $10^{-7}$ M. Current work in our lab is focused on reducing the sensing time of the system to make it more amenable for field applications.

The final step in the technological evolution of our arsenite sensing system was to incorporate it into a dynamic higher-order system that could be easily transported to a test site. The nematodes *C. elegans* are bacteria-consuming roundworms found in the soil and can be maintained in small petri dishes on the order of weeks to months. *C. elegans* are ideal higher-order systems for the incorporation of sensing elements due to their optical transparency, ease of maintenance, and the cost-effectiveness of cultivation (221). To this end, we employed *C. elegans* in conjunction with genetically encoded sensing systems in bacterial cells and as genetically engineered organisms which can respond to an analyte. First, wild-type N2 animals were placed on lawns of *E. coli* AW10 cells harboring plasmid pSD10 which contains the genes for *ars*R and the green fluorescent protein ($gfp_{uv}$) under control of the *ars* operon. Although nematodes have been shown to exhibit negative food preferences (222-224), the wild-type N2 animals used in this study did not appear to exhibit any adverse effects from being switched from the laboratory *E. coli* strain, OP50, to a temporary overnight diet of *E. coli* AW10 prior to exposure to arsenite. The animals were transferred directly from the overnight AW10 plates to a 15 mL tube and after three successive washing steps, were transferred either to 12-well or 96-well plates containing sodium arsenite. To optimize incubation time, the worms were exposed to the arsenite for 1 - 4 h before taking measurements. The signal intensity increased for the first three hours, and then slightly decreased after the 4 h incubation (Figure 3.6A). Next, the *C. elegans* were again fed the *E. coli* AW10 cells overnight, washed, and transferred to 96 well plates containing sodium arsenite and incubated for 2 h prior to

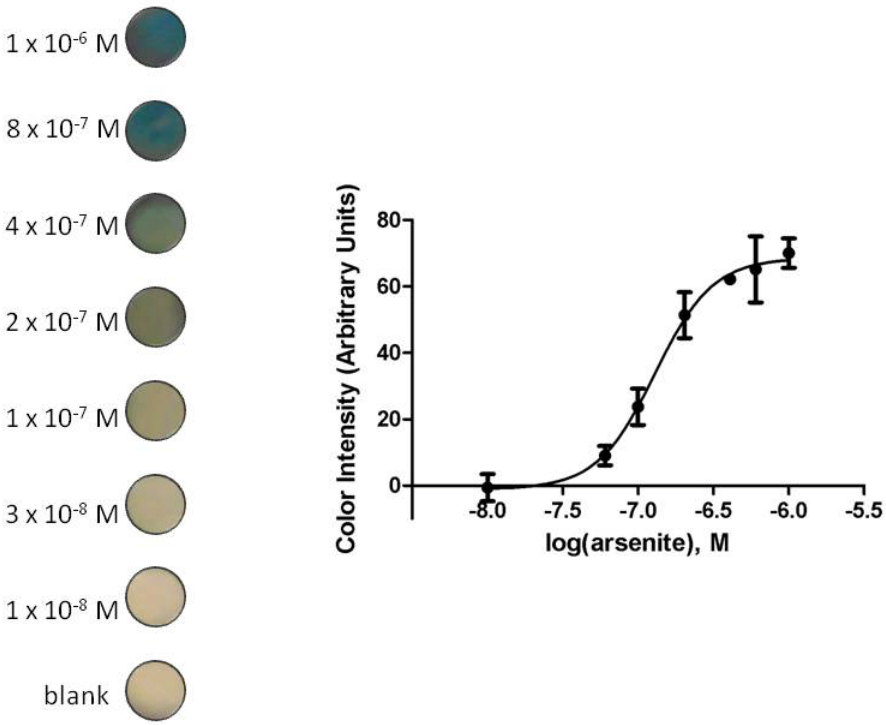


**Figure 3.5.** The dormant spores were spotted on Whatman filter paper and incubated overnight at RT in culture tubes with LB broth and various concentrations of arsenite. A) After a 3h incubation period, the strips were removed and lysozyme and X-gal were added to the spots. After 30 min of exposure, the blue color began to develop. B) The color intensity was quantified using ImageJ software to create a dose response curve. The data represent the average ± one standard error of the mean (n=3).

measurement. It is helpful to note that the wild-type nematodes have been shown to be less susceptible to arsenic-induced oxidative stress than gamma-glutamylcysteine synthetase (gcs-1) mutant nematodes (225-226). Additionally, a previous study showed that arsenite-inducible, cysteine- and histidine-rich RNA-associated protein (AIRAP) and its homologue, AIP-1, derived from nematodes offered protection of murine kidney cells from the toxic effects of arsenite (227). Thus, *C. elegans* have been shown to survive exposure to arsenite, especially for the short time period needed for the ingested *E. coli* AW10 cells to respond to the arsenite in solution. Signal quantification was approached by two methods, imaging with a microscope and a microtiter plate assay. Rather than

imaging a large number of bacteria, each worm can be seen to fluoresce discreetly upon exposure to arsenite. Larger worms are easier to visualize and appear to fluoresce more, perhaps due to increased consumption of the available food source. Figure 3.6B shows the average fluorescence at 510 nm (normalized to a zero arsenic control) for samples of various arsenite concentrations. The detection limit was found to be $1 \times 10^{-9}$ M, which is well within the acceptable range of arsenic accepted by the EPA for arsenic.

The next step in the evolution of a biosensor is the incorporation of sensing elements into higher level organisms so that organism itself can be the sensing system. To make the first steps toward this goal, we have employed a mutant strain of *C. elegans*, SJ4001 which has been modified to control the expression of GFP by the AIRAP promoter, previously described. In the presence of arsenic, the expression of GFP is most pronounced in hypodermal cells (227). Figure 3.6C shows a fluorescence microscopy image of a nematode after incubation in the presence of 0.1 mM arsenite as compared to the nematode in the absence of arsenite, indicating the nematodes can be used as an on/off type sensor.

Herein, we have demonstrated the technological evolution of genetically engineered sensing systems based on the regulatory protein ArsR. Just as organisms evolve to adapt to their environments, scientific technology is always evolving to adapt to address specific issues. In the genetically engineered sensing system on the standard microtiter plate platform to detect arsenic and organoarsenicals, the assay proves to be time consuming. Although the incubation time with the analyte is 1 h, a culture must still be grown to an $OD_{600}$ of 0.6 before the incubation. One way to circumvent this issue is to begin with bacterial spores or to lyophilize the bacteria. In this study and others (146,

188), we have demonstrated that dormant bacterial spores can be prepared in advance and stored until sample analysis. Previous reports also demonstrate that these spores are stable under a variety of environmental conditions such as an elevated humidity, desiccation, and extreme temperatures (149). To overcome issues pertaining to the cost of analysis, we have evolved the technology to include the use of paper-based platforms for analysis. These platforms are advantageous due to their low cost, ease of fabrication, and disposability. The assay times on paper versus traditional microtiter plate platforms are comparable when using cells which are in a vegetative state; however, when spores are present, it was necessary to include $Ca^{2+}$-DPA in the nutrient media to decrease the germination time from 16 h to 3 h. Previous reports have demonstrated the use of the arsenic whole-cell biosensor for analysis of environmental and biological samples; however, soil analysis using the arsenic whole-cell biosensor had not been demonstrated. Therefore, we have employed our genetically engineered sensing system for the detection of arsenic in soil. Genetically engineered sensing systems, however, have limitations in the analysis of soil samples due to traditional extraction techniques which use organic or acidic extractions which may be toxic to living systems. To overcome this issue, a phosphate extraction was employed in our soil samples. Each of steps of evolution described above has employed *B*. *subtilis* cells harboring pMUTin-23. The detection limit during each stage of technological evolution is shown in Table 3.2. It is important to note that the detection limit did not vary greatly between each step in the evolution, indicating that genetically engineered sensing systems are robust, ideal systems to apply to a number of applications. The final step in the evolution of genetically engineered sensing systems was the incorporation of the whole-cell into *C*. *elegans*. The transparent nature of

this species allows for facile detection of optical reporters. Additionally, *C. elegans* can be dispersed onto sites where contamination is possible and their mobility allows for detection over broad areas. Each of the experiments described herein are stepping stones to the technological evolution of a whole-cell biosensor which can be further optimized for future studies.

### 3.4 Conclusions

Genetically engineered sensing systems have had numerous applications throughout the years. These systems are ideal for analytical applications due to the natural selectivity of the regulatory proteins involved in the sensing network. Herein, we have demonstrated for the first time the technological evolution of a genetically engineered sensing system by employing cells containing the ArsR regulatory protein for the detection of arsenic. Genetically engineered sensing systems are capable of being tailored for a specific analyte, amenable to various platforms, and can be packaged for long-term storage. Additionally, Table 2 demonstrates that genetically engineered sensing systems can be amended to all of these platforms and still maintain the detection limit of the vegetative cells in a traditional microtiter plate. The studies herein also glimpse into the future of genetically engineered sensing systems by exploiting an optically transparent nematode as a carrier for the sensing technology. Furthermore, the nematode itself can be genetically manipulated to serve as the sensing element. As advancements are made in the fields of molecular biology and materials engineering, genetically engineered sensing system technology will continue to evolve and novel designer systems can be fabricated for a plethora of analytical and biomedical applications.

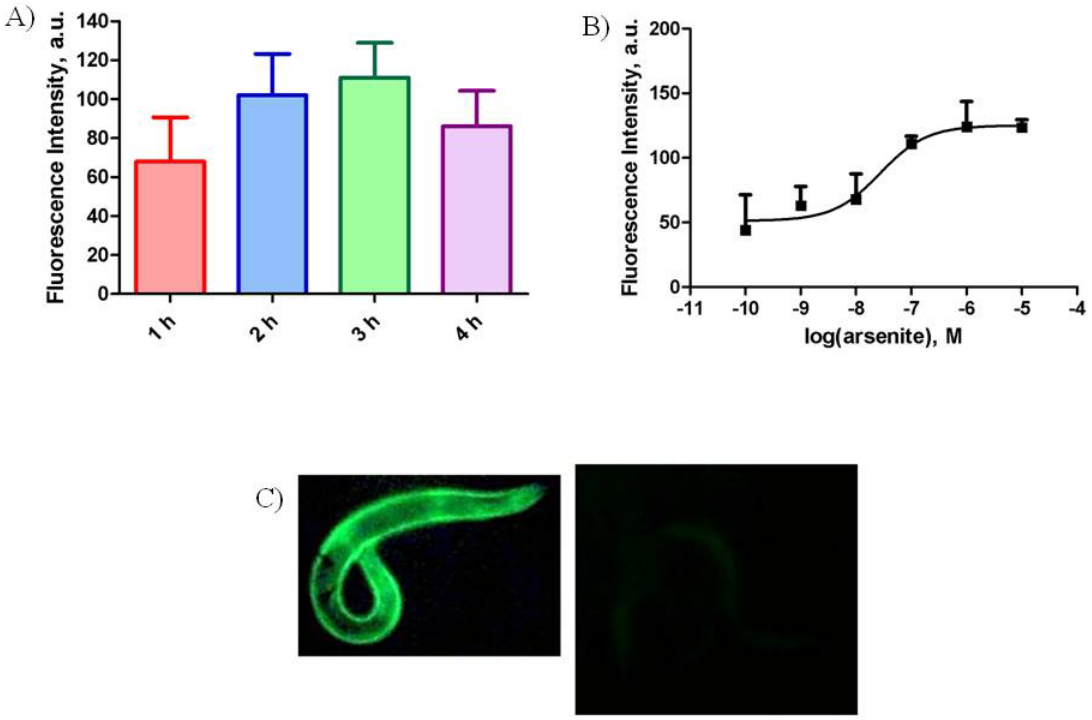


**Figure 3.6.** *C. elegans* were employed as vehicles for sensing arsenic. A) Worms were transferred onto NGM plates with *E. coli* AW10 cells containing the plasmid pSD10 as the sole food source. The worms were washed and placed in microtiter plates with 1 x $10^{-6}$ M arsenic. A time study was performed to determine the optimal incubation time to elicit a signal from the cells consumed by the nematodes. B) The worms were fed *E. coli* AW10 cells overnight. The worms were then washed and placed in a microtiter plate with various concentrations of arsenic. After 2 h incubation, the fluorescence intensity was measured and it was found that there was a dose-dependent increase in fluorescence. The values shown are averages ± 1 standard error of the mean (n=2). C) In addition to allowing worms to consume the whole-cell biosensor, SJ4001 worms which were genetically modified to express GFP under the control of the arsenite-inducible RNA-associated protein were used [47]. The image on the left shows the fluorescence of the worm after 4 h incubation in presence of 1 x $10^{-4}$ M arsenite. The fluorescence image on the right is a worm that was incubated in the presence of Milli-Q purified water. Images were taken on using an Iphone 4S and were adjusted in Adobe Photoshop using the same parameters to remove background fluorescence.

**Table 3.2.** Limit of detection of the arsenic genetically encoded biosensing system when implemented into various platforms.

| | Limit of Detection * |
|---|---|
| **Microtiter plate- No sporulation** | $3.2 \times 10^{-8}$ M |
| **Vegetative cells on paper microtiter plate platform** | $1.7 \times 10^{-7}$ M |
| **Microtiter plate-After sporulation and germination** | $2.0 \times 10^{-7}$ M |
| **Spores on paper strips** | $1 \times 10^{-7}$ M |
| **Cells consumed by *C. elegans*** | $1 \times 10^{-9}$ M** |

*Limit of detection is defined as the analyte concentration which produced a signal equal to or higher than the signal produced by the blank plus three standard deviations.
**The sensor consumed by the *C. elegans* is the *E. coli* AW10 strain, which is different than the sensor used in the other studies herein

# Chapter 4. Paper Strips for Arsenic Detection Based on Engineered Sensing Spores

## 4.1 Overview

There is a need for rugged sensing platforms which allow for stable, long-term storage and rapid on-site detection. This is of particular importance in resource poor settings where detection of analytes with biomedical or environmental relevance is necessary. Whole-cell biosensors are ideal vehicles for these sensing platforms due to their rapid growth rate, large population size, low cost and easy maintenance (228). Further, whole-cell biosensors provide information about the bioavailability and toxicity of an analyte of interest. Certain bacteria, such as those of the species *Bacilli*, have the ability to transition to a dormant state when subjected to adverse environmental conditions by forming protective shell around their genetic material, termed spores. These spores are able to withstand a variety of environmental conditions and have been shown to survive for millions of years (229). These spores have been exploited for numerous applications in biotechnology (143). Herein, we describe the use of whole-cell biosensors, which have been sporulated, in combination with paper-based platforms for the detection an environmental contaminant, arsenic.

Arsenic is a well-known toxic environmental contaminant prevalent in natural and polluted waters and soils. Human exposure can lead to cancer of the lungs, skin, and kidneys (230), and its exposure *in utero* or in early life has been linked to altered motor function and neurodevelopment, impaired lung and thalamic function, and an increased susceptibility to infection (231). Arsenic contamination is water supplies is prevalent in certain areas of the world, such as Bangledesh, where up to 77 million people are

exposed to toxic levels of arsenic in drinking water (232-233). The gold standard for arsenic detection is inductively coupled plasma atomic absorption spectroscopy (ICP-AAS), but this technique is expensive, requires trained personnel, and may not be suitable for on-site applications. Currently, there are a number of kits used for on-site analysis of arsenic in drinking water. These kits, however, have numerous shortcomings such as lack of selectivity, production while detection of unwanted byproducts such as arsine gas, and results not comparable to those obtained with standard laboratory measurement techniques (234). Therefore, there is a need for an arsenic detection kit that is transportable, does not rely on corrosive or toxic components, and does not produce unwanted byproducts. This detection kit must be sensitive, selective, robust, allow for rapid analysis and be able to be performed with minimally trained or untrained personnel.

In recent years, paper has been employed as an inexpensive substrate for the creation of microfluidic devices for use in diagnostic tests and detection kits (209). This is accomplished by patterning hydrophobic barriers onto paper to create hydrophilic channels and control sample flow through the device. Numerous methods have been investigated for patterning paper-based microfluidics including photolithography (209-210), PDMS printing (211), inkjet etching (212-213), and printed circuit technology (235), to name a few. These techniques, however, are not amenable to mass manufacturing due to the need for multistep fabrication and relatively high cost (215). Fabrication techniques, such as wax patterning, have emerged that are low cost, employ non-toxic reagents, and are easily manufactured on a large scale. Screen printing, dipping, and wax printing have been explored as part of these technologies. Screen printing is achieved by creating a mask on a transparency using a laser printer and

fabricating screens through which solid wax is rubbed through onto the paper and melted to create the device (236). The second method, wax dipping, uses an iron mould, formed via laser cutting, which is magnetically sealed to the paper, and dipped into molten wax (237). Although these methods utilize relatively simple fabrication techniques, they are limited due to the need for multiple steps in the fabrication and inflexibility in patterning. To overcome these obstacles, wax printing has recently been explored. In this technique, a design is created using a computer program and is printed on a paper substrate using a wax printer (238-239). By this method, multiple copies of devices can be reproducibly fabricated in minutes to achieve mass numbers of paper devices at a low cost.

These paper-based sensing platforms are especially useful for on-site sensing compounds of environmental relevance. Specifically, environmental sensing is important for the detection of dangerous heavy metals in water sources, especially in developing countries lacking adequate infrastructure for testing and decontaminating water (240). A previously reported sensor demonstrated the feasibility of using paper-based approaches for the detection of a number of metals, namely Hg(II), Ag(I), Cu(II), Cd(II), Pb(II), Cr(VI), and Ni(II) (241). This assay, however, lacks selectivity and further analysis needs to be performed to determine the identity of the metal that is present as the sensor cannot discriminate which of the metals listed above is present. An approach to improving selectivity of a sensor is to take advantage of the exquisite selectivity of molecular recognition find in nature. For example, biosensors have employed proteins as the sensing element to develop biosensors that selectively respond to an analyte of interest. These biomolecules, however, have their own disadvantages in that they are typically unstable at elevated temperatures, limiting their transport, storage, and use conditions. To

overcome the temperature instability of proteins in particular, we have previously employed paper strip whole-cell biosensors for the detection of quorum sensing molecules (108). Whole-cell biosensing systems are advantageous when incorporated in on-site detection devices and kits in that they provide information on analyte bioavailability, have high sensitivity and selectivity, and are cost effective, while providing a natural packaging for labile biomolecules that protects them from environmental, potentially harsh, conditions (105-106). Previous methods that have been employed for the preservation of bacterial whole-cell sensors include freeze-drying, vacuum drying, continuous cultivation, and immobilization in organic and inorganic polymers, all of which can be time-consuming and costly (219). Recently, our laboratory has demonstrated that bacterial spores are ideal for use as transport and storage vehicles for whole-cell sensing systems (188). Bacterial spores have been shown to undergo numerous germination/sporulation cycles and still maintain the initial analytical characteristics of the sensor. Further, it has been demonstrated that *Bacillus subtilis* spores can withstand a range of environmental conditions such as extreme temperatures, humidity levels, and desiccation, making them ideal for on-site as well as remote analysis (149).

In the current work, we have combined the transport and enhanced storage properties of self-contained *B. subtilis* spores containing an arsenic sensing system with easy to use and cost-effective wax printed paper strips. The sensing system employs β-galactosidase as the reporter protein, which, upon addition of an appropriate substrate, can be visually detected. The wax printed paper is inexpensive and coupled with the

spores allows for development of a stable device for on-site analysis without the need for laboratory infrastructure or trained personnel.

## 4.2 Materials and Methods

### 4.2.1 Chemicals and Apparatus

Sodium arsenite was purchased from Ricca Chemical Co. (Arlington, TX). Whatman cellulose chromatography paper, Grade 1, was purchased from GE Healthcare (Piscataway, NJ). The chemiluminescence detection kit, Beta-Glo assay system, was purchased from Promega (Madison, WI). The 96-well microtiter plates were purchased from Costar (Corning, NY). Luria-Bertani (LB) broth and dipicolonic acid were purchased from Fisher Scientific (Pittsburg, PA). The agar, alanine, potassium chloride, glucose, fructose, calcium chloride, magnesium sulfate, potassium phosphate, chromogenic substrate X-gal (5-bromo-4-chloro-3-indolyl-β-D-galactopyranosidase), and lysozyme were purchased from Sigma Aldrich (St. Louis, MO). All standards were prepared in Milli-Q purified water or tap water from the University of Miami as indicated. Chemiluminescence measurements were performed using a POLARstar OPTIMA microplate reader from BMG Labtech (Durham, NC). Paper strips were printed using a Xerox ColorQube 8570N printer (Norwalk, CT). An iPhone 4S was used to take jpeg images of the strips. All colorimetric data was analyzed using ImageJ software from the NIH (Bethesda, MA).

### 4.2.2 Plasmids, Bacterial Strains, and Culture Conditions

*Bacillus subtilis* strain 23 was transformed with plasmid pMUTin-23 which contains three genes conferring arsenic resistance (*ars*R, *ars*B, *ars*C). ArsR is a DNA-binding repressor protein which, upon binding to As(III), releases its promoter and begins

the transcription of the reporter gene, *lacZ*. ArsB is a membrane protein that forms a channel which allows As(III) to be effluxed from the cell. ArsC reduces As(V) to As(III) so it can be removed from the cell (105).

**4.2.3 Dose-Response Curves in Microtiter Plates**

Cells from a glycerol stock were grown in 5 mL of LB broth containing 25 µg/mL of erythromycin overnight at 37 °C, 250 rpm. The overnight culture was then used to inoculate a 50 mL flask of fresh LB broth containing 25 µg/mL erythromycin and grown at 37 °C and 250 rpm until an $OD_{600}$ of 0.6 - 0.8 was obtained. Commercially available sodium arsenite was dissolved in either Milli-Q purified water or tap water. Arsenite solutions of concentrations ranging from $1 \times 10^{-6}$ M – $1 \times 10^{-8}$ M were prepared. This concentration range was chosen to encompass the linear range of the sensor. Milli-Q purified water or tap water was used as the blank. A 10 µL volume of each of the arsenite solutions was added in triplicate to a 96 well microtiter plate containing 90 µL/well of sensing cell culture. The microtiter plate was incubated at 37 °C and 175 rpm for 1 h. β-Galactosidase expression was quantified using the chemiluminescence assay detection kit, β-glo Assay System, following the manufacturer's instructions. The results were plotted using GraphPad Prism 5 by GraphPad Software, Inc. (San Diego, CA).

**4.2.5 Bacterial Spores**

Spores were generated using a previously established protocol (189). Briefly, 5 mL cultures of cells were grown overnight in LB broth plus 25 µg/mL erythromycin. The overnight culture was used to inoculate 500 mL of Difco Sporulation Media which consisted of Bacto nutrient broth (8g/L), 10 mL of 10% (w/v) KCl, 10 mL of 1.2% (w/v) $MgSO_4 \cdot 7\ H_2O$, adjusted to pH 7.6 with NaOH. After autoclaving, filtered solutions of 1

mL each of 1 M $Ca(NO_3)_2$, 0.01 M $MnCl_2$, and 1 mM $FeSO_4$ were added to the solution. The inoculated broth was then grown at 37 °C and 250 rpm for 48 h or until >90% of the culture contained free spores when examined under a microscope. The cells were then centrifuged at 8,000 rpm for 20 min. The resultant pellet was resuspended in Milli-Q purified water and was sonicated on ice for 10 min with 10 s on/off intervals. After sonication, the spores were centrifuged again at 8,000 rpm for 15 min and washed 3 times in 125 mL of a 1 M KCl, 0.5 M NaCl solution. The spores were then resuspended in 50 mM Tris buffer, pH 7.2 and incubated with 50 µg/mL lysozyme at 60 °C for 60 min to remove any vegetative cells. After incubation, the spores were washed three times with Milli-Q purified water, resuspended to an $OD_{600}$ of 6.0 and stored at 4 °C until further use.

### 4.2.6 Preparation of Paper Strips

Paper strips were designed using Adobe Photoshop such that 108 strips were able to be fitted onto one piece of 8.5 in. x 11 in. of Whatman chromatography paper, type 1, which was printed using a Xerox ColorCube Wax Printer. The printed strips were then baked for 30 s on each side in an oven at 110 °C to allow the wax to form a hydrophobic barrier throughout the chromatography paper. *B. subtilis* spores were diluted to an $OD_{600}$ of 2.0 in Milli-Q purified water and mixed in equal volume with a 4% agar, 50 mM Tris KCl solution at pH 8.0. A volume of 20 µL of this mixture was spotted on each strip within the hydrophobic barrier created via wax printing. After allowing the strips to dry, the strips were either used immediately or stored at RT until use.

### 4.2.7 Optimization of Germination Time on Paper Strips

Commercially available arsenite was diluted using Milli-Q purified or tap water to obtain standards ranging from $1 \times 10^{-6}$ M - $1 \times 10^{-8}$ M arsenite in a total volume of 1 mL of LB broth, 12 mM $CaCl_2$ and 12 mM DPA in culture tubes. Paper strips were added to each tube and were left to incubate for various time periods at 37 °C and 250 rpm. After incubation, the strips were removed and 10 µL of 50 mg/mL X-gal and 10 µL of 20 mg/mL lysozyme were added to each strip and the color development was allowed to continue for 60 min. The color intensities were then measured using ImageJ software upon digital image acquisition as previously described (108). The final color intensity variations are due to environmental illumination while the picture was being taken and were corrected by measuring the color intensity of the strip just above the sensing area.

### 4.2.8 Dose-response Curves on Paper Strips

Commercially available arsenite was diluted using Milli-Q purified or tap water to obtain standards ranging from $1 \times 10^{-6}$ M - $1 \times 10^{-8}$ M arsenite in a total volume of 1 mL of LB broth, 12 mM $CaCl_2$ and 12 mM DPA in culture tubes. Paper strips were added to each tube and were left to incubate for 3 h at 37 °C and 250 rpm. After incubation, the strips were removed and 10 µL of 50 mg/mL X-gal and 10 µL of 20 mg/mL lysozyme were added to each strip and the color development was allowed to continue for 60 min. The color intensities were then measured using ImageJ software upon digital image acquisition as previously described (108). The final color intensity variations are due to environmental illumination while the picture was being taken and were corrected by measuring the color intensity of the strip just above the sensing area.

### 4.2.9 Analysis of Environmental Samples on Paper Strips

Initially, 0.5 g of top soil was spiked with 100 µL of varying arsenite concentrations. The spiked samples were incubated at room temperature and 175 rpm overnight. After incubation, the samples were dried by incubation in an oven set to 100 °C to remove any water from the soil. After drying, 12.5 mL of 300 mM phosphate buffer, pH 7.5, was added to each sample and incubated at 40 °C and 300 rpm for 16 h. The samples were then filtered to separate the aqueous layer containing the arsenic from the soil and 10 µL of each sample was added to 90 µL of vegetative cells and incubated for 1 h at 37°C and 175 rpm. β-galactosidase expression was quantified using the chemiluminescence assay detection kit, β-glo Assay System, following the manufacturer's instructions. Simultaneously, 100 µL of each sample was added to culture tubes containing 1 mL of LB broth, 12 mM $CaCl_2$ and 12 mM dipicolonic acid (DPA) and incubated with paper strips which have spores immobilized on them for 3 h. After incubation, the strips were removed from the solution and 10 µL of 50 mg/mL X-gal and 20 mg/mL lysozyme were added to the strips to allow for color development. Images were acquired using an iPhone 4S and the color intensity was quantified using ImageJ software. The results were validated by ICP-MS.

### 4.2.10 Reducing Assay Time For On-Site Detection

Strips were spotted as previously described and incubated at 37 °C and 250 rpm for various times (1 h, 2h, 3h, 4h) in 900 µL of LB broth containing 12 mM $Ca^{2+}$-DPA. Additionally, the strips were incubated at RT without shaking overnight at room

temperature in 900 μL of LB broth. After incubation, 10 ppb arsenic was added to each solution and incubated for various time points (15, 20, 25, 30, 35, 45, or 60 min). X-gal and lysozyme were then added for color development.

**4.3 Results and Discussion**

The facile, sensitive, selective detection of environmentally persistent analytes that impact human health is of upmost importance. One of such compounds is arsenic, known to cause toxic effects to humans that can lead to cancer, dermatitis, and vascular disease (242). Arsenic is of special concern because it is not only a pollutant, but also present naturally in soils and waters. Due to the prevalence of arsenic presence in developing countries, robust sensors are needed that are amenable to field studies in locations where infrastructure and other resources are limited. Our research group has previously shown that genetically engineered sensing bacterial systems allow for the selective and sensitive detection of a number of different classes of environmental analytes, including arsenic (188). Further, we were first to report that bacterial spores provide stable packaging for whole-cell biosensors, and therefore, are an ideal vehicle for their inexpensive storage and transport under a variety of environmental conditions (149). We have also shown that *B. subtilis* sensing cells are amenable to field applications using portable, centrifugal microfluidic platforms (183). These platforms, however, are still limited for on-site analysis due to the need for devices for sampling and detection that are not practical for use in developing areas. To address this issue, we have designed and constructed a new wax printer based paper strip platform onto which sensing cells can be immobilized for visual signal detection (Figure 4.1). To this end, we have employed a *B. subtilis* strain harboring a plasmid that contains the *arsR* gene, which recognizes arsenic,

along with the *lacZ* gene responsible for the production of the reporter enzyme β-galactosidase. When arsenic is present, it binds to ArsR, causing the subsequent transcriptional regulation and expression of the *lacZ* gene, which, in the presence of its substrate, produces a signal that is directly proportional to the arsenic present in the environment.

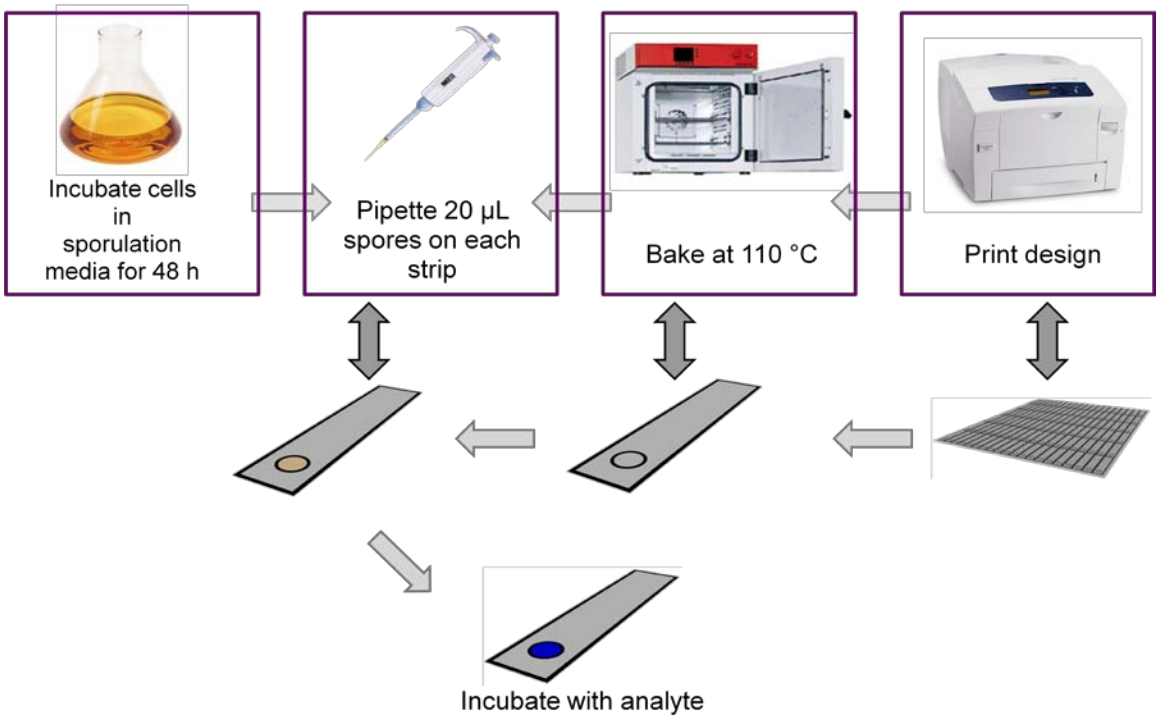


**Figure 4.1.** Schematic demonstrating the fabrication of the paper strips. Initially, a design is printed on a wax printer. After printing, the paper is baked at 110 °C for 30 s on each side to form a wax barrier through the paper. Aliquots of 20 µL of a 1:1 spore agar solution are spotted into the sensing area on the strip. The strips are then incubated in the presence of analyte for 3 h to allow for germination and detection. The strips are removed from the solution and X-gal and lysozyme are added for signal visualization.

Initial studies were performed to evaluate the analytical performance of the *B. subtilis* sensing cells by exposing them to varying concentrations of arsenite from $1 \times 10^{-6}$ M to $1 \times 10^{-8}$ M and monitoring the expression of β-galactosidase using chemiluminescence (188). The detection limit, defined as the signal of the blank plus

three standard deviations, was found to be $1 \times 10^{-7}$ M (Figure 4.2), which is within the current EPA standard for drinking water of 10 ppb, or $7.6 \times 10^{-7}$ M arsenic (http://water.epa.gov/lawsregs/rulesregs/sdwa/arsenic/). To employ the sensing system for detection of arsenic in environmental samples, the effect of other substances in the sample (matrix effects) were evaluated with our sensor by dissolving the analyte in Milli-Q purified water or tap water to determine if the presence of ions affected the analytical characteristics of the arsenic sensor. Figure 4.2 shows the comparison of a reference dose-response curve for arsenic detection in double-distilled water to a dose-response curve in tap water in the same analytical run. The detection limits for arsenic are similar, thus showing no significant impact from other metal ions that may be present in municipal tap water.

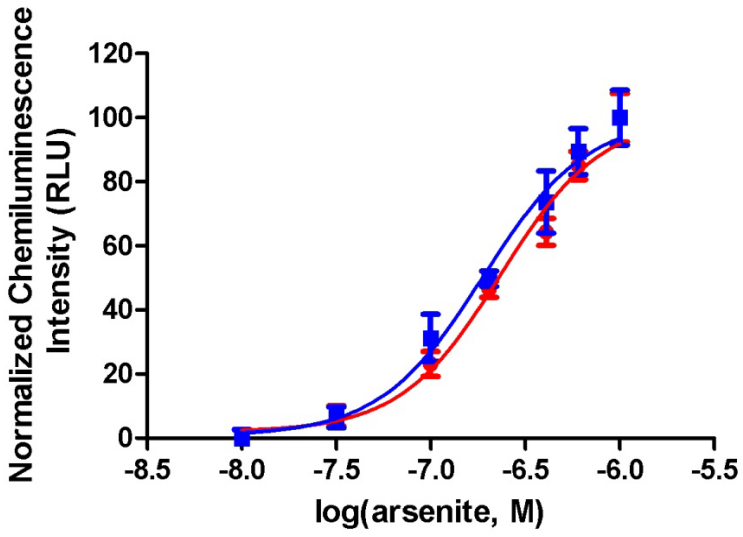


**Figure 4.2.** To evaluate the effect of the presence of ions in the sample, dose-response curves were generated using both Milli-Q purified water (red) and tap water (blue) in a microtiter plate on the same analytical run. The chemiluminescence signals have been corrected with respect to each blank and have been normalized for comparison. Data shown are the average ± 1 SD (n=3).

After evaluation of the analytical characteristics of the whole-cell sensing system in vegetative or "alive" cells, we evaluated the performance of the *B. subtilis* arsenic sensing system after turning the cells into spores and germinating "reviving" the cells after given periods of times. Previous work described that germination of spores to cells and subsequent sensing of the cells was achieved with an incubation time of 2 h in a microtiter plate (188). In this case, a chemiluminescent substrate was also employed for generation of the signal from the reporter enzyme, β-galactosidase. The validation of the spores' ability to germinate and be employed for sensing lead to the preparation of paper strips sensors for detection of arsenic. The spores were immobilized on the strip by first diluting the spores to an $OD_{600}$ of 2.0 and mixing them in an equal volume of 4% agar in a 50 mM Tris KCl buffer, pH 8.0, followed by spotting the spore solution on the paper strip and allowing the spores to dry on the paper. The strip was then incubated in a culture tube for 2 h with LB broth and the appropriate amount of analyte. After incubation, the strips were removed from the tubes and an easy to visualize chromogenic substrate for b-galactosidase, X-gal, and lysozyme, an enzyme that facilitates cell wall opening for sensing, were spotted onto the detection area of the strip. In such a system, the measured color intensity is directly proportional to the amount of arsenic present in the environment of the sensing cells. However, no color change was noted after several hours of incubation of the spores with only X-gal and lysozyme. To determine if the spores were germinating, a time study was performed using the paper strips with the immobilized spores. Initially, no color change was noted until after 16 h of incubation (data not shown). This incubation time was previously shown to be necessary for *B. subtilis* spores that have previously been employed for paper-based detection of Zn (II)

and bacitracin (220). For portable field kits, however, this is a lengthy incubation time and is unsuitable for on-site analysis. Therefore, we investigated methods to decrease the germination time and, thus, decrease assay time. To that end, we explored two methods for spore germination. First, it is well known that dipicolinic acid (DPA) comprises ~20% of the core dry weight of a spore (243). DPA exists as a 1:1 chelate with divalent cations, specifically $Ca^{2+}$. It is hypothesized that the role of DPA is to lower water content of the spore, which in turn protects core proteins from inactivation or denaturation from wet heat (244). Previous studies investigating *B. subtilis* spores on solid surfaces have shown that a 1:1 chelate of $Ca^{2+}$-DPA enhanced germination by 5-8 fold in thin silica layers (245). Therefore, we hypothesized that $Ca^{2+}$-DPA could be necessary to enhance germination on our paper strips. Our second option to expedite germination was to add L-asparagine, D-glucose, D-fructose, and potassium (AGFK) media to the spores. Previous studies report that certain receptors on the surface of the spores, such as GerB and GerK, cooperate to respond to AGFK media and initiate germination (246). To determine which of these methods were more efficient for the germination of our system, studies were conducted in a microtiter plate by adding 45 µL of spores of an $OD_{600}$ of 2.0 and incubating in the presence of $1 \times 10^{-6}$ M arsenic with a final concentration of either 60 mM $CaCl_2$ and 60 mM DPA or AGFK media in triplicate and the assay was evaluated at different time points to monitor the germination. It was found that six hours was necessary to achieve a reproducible signal above the background. Figure 4.3a shows that there is a significant difference in the signal intensity of the two germination methods after six hours ($p < 0.01$). It is important to note, however, that in this study, the only source of nutrients to stimulate germination was the $Ca^{2+}$-DPA or AGFK. Therefore, we

hypothesized that the germination process could be sped up further by the addition of a nutrient rich media such as LB broth in conjunction with $Ca^{2+}$-DPA which was used in subsequent experiments when employing the paper strips for sensing. However, when this concentration was used in the presence of nutrients, no germination was observed in the six hour time period. We hypothesized that the DPA may be chelating other divalent ions in the media as opposed to the $Ca^{2+}$. To overcome this obstacle, we performed a study in which we incubated the spores immobilized on the paper strips in the presence of various concentrations of $Ca^{2+}$-DPA. Figure 4.3B shows the color intensity decrease with increasing $Ca^{2+}$-DPA and Figure 3C shows the quantitative results obtained from ImageJ. As expected, higher concentrations of $Ca^{2+}$-DPA actually hindered the germination. At lower concentrations, i.e. 12 mM, the germination increased significantly over the blank. Therefore, 12 mM $Ca^{2+}$-DPA was used for subsequent experiments.

After optimizing the germination media in the microtiter plate, the germination time on the strips needed to be optimized. The spores were spotted on the strips as previously described and incubated in culture tubes containing 1 mL of a solution of LB broth with 12 mM $CaCl_2$, 12 mM DPA and 1 x $10^{-6}$ M arsenite at 37 °C and 250 rpm for various times (2 h, 2.5 h, 2.75 h, 3 h, 4 h, and 5 h). After the appropriate incubation time, the strips were removed from the tube and X-gal and lysozyme were spotted onto the strip for development of the blue color. No color development was seen after a 2 h incubation period, while the color intensity was visible at 2.75 h incubation and significantly enhanced at 3 h and beyond (Figure 4.4A). Figure 4.4B shows the quantification of the visual results after analysis of the color intensities with ImageJ software. From the obtained data, an incubation time of 3 h was chosen for further assays.

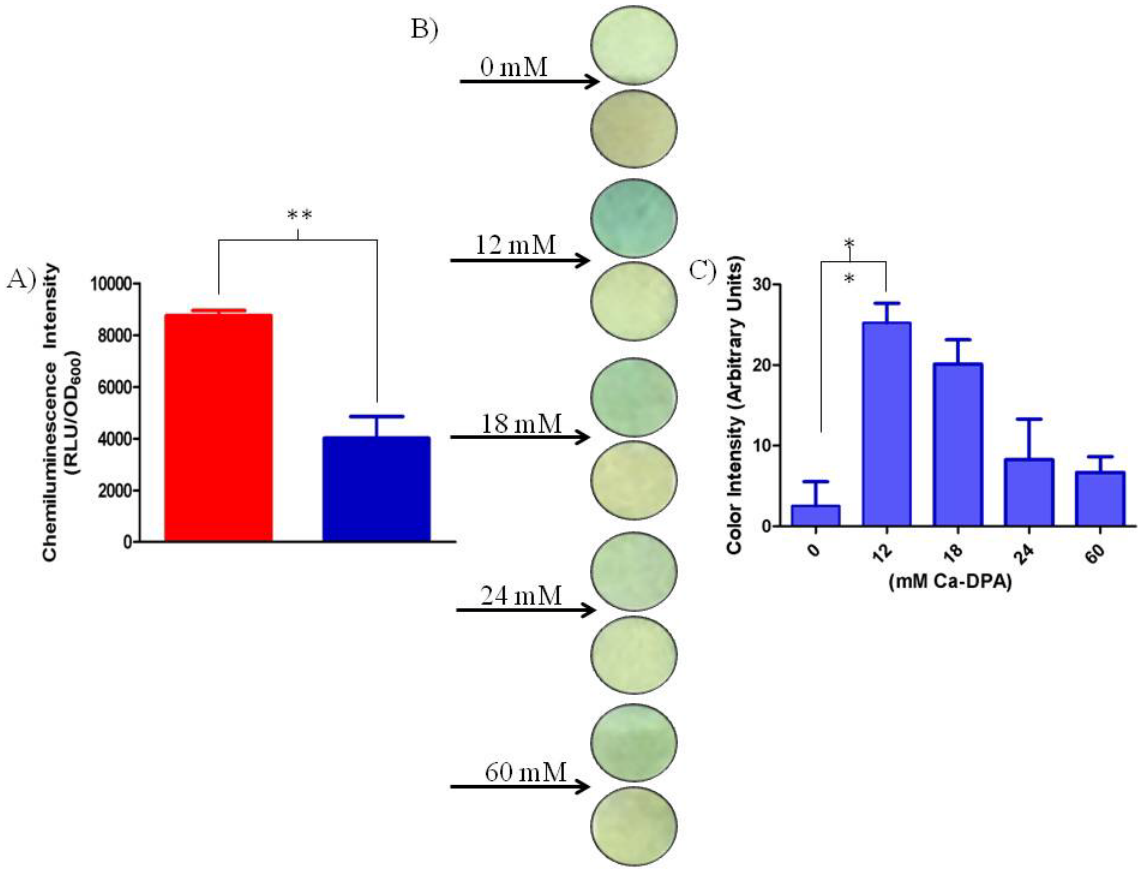


**Figure 4.3.** (A)Two methods were compared to optimize the germination time of the spores immobilized on the paper strips. The first method was the addition of 12 mM $CaCl_2$ and 12 mM DPA (red) and the second was the use of AGFK media to promote germination (blue). The spores were placed in the appropriate media and allowed to germinate for 6 h in the presence of $1 \times 10^{-6}$ arsenite. The $Ca^{2+}$-DPA media enhanced signal output significantly as compared to the AGFK media (p= 0.006). Data shown are the average ± 1 SD (n=3). The spores were spotted on the wax-printed paper strips and incubated for 3 h in the presence of varying concentrations of $Ca^{2+}$-DPA, LB broth, and $1 \times 10^{-6}$ M arsenite. (B) Image of the detection areas of the strips showing the amount of $Ca^{2+}$-DPA each strips was incubated in the presence of. The images were quantified using ImageJ software and the results are shown in (C). A concentration of 12 mM $Ca^{2+}$-DPA was significantly different than the blank (p=0.0042) and was used in subsequent experiments. All data are shown as averages ± 1 SEM (n=3).

It was hypothesized that by printing the detection chambers on the paper strips, a hydrophobic barrier would be formed to prevent the spores from spreading through the paper. By confining the same number of spores to a smaller space, the signal intensity,

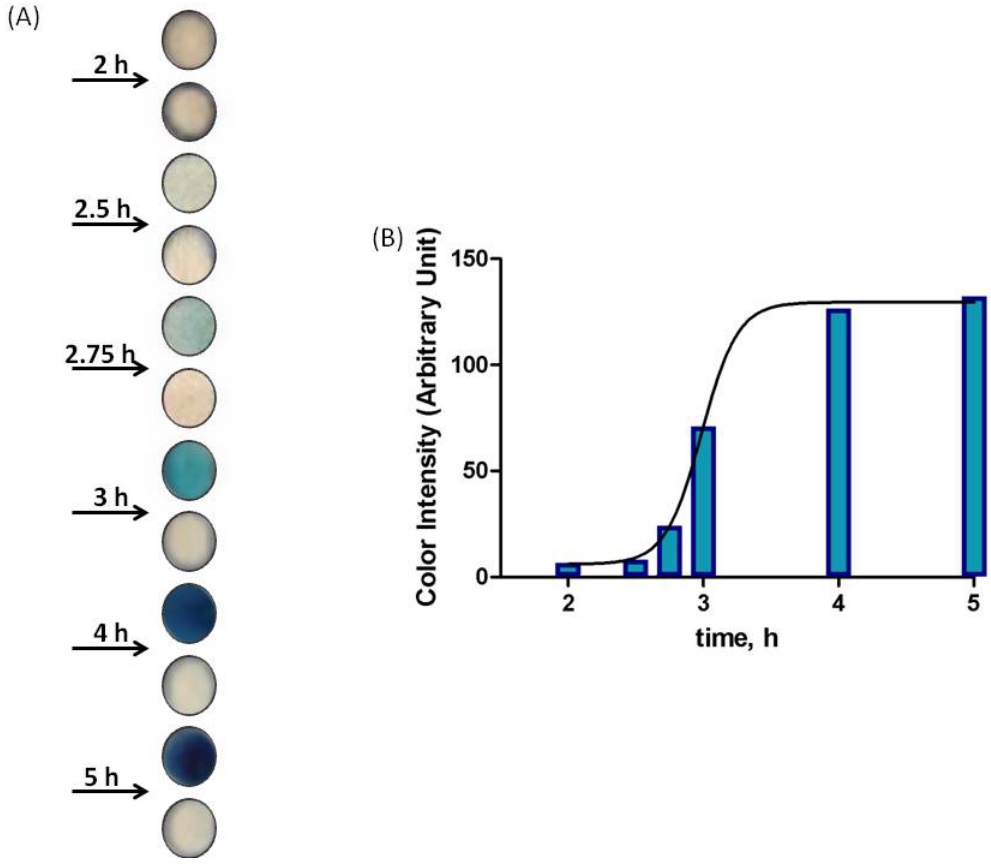


**Figure 4.4.** Time study to determine germination and sensing time for spores immobilized on paper strips. (A) The spores were incubated for various times in the presence of LB, $Ca^{2+}$, DPA, and $1 \times 10^{-6}$ M arsenite at 37 °C and 250 rpm. After incubation, X-gal and lysozyme were added to the detection area on the strip for blue color development. The top strip represents the color change in the presence of arsenite at each time point and the bottom strip represents color change in the presence of the water blank for that time point. (B) The intensity of the color development was analyzed using ImageJ software. The signals have been corrected with respect to the blank and variations in color intensity due to differences in environmental illumination while the pictures were taken. The time study was performed three times with values of ≤10% RSD.

and thus sensitivity, of the sensor should increase. To test this hypothesis, strips of identical dimensions were cut from the chromatography paper, but were not wax printed, and were incubated alongside wax printed strips in $1 \times 10^{-6}$ M arsenite for 3 h. After incubation, the chromogenic substrate X-gal was added to the strips and the color intensity was generated in less than 1 h (Figure 4.5A). Upon quantification, it was found

that the signal intensity of the wax printed strips was significantly higher than the intensity of the plain paper strips (p=0.0232) (Figure 4.5B). These data indicate that the sensitivity of the sensor is enhanced by printing a hydrophobic barrier around the detection area of the strip.

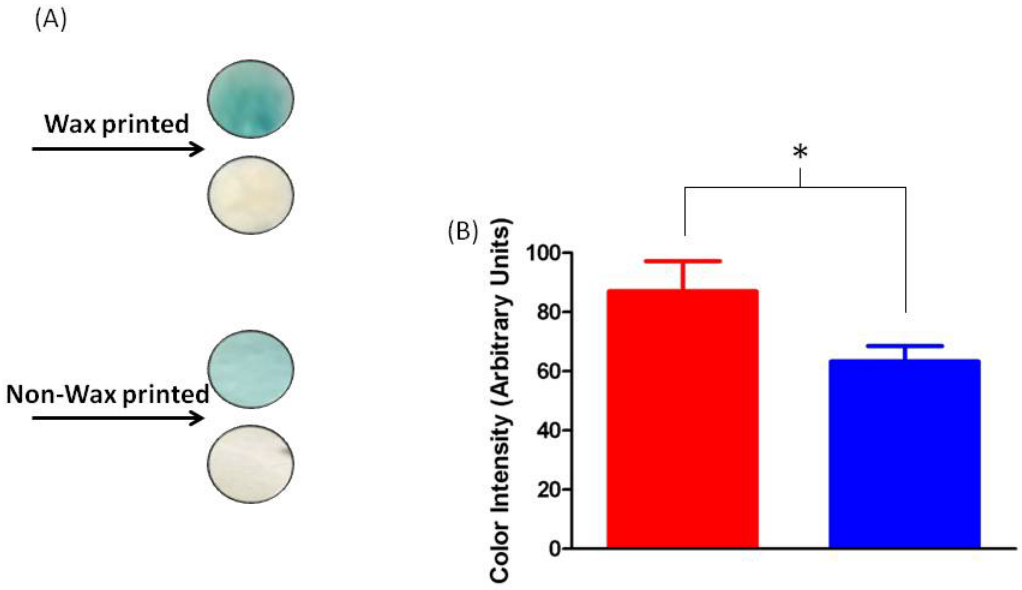


**Figure 4.5.** Spores were spotted on paper strips that were plain or wax printed for 3 h in the presence of $1 \times 10^{-6}$ M arsenite. (A) Image of the detection areas of the strips which had not been wax printed and its respective blank (top) and had been wax printed with its respective blank (bottom). (B) The images were analyzed using ImageJ software. The color intensity generated by the cells on the wax printed paper strips was statistically higher than the plain paper strips. All data are shown as averages ± 1 SEM (n=3).

After time optimization, a dose-response curve was generated by placing the paper strips containing the spores in contact with a solution containing various concentrations of arsenic. Figure 4.6A shows the strips after incubation in a solution of arsenic in Milli-Q purified water while figure 4.6B shows the strips after in a solution of arsenic in tap water. The strips were analyzed with imaging software and it was determined that there was not a significant change in the detection limit of the sensor in

the two different types of water (Figure 4.6C), with both sensing strips showed a limit of detection of 1 × $10^{-7}$ M. Strips which had been spotted with spores were also stored at room temperature and evaluated for arsenic detection after 7 months. It was found that

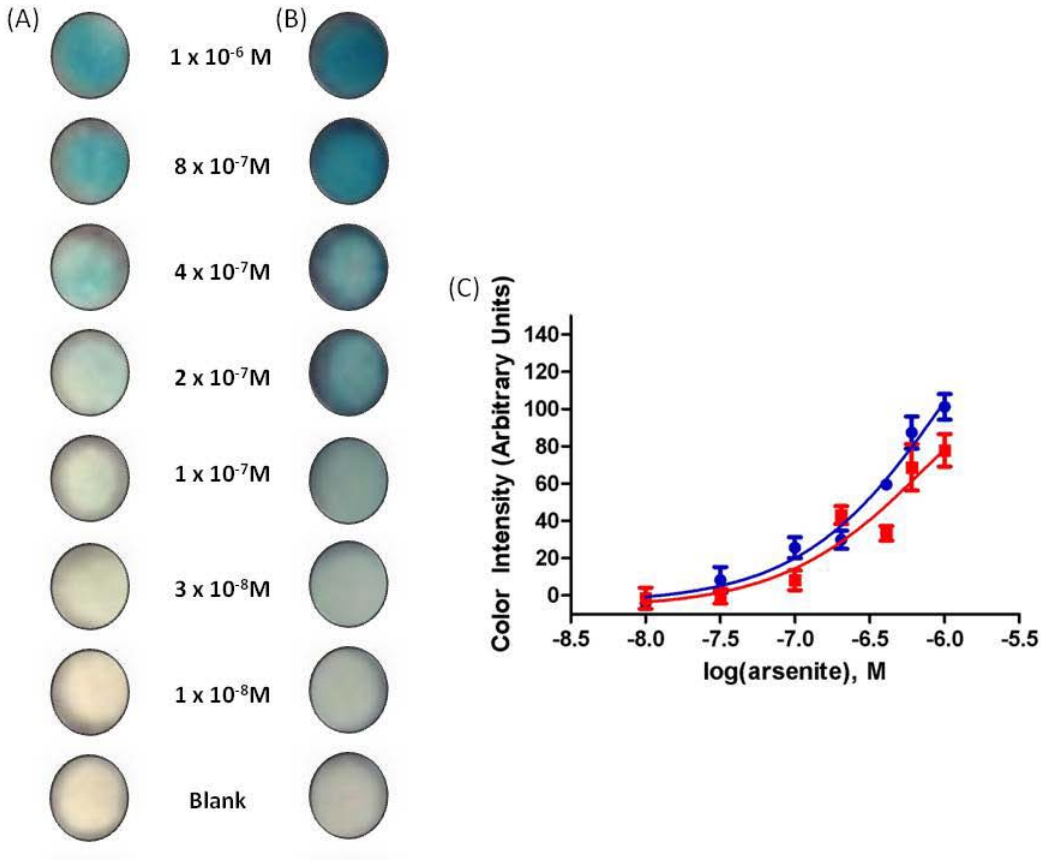


**Figure 4.6.** *B. subtilis* spores containing plasmid pMUTin-23 were immobilized on the paper strips and incubated with various concentrations of arsenite, LB broth, and $Ca^{2+}$-DPA for 3 h at 37 °C and 250 rpm. (A) Dose-response data for the paper strips incubated in Milli-Q purified water. Milli-Q purified water served as the blank. After incubation, the strips were removed from the solution and 10 µL of X-gal (50 mg/mL) in DMF and lysozyme (20 mg/mL) in water were added to the detection area of the strip. Color development was carried out for 1 h. (B) Dose-response data for paper strips incubated in tap water. The assay was carried out as described above except tap water served as the blank. (C) The intensity of the blue color development on the Milli-Q purified water (red) and tap water (blue) sensing strips was measured using the software ImageJ upon digital acquisition of each image. The signals have been corrected with respect to the blank and variations in color intensity are due to differences in environmental illumination while the pictures were taken. All data are shown as averages ± 1 SEM (n=3).

the strips maintained a sensitivity level comparable to that of freshly spotted strips (Figure 4.7), thus demonstrating the stability of spore-based paper strips. This is an indication that the innate stability of the spore will result in durable sensing strips under a

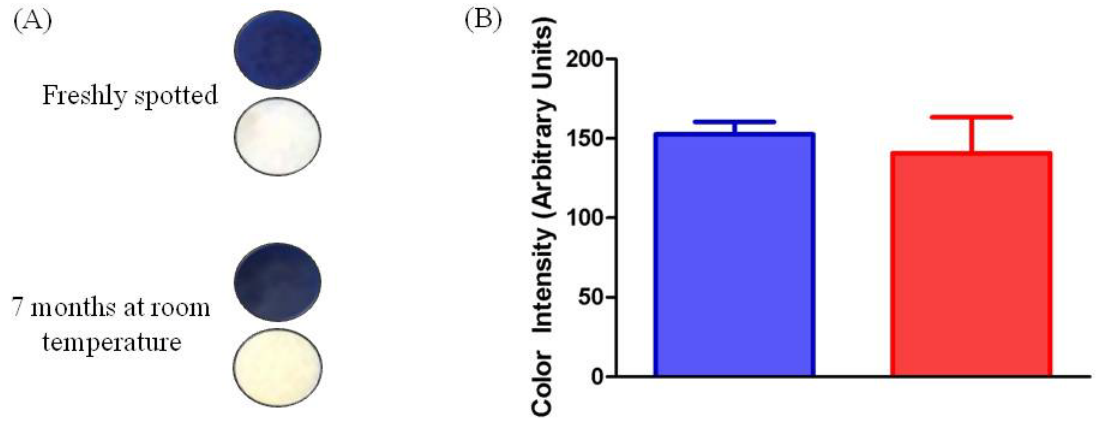


**Figure 4.7.** Stability of spores on paper strips over time. (A) Freshly spotted spores and spores that had been stored at RT for seven months were incubated with 1 x $10^{-5}$ M arsenite (top) or Milli-Q purified water (bottom). (B) The blue color intensity of the sensing strips was measured with ImageJ upon digital acquisition of each image. Upon storage for 7 months at room temperature, there is no significant difference in signal intensity as compared to freshly spotted spores. The signals have been corrected with respect to the blank and variations in color intensity are due to differences in environmental illumination while the pictures were taken. All data are shown as averages ± 1 SEM (n=3).

variety of environmental conditions, as previously described by our group with other spore-based platforms (149).

To validate our recently developed paper strip biosensor we employed it in the detection of arsenic in a soil sample from Blanche Park in Miami, FL, that has been reported to have high levels of arsenic contamination. Levels of 3600 ± 800 ppb arsenic were detected using our paper strips (Figure 4.8). ICP-MS confirmed levels of 4200 ppb, indicating that the strips can be used to detect arsenic in environmental samples. The sensor was also employed to detect arsenic in water samples from Guanica Bay, Puerto Rico. No arsenic was dectable by our sensor or by ICP-MS analysis.

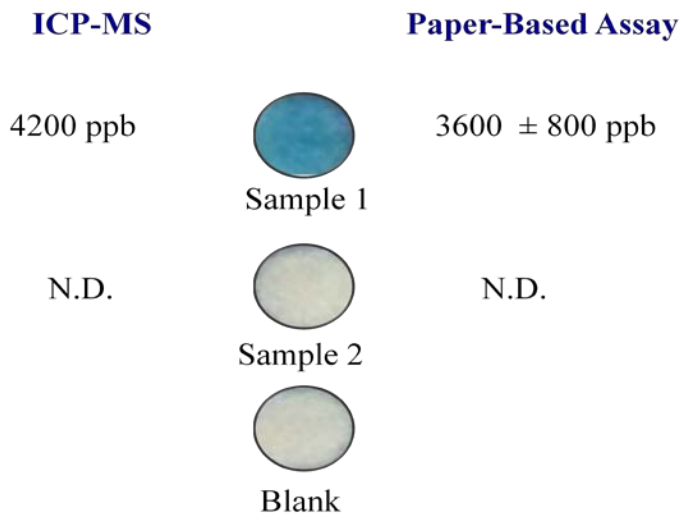


**Figure 4.8.** Analysis of arsenic levels in environmental samples. Sample 1 was taken from a water sample from Guánica Bay, Puerto Rico. No arsenic was detected using the paper strips or by ICP-MS analysis. Sample 2 was taken from Blanche Park in Miami, FL. ICP-MS confirms the presence of 4200 ppb arsenic. The paper strips also indicate 3600 ±800 ppb arsenic which confirms the use of the paper strips for analysis of arsenic levels in environmental samples.

For on-site applications, it is important to reduce assay time to analysis. Currently, the developed assay time described above is 4 h, including color development. Although this is a marked improvement on previously reported assay times that employ paper-based spore sensing (220), it may not be optimal for on-site detection. To further optimize the assay time for on-site detection, we investigated germinating the spores immobilized on the paper strip prior to incubation with the sample. We envision that if an on-site test is being completed, one could begin germinating the spores before leaving for the analysis. Thus, the innate stability of the spores could still be exploited until time for analysis. The spores immobilized on the paper strips were incubated in germination media at 37 °C and 250 rpm for various times (1, 2, 3, or 4 h). After incubation, 10 ppb arsenite was added to each sample and left at RT without shaking for 1 h. We chose 10 ppb because that is the lower EPA limit for arsenic contamination in water samples. After

color development, it was found that a 3 h incubation time was optimal to see a color change significantly above the blank. Next, the strips were incubated for 3 h in germination media at 37 °C and 250 rpm. Then, 10 pbb was added to the sample and incubated for various times (15, 20, 25, 30, 35, 45, and 60 min). X-gal and lysozyme were added to the strips. After 40 min of color development, it was found that a 35 min incubation time in the presence of analyte gave a significant color change (Figure 4.9A). Additionally, were incubated the spores immobilized on the paper strips at RT without shaking overnight. This would be ideal if the on-site analysis was going to occur in a resource poor setting where electricity was not available. After ON incubation, 10 ppb arsenic was added to each tube and incubated for various times (15, 20, 25, 30, 35, 45, and 60 min). X-gal and lysozyme were added to the strips. As before, after 40 min of color development, it was found that a 35 min incubation time in the presence of analyte gave a significant color change as compared to the blank (Figure 4.9B). By germinating the spores before analysis, the assay time decreases significantly from 4 h to 75 min.

**4.4 Conclusions**

Herein, we have developed a portable paper strip sensing system based on genetically engineered *B. subtilis* spores immobilized on the surface of wax printed paper strips for the semi-quantitative visual monitoring of arsenic in environmental samples. The spores function as a stable vehicle for transport, storage, and preservation of the whole-cell sensing system that, when paired with a paper strip platform, allows for on-site detection. Further, we have optimized the germination time of the spore on the paper strips to significantly decrease assay time (from 16 h to 3 h) and a long shelf-life (at least 7 months), both of which make these spores more amenable for on-site detection. The use

of spores in conjunction with paper-based platforms can be used for a variety of environmental analytes for which cell-based biosensors are available to provide a robust, sensitive and selective sensor for on-site detection of environmental compounds (85, 247).

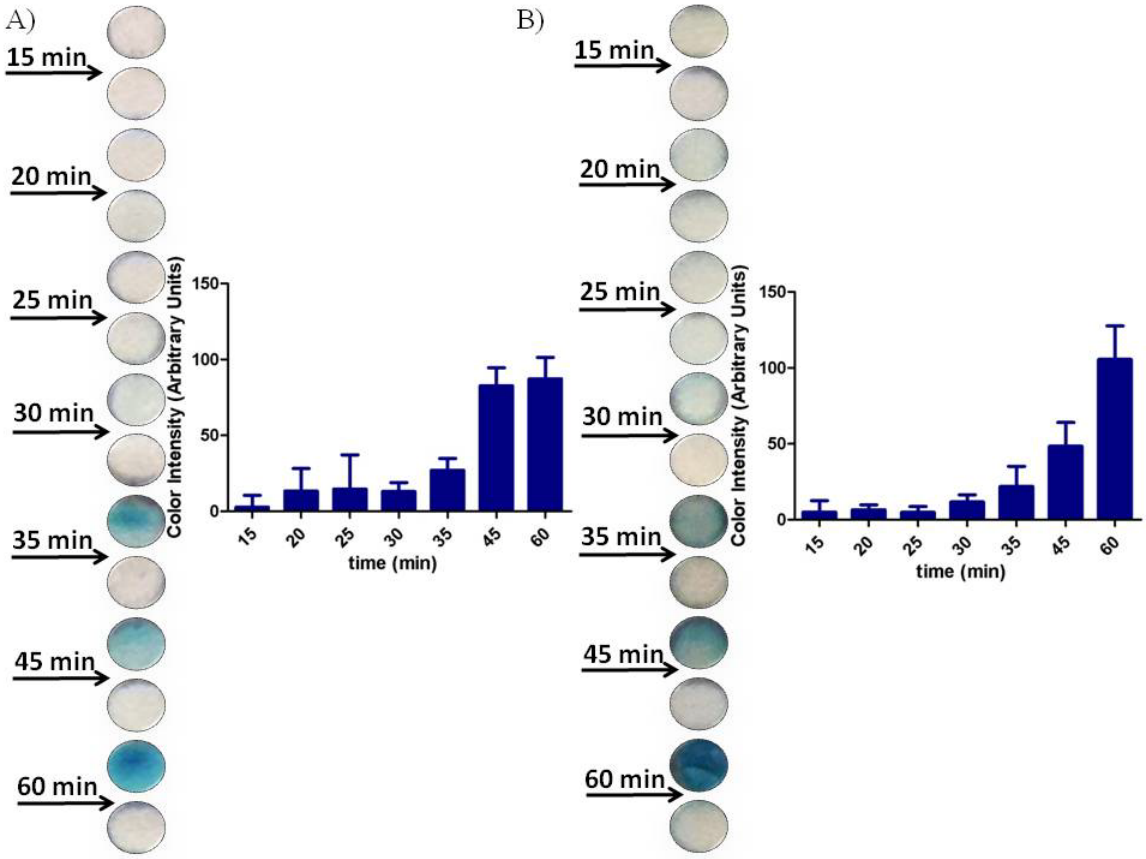


**Figure 4.9.** Spores immobilized on paper strips were germinated prior to incubation with 10 ppb arsenite. (A) The strips were incubated at 37 °C and 250 rpm for 3 h. After incubation, 10 ppb arsenite was added to the solution and incubated for various time points before color development. (B) The strips were incubated at RT without shaking ON. After incubation, 10 ppb arsenite was added to the solution and incubated for various time points before color development. The color change is shown on the left and the quantified color intensities using ImageJ software is shown on the right of each figure. Data are shown as averages ± 1 SEM (n=3).

# Chapter 5. Nanoparticle Mediated Remote Control of Enzymatic Activity

## 5.1 Overview

Nanomaterials with unique energy absorbing (*e.g.*, radiofrequency, optical, *etc*.) and physical properties have built the foundation for a new field of remote controlled (RC) materials(248-250). Due to such unique features, these materials have found many uses in medicine and biotechnology (251-254). One example is the use of gold nanoshells for photothermal cancer therapy (255). These materials absorb energy in the form of near-infrared light (NIR) and dissipate it as heat, which can be applied to induce photothermal ablation of cancer cells. Additionally, Wijaya *et al*. demonstrated that laser-induced melting of nanorods was shown to selectively release oligonucleotides from the nanorods, which may prove useful in drug delivery applications (256). Carbon nanotubes (CNTs) have also been used for their unique heating abilities in the presence of NIR and other wavelengths of energy. Miyako *et al*. were able to control the activity of two thermophilic enzymes, Taq DNA polymerase and cyclomaltodextrin glucanotransferase, *via* heating CNTs with NIR laser irradiation (257). This was one of the first demonstrations of remotely controlled enzymatic reactions using the heating properties of CNTs. Although these materials have been shown to be heated remotely, their uses *in vivo* are limited due to the minimal penetration depth of NIR light (258). To overcome this limitation, nanoparticles have been explored as an alternative source for the production of localized heat when exposed to an alternating magnetic field (AMF) (259-261). Iron oxide nanoparticles are of particular interest because they not only function as heating sites and as vehicles for drug delivery, but they can also be visualized using

conventional imaging techniques (262-265). For instance, Thomas *et al.* developed a drug delivery system based on zinc-doped iron oxide nanocrystals encapsulated within mesoporous silica nanoparticles (266). When heated in the presence of an AMF, temperature responsive valves opened to release the encapsulated drug. Importantly, it was demonstrated that no compound was released in the absence of the field. Recently, Stanley *et al.* demonstrated that by coating iron oxide nanoparticles with antibodies, they could be targeted to a temperature-sensitive $Ca^{2+}$ ion channel (267). When the nanoparticles are heated with an AMF, the channels open allowing for an influx of $Ca^{2+}$ ions. In turn, a bioengineered $Ca^{2+}$ driven promoter is activated, thus intitiating the transcription of insulin. This is one of the first examples of using the heating properties of iron oxide nanoparticles to remotely control gene expression.

Nanocomposites containing magnetic nanoparticles have also been used to enhance or control the properties of stimuli-responsive hydrogels (268-271). There are numerous classes of stimuli-responsive hydrogels that have been developed and are able to, depending on their composition, respond reversibly to external stimuli such as temperature, pH, electric potential, and analyte concentration (272-274). By combining the remote heating capabilities of the nanoparticles with the stimuli-responsive properties of hydrogels, multifunctional materials can be designed for targeted applications such as drug delivery, hyperthermia cancer treatment, and as stimuli-responsive microfluidic valves (260, 275-277). Zadrazil *et al*. encapsulated iron oxide nanoparticles in a thermo-responsive polymer poly(*N*-isopropylacrylamide), (PNIPAM), to form a temperature responsive hydrogel sponge that could release an oil, kerosene, in the presence of an responsive polymer with the iron oxide nanoparticles, a drug delivery system for

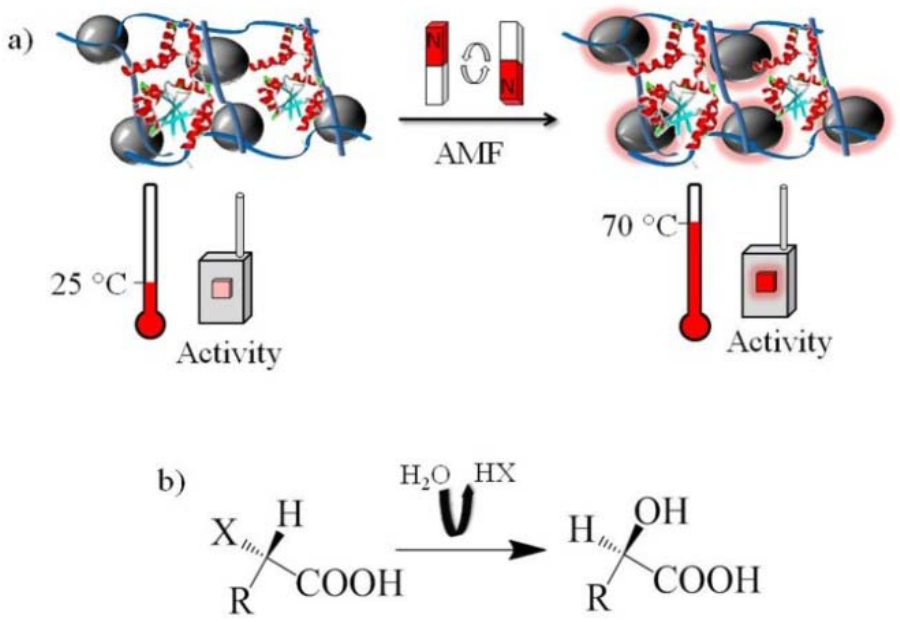


**Figure 5.1.** Schematic demonstrating enhanced activity of the enzyme in the presence of an AMF. a) L-2-$HAD_{ST}$ immobilized in a hydrogel network containing $Fe_3O_4$ nanoparticles. At room temperature, the enzyme activity is minimal. In the presence of the AMF, the nanoparticles heat, thus heating the environment around the L-2-$HAD_{ST}$ and increasing the activity of the enzyme. b) L-2-$HAD_{ST}$ functions by replacing the halogen (X) on an L-2-haloalkanoate with a hydroxyl group. The result is the formation of an D-2-hydroxyalkanoate.

hydrophobic compounds could be developed with on-demand release by exposure to an AMF.

Herein, we demonstrate that by combining enzyme-modified responsive hydrogels with $Fe_3O_4$ nanomaterials, RC nanocomposites can be developed that could find applications not only in the remote decontamination of environmental samples, but also as "on/off" switches for heating and activating proteins in other biomedical, industrial, and pharmaceutical applications. Specifically, the incorporated $Fe_3O_4$ nanoparticles controllably heat the hydrogel matrix in the presence of an AMF, thus allowing for the remote control of the temperature within the system (260). By exploiting

this selective heating capability, enhancement of catalytic activity was achieved by turning on the co-encapsulated thermophilic enzyme. The reactivity of the biomolecules is enhanced at higher temperatures (Figure 5.1a), where combining the divergent materials results in a remotely controlled system. Specifically, we demonstrated the ability to remotely activate a model enzyme, L-2-$HAD_{ST}$, a thermophilic dehalogenase isolated and characterized from the thermophile archaea *Sulfolobus tokodaii.* This enzyme catalyzes the stereospecific dehalogenation of L-2-haloalkanoates to D-2-hydroxyalkanoates (Figure 5.1b). By encapsulating the enzyme into the hydrogel, it allows for the use of the biocatalyst through many enzymatic cycles with different substrates without the need for complicated separation and/or regeneration steps.

## 5.2 Materials and Methods

### 5.2.1 Chemicals and Apparatus

Sodium hydroxide, sodium chloride, ammonium persulfate (APS), sodium phosphate dibasic, sodium phosphate monobasic, acrylamide, and bisacrylamide were purchased from Sigma (St. Louis, MO). L-2-chloropropionic acid (CPA), acrylic acid, 1-ethyl-3-[3-dimethylaminopropyl]carbodiimide hydrochloride (EDC), N-hydroxysulfosuccinimide (Sulfo-NHS), tetramethylethylenediamine (TEMED), and glycine were obtained from Fisher Scientific (Pittsburgh, PA). All chemicals were reagent grade or better. All solutions were prepared using reverse osmosis water (Milli-Q Water Purification System, Millipore, Bedford, MA). Nanoparticles were purchased from Nanostructured & Amorphous Materials Inc. (Houston, TX). The 15-mL centrifuge tubes were purchased from Sarstedt (Newton, NC). Chloride concentrations were determined using a chloride ion selective electrode (VWR, West Chester, PA). Alternating magnetic

field studies were performed on an induction power supply (MMF-3-135/400-2, Taylor Winfield, Brookfield, OH) equipped with a solenoid (1.5 cm diameter, 5 turns). All results were analyzed using GraphPad Prism version 5.0 (GraphPad Software, Inc., La Jolla, CA).

### 5.2.2. Enzymatic Activity Determination of Free L-2-HAD$_{ST}$ Using the Chloride ISE

A stock solution of CPA (10 mM) substrate was prepared in glycine buffer (20 mM, pH 9.5). After addition of the substrate to the buffer, the pH was readjusted with NaOH to 9.5. From this stock solution, dilutions of CPA (0, 0.5, 1.0, 1.5, 2.0, 2.5, and 3.0 mM) were prepared in glycine buffer (20 mM pH 9.5). Triplicate aliquots (2-mL) were obtained from each CPA solution. Then, L-2-HAD$_{ST}$ (0.003 mg) was added to each sample and incubated for 10 min at 70 °C. Blank samples were prepared by adding an equivalent volume of glycine buffer to the protein without substrate. Upon cooling, a commercial chloride ISE was used to determine chloride concentration.

### 5.2.3 Hydrogel Fabrication

The first step of the covalent immobilization of the L-2-HAD$_{ST}$ into a hydrogel network involved the chemical conjugation of the lysine residues of the enzyme to the carboxylic groups of acrylic acid monomers using well-established carbodiimide-mediated coupling reaction protocols. First, acrylic acid (170 μL of a 1 x $10^{-3}$ M stock solution) was added to a reaction mixture of EDC (0.115 mg) and sulfo-NHS (0.575 mg) and left to react at room temperature for 15 min. To this mixture, enzyme (2.0 mg) was added at RT for 2 h and left to react, without stirring, at 4 °C overnight. The conjugated protein was then centrifuged in an Amicon centrifuge filter with a 3000 MW cutoff to remove any unreacted acrylic acid.

Before polymerization of the hydrogels, the hydrogel cast was weighed, and the mass recorded. For hydrogel fabrication, acrylamide (300 mg) and bisacrylamide (576 μL) were added to 2-(*N*-morpholino)ethanesulfonic acid (MES) buffer (2.35 mL, pH 5.5). Next, $Fe_3O_4$ (10% w/v) nanoparticles were added to the precursor solution, which was then sonicated for 20 min to disperse the $Fe_3O_4$ nanoparticles. After dispersion, either (2 mL,1 mg/mL) of the L-2-$HAD_{ST}$-acrylamide functionalized enzyme or buffer (control hydrogels) were added to the solution. Next, APS (60 μL) and TEMED (25 μL) were incorporated into the solution and the hydrogels were allowed to polymerize for 1 h at 4 °C. After allowing it to warm to room temperature, the hydrogel and cast were again weighed. The mass of the cast was subtracted from the mass of the hydrogel plus cast to get an accurate mass of the hydrogel. The polymerized matrix was then removed from the cast and washed overnight in 20 mM glycine buffer, pH 9.5, to remove any of the unreacted monomer from the hydrogel. The hydrogels were then cut into 4-mm diameter round pieces. Eight of these pieces were weighed and their masses averaged. This average was expressed as a percent of the total hydrogel mass. To estimate the average mass of protein in each hydrogel piece, the percentage of mass found for an individual piece was multiplied by the total protein concentration incorporated into the hydrogel matrix.

### 5.2.4 Determination of Hydrogel Encapsulated L-2-$HAD_{ST}$ Activity in a Water Bath

A stock solution CPA (10 mM) substrate was prepared in glycine buffer (20 mM, pH 9.5). After addition of the substrate to the buffer, the pH was readjusted with NaOH to 9.5. From this stock solution, dilutions of CPA (0, 0.5, 1.0, 1.5, 2.0, 2.5, and 3.0 mM) were prepared in glycine buffer (20 mM, pH 9.5). Triplicate aliquots (2-mL) were

obtained from each CPA solution. Hydrogel pieces were added to the solutions that either contained the immobilized L-2-$HAD_{ST}$ or no protein (control hydrogels). Each sample was incubated for 30 min at 21 °C (room temperature), 50 °C (water bath), or 70 °C (water bath). They hydrogel pieces were immediately removed. Upon cooling to room temperature, a commercial chloride ISE was used to determine chloride concentration.

### 5.2.5 Long-Term Stability of Hydrogel Encapsulated L-2-$HAD_{ST}$ in a Water Bath

The activity of the enzyme was determined as described above. Specific activity was evaluated at 70 °C each month for three months from the same set of hydrogels.

### 5.2.6 Alternating Magnetic Field Studies

The hydrogels with the encapsulated enzyme and control hydrogels were incubated at various field amplitudes for 10 min in the presence of CPA (0.5 mM). Simultaneously, hydrogels with the encapsulated enzyme and control hydrogels were also incubated for 10 min in the presence of CPA (0.5 mM) at room temperature. Next, the hydrogel was removed from solution, and the chloride concentration was measured. All measurements were blank subtracted to account for the chloride formation at room temperature. After determining the field amplitude for optimum enzymatic activity, an assay was performed to evaluate the enzymatic efficiency. Stock solutions of the substrate were prepared as described above. The hydrogels were exposed to a field amplitude of 26.2 kA/m for 10 min in the presence of various amounts of substrate as described previously, then the hydrogel was removed and the chloride concentration determined *via* the chloride ISE.

### 5.2.7 Time Study of Free L-2-HAD$_{ST}$

A time study was performed to find an optimal incubation time for L-2-HAD$_{ST}$ activity. The substrate concentration was kept constant at 2.0 mM CPA in 20 mM glycine buffer, pH 9.5. Each sample in triplicate was incubated for the desired time (5, 10, 15, 30, 45, and 60 min) in a water bath at 70 °C. After incubation, the tubes were cooled to room temperature and a commercial chloride ISE was used to determine chloride concentration.

### 5.2.8 Time Study of Hydrogel Encapsulated L-2-HAD$_{ST}$

The hydrogels were incubated in a 20 mM glycine buffer, pH 9.5, with 0.5 mM substrate for different time intervals (5, 10, 15, 20, 30, 45, and 60 min) in a water bath at 70 °C. After incubation, the hydrogels were removed and the samples allowed to cool to room temperature. The chloride concentration was then determined *via* a commercial chloride ISE.

### 5.2.9 Heating Profile of Hydrogel

The wet hydrogel was wrapped in saran wrap and placed on the top of the coil of the AMF apparatus. The field strength was set at 19.9 kA/m and the temperature of the hydrogel was visualized using an AGEMA Thermovision 470 IR camera (FLIR, Boston, MA).

## 5.3 Results and Discussion

L-2-HAD$_{ST}$ catalyzes the dehalogenation of organic compounds, such as the model substrate S-2-chloropropionic acid (CPA). The reaction results in the stereospecific dehalogenation of CPA and formation free chloride, which can be measured by a chloride ion-selective electrode (ISE). L-2-HAD$_{ST}$ has optimal activity at

pH 9.5 and 70 °C, and maintains its activity when immobilized on a solid matrix (278). The demonstration of the long-term activity of the enzyme in solution, as well as its ability to work under extreme conditions and retain activity upon immobilization, allowed us to formulate the hypothesis that L-2-$HAD_{ST}$ can maintain its enzymatic activity after chemical conjugation to acrylic acid monomers and polymerization into a hydrogel network. Purification of the enzyme used for all the studies was performed using a previously established protocol (278). After purification, L-2-$HAD_{ST}$ was incorporated into a hydrogel network by chemical conjugation to acrylic acid functional groups *via* the lysines on the protein. An acrylamide hydrogel containing the L-2-$HAD_{ST}$ was then polymerized with 1.5 wt% bisacrylamide crosslinking in the presence of 10% (w/v) $Fe_3O_4$ nanoparticles. Previous modeling studies indicated that such a nanoparticle concentration would be needed to reach and maintain the desired temperatures.(279) Additionally, a control hydrogel was polymerized by replacing the enzyme solution with the same volume of 20 mM glycine buffer, pH 9.5. The hydrogel was used as a mechanism by which the encapsulation of both the enzyme and the nanoparticles was possible, thereby allowing for remote heating of the system in the presence of an AMF. This is envisioned to allow for activation of the system for bioremediation capabilities with facile recollection of the materials when the process is finished. Although this technique was implemented to immobilize the enzyme in the hydrogel, other strategies may be employed to directly immobilize enzymes to the nanoparticles (280). The immobilization can lead to enhanced stability of the enzyme, as previously demonstrated (281).

With the enzyme incorporated into the hydrogel network, a time study was conducted to determine the optimal incubation time for the substrate. The hydrogel-encapsulated enzyme was incubated with 0.5 mM CPA for various periods of time ranging from 10 min to 1 h at 70 °C. The incubation time used for subsequent studies was determined to be 30 min (Figure 5.2a). Although the time study showed a constant increase in activity over the hour incubation, the 30 min time point is long enough to detect activity significantly above the blank, yet short enough to optimize assay time. After determining the time of incubation for the hydrogel-encapsulated enzyme with the substrate, it was important to demonstrate the activity trend when exposed to varying temperatures. To demonstrate temperature effects on activity, we evaluated the enzyme turnover at three different temperatures (~21, 50, and 70 °C). The highest temperature chosen was 70 °C, the optimal temperature for enzyme activity. Higher temperatures were not used because the aim of the study was to evaluate if the enzyme could be remotely heated using an AMF, not to determine stability of the hydrogel-encapsulated enzyme. First, the activity of the hydrogel-encapsulated enzyme at room temperature (RT, ~21 °C) was evaluated. The hydrogels were placed in a 20 mM glycine buffer, pH 9.5, containing various substrate concentrations (Figure 5.2b). After incubating for 30 min, the hydrogels were removed and the chloride concentration was measured. For each substrate concentration, triplicate measurements were performed using hydrogels containing the enzyme and control hydrogels prepared in the absence of the enzyme. The latter was used to determine the contribution of substrate autohydrolysis during the incubation period, which was taken into account by subtracting the chloride concentration in the controls from the total chloride concentration in the test samples. The protein in the

hydrogel was found to have a $k_{cat}$ of 4.02 ± 0.18 × $10^{-5}$ $s^{-1}$ and a $K_m$ of 1.03 ± 0.27 mM. Furthermore, the enzymatic efficiency at room temperature was found to be 0.39 ± 0.10 × $10^{-4}$ $mM^{-1}$ $s^{-1}$.

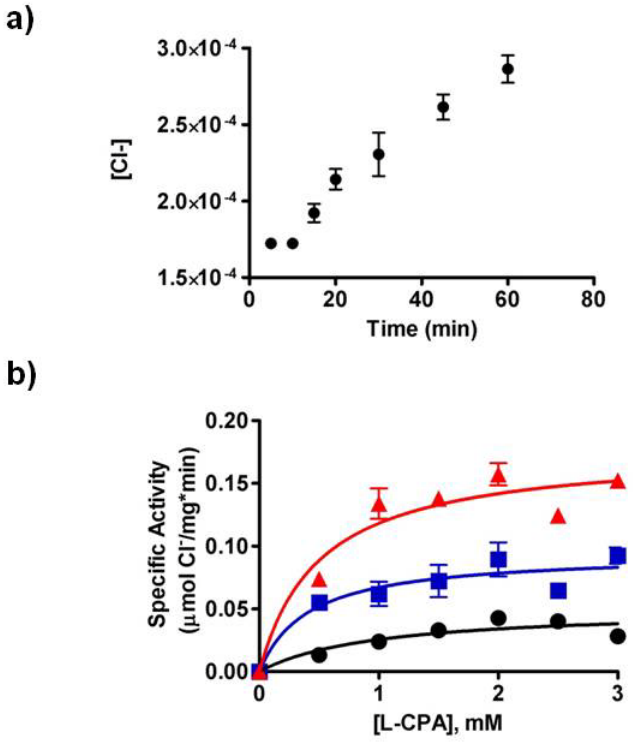


**Figure 5.2.** Enzymatic activity of L-2-$HAD_{ST}$ immobilized in a hydrogel in a water bath. a) The protein was encapsulated in the hydrogel and a time study was performed by allowing the nanocomposite hydrogel pieces to incubate with 0.5 mM CPA for various periods of time. Data are blank subtracted and shown as averages ± one standard deviation (n=3). The time point chosen for subsequent experiments was 30 min. b) To test the activity of the immobilized protein, the hydrogel-encapsulated L-2-$HAD_{ST}$ was incubated for 30 min at 21 °C (circles), 50 °C (squares), and 70 °C (triangles) with various concentrations of CPA. Data are blank substracted and shown as averages ± one standard deviation (n=3).

Next, the activity of the hydrogel-encapsulated enzyme was evaluated at 50 °C, which is still lower than the optimum temperature for reactivity (70 °C). The experiments were performed as described above by incubating for 30 min at 50 °C in a water bath.

After the incubation period, the hydrogels were removed and the samples allowed to cool to room temperature before measuring the chloride concentration. The enzyme was found to have a $k_{cat}$ of 17.9 ± 2.6 × $10^{-5}$ $s^{-1}$ and a $K_m$ of 0.41 ± 0.01 mM. The enzymatic efficiency was 4.39 ± 0.65 × $10^{-4}$ $mM^{-1}$ $s^{-1}$, representing a >7 fold increase in functionality as compared to the system at room temperature, which was expected as L-2-$HAD_{ST}$ is a thermophilic enzyme with optimal reactivity observed at higher temperatures. Additionally, the $K_m$ also decreased at 50 °C compared to the hydrogel at room temperature. This demonstrates that the enzyme is still able to more favorably bind the substrate for enzymatic activity at the higher temperature when encapsulated in the hydrogel.

Finally, the experiments were repeated as above by incubating the hydrogels for 30 min in a water bath at 70 °C, the optimum temperature for enzymatic activity. The $k_{cat}$ was determined to be 27.6 ± 0.6 × $10^{-5}$ $s^{-1}$, the $K_m$ was 0.52 ± 0.15 mM, while the enzymatic efficiency was 5.33 ± 1.54 × $10^{-4}$ $mM^{-1}$ $s^{-1}$. The efficiency increased by almost 1.5 times when the hydrogel encapsulated enzyme was heated at 70 °C as compared to 50 °C and by ~15 fold as compared to the enzyme at room temperature. This remarkable increase in activity as a function of temperature is based upon the thermophilic nature of the system. To that end, higher temperatures are required for maximal activity. The $K_m$ value did not vary significantly for the enzyme at 70 °C as compared to 50 °C. Previously published studies also suggest that the $K_m$ values at these temperatures are comparable.[32,36] Unfortunately, global heating of the system, which includes the hydrogel

and surrounding environment, is highly energy inefficient and can result in unwanted side effects. This is especially true when applying the materials for selective functionality in a complex matrix.

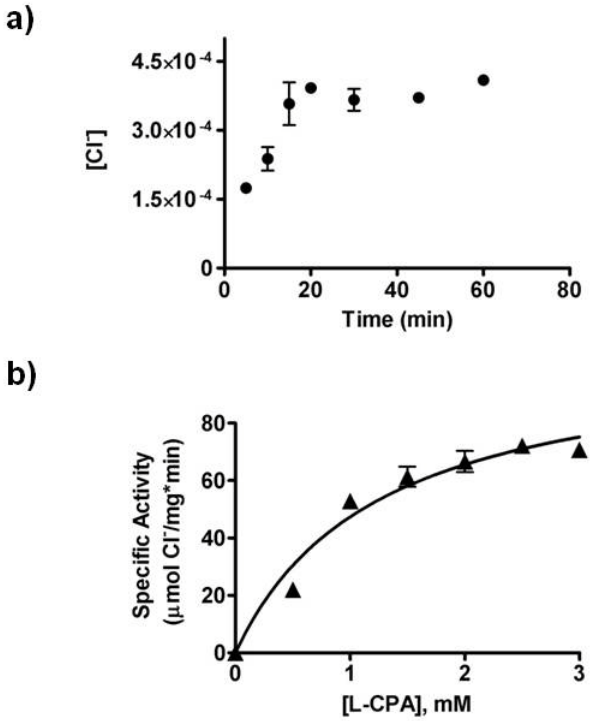


**Figure 5.3**. Enzymatic activity of free L-2-$HAD_{ST}$. a) The protein was incubated at 70 °C with 2 mM CPA for various periods of time. Data are blank subtracted and shown as averages ± one standard deviation (n=3). The optimal incubation time chosen was 10 min. b) To test the activity of the free protein, 0.003 mg L-2-$HAD_{ST}$ was incubated at 70 °C in the presence of various concentrations of CPA for 10 minutes. Data are blank subtracted and shown as averages ± one standard deviation (n=3).

Studies were also carried out to characterize the free enzyme in order to compare its activity to that of the enzyme immobilized in the hydrogel network. A time study was performed using 2.0 mM of CPA (Figure 5.3a), which demonstrated an optimal incubation time at 70 °C of 10 min. Next, L-2-$HAD_{ST}$ was incubated with various concentrations of substrate in 20 mM glycine buffer, pH 9.5 for 10 min and its activity

was measured by determining the concentration of chloride with an ISE. Characterization of the Michaelis-Menten kinetics (Figure 5.3b) found a $k_{cat}$ of 213.4 ± 8.7 × $10^{-5}$ $s^{-1}$, $K_m$ of 1.25 ± 0.16 mM, and an enzymatic efficiency ($k_{cat}/K_m$) of 17.02 ± 2.28 × $10^{-4}$ $mM^{-1}$ $s^{-1}$. The activity of the free enzyme in the water bath at 70 °C was compared to the hydrogel-encapsulated enzyme at varying temperatures are summarized in Table 5.1. From this study, it was determined that the enzymatic efficiency of the immobilized enzyme was about 30% of the efficiency of the free enzyme at the same temperature; however, activity was maintained even after protein modification and hydrogel encapsulation. A decrease in enzymatic efficiency was seen previously when the enzyme was immobilized on a sepharose resin (282). The decreased enzymatic efficiency observed in our study is likely due to the immobilization of the enzyme in the hydrogel network and the diffusion limitation of the substrate into the hydrogel (283-284). By conjugating the enzyme to the hydrogel through non-specific lysines, some protein may become denaturated, or the enzymatic pocket may become inaccessible to the substrate as a result of immobilization. Even so, the enzymatic efficiency increased with increasing the temperature from room temperature to the optimum temperature for activity (70 °C) within the hydrogel. This suggests that although there may be enzyme molecules where the binding pocket is inaccessible to the substrate, there is a significant fraction of immobilized enzyme that maintains function.

Once the above parameters were established, we hypothesized that the hydrogel with encapsulated $Fe_3O_4$ nanoparticles could be heated remotely *via* an AMF, thus increasing the activity of the incorporated enzyme. Successful remote heating would allow for use of the materials in self-contained remote sites, making them ideal for

environmental field applications. Initially, studies were performed with the hydrogel-encapsulated enzyme containing $Fe_3O_4$ nanoparticles to ensure that it could be remotely heated to 70 °C, which is required for optimum L-$HAD_{ST}$ activity. The hydrogels were exposed to a magnetic field amplitude of 19.9 kA/m for 15 min on an induction power supply equipped with a solenoid (1.5 cm diameter, 5 turns). Using this approach, the temperature of the hydrogel was measured every 30 s with an infrared thermal imaging camera. Approximately 2.5 min into the exposure, the hydrogel heated to 70 °C and maintained that temperature for at least 15 min (Figure 5.4a). The images taken using the IR camera demonstrate that when the hydrogel was not in the presence of the AMF (time=0), there is no heating. After exposure to the AMF after 60 seconds, the hydrogel begins to heat up and continues to do so until about 150 seconds. At this time, the hydrogel is at the maximum temperature for that field amplitude and it maintains that temperature until the field is removed (Figure 5.4b). Although this study was important to demonstrate that the temperate could be controlled in a narrow range by heating with the AMF, the temperatures were measured with an IR camera and not in solution. Due to the need for the hydrogel-air interface, the parameters used in this study may not directly correlate to the system when immersed in buffer. Therefore, further optimization for the hydrogel heating had to be conducted for the hydrogel in solution. This was assessed by using 0.5 mM substrate and measuring L-2-$HAD_{ST}$ activity after a 10 min exposure time to various magnetic field amplitudes (14.2, 21.7, 26.2, and 30.6 kA/m). As a control, the hydrogels were incubated with 0.5 mM substrate for 10 min at room temperature in the

**Table 5.1.** Summary of kinetic data for L-2-$HAD_{ST}$ under various conditions. Data are shown as averages ± one standard deviation (n=3).

| | FP, 70 °C* | HE, 21 °C | HE, 50 °C* | HE, 70 °C* | HE, AMF |
|---|---|---|---|---|---|
| $k_{cat}$ ($\times 10^{-5}$ $s^{-1}$) | 213.4 ± 8.7 | 4.02 ± 0.18 | 17.9 ± 2.6 | 27.6 ± 0.6 | 31.3 ± 8.1 |
| $K_m$ (mM) | 1.25 ± 0.16 | 1.03 ± 0.27 | 0.41 ± 0.01 | 0.52 ± 0.15 | 0.30 ± 0.07 |
| $k_{cat}/K_m$ ($\times 10^{-4}$ $mM^{-1}s^{-1}$) | 17.02 ± 2.28 | 0.39 ± 0.10 | 4.39 ± 0.65 | 5.33 ± 1.54 | 10.11 ± 3.52 |

*incubation in a water bath at the specified temperature
FP- Free protein, HE- hydrogel-encapsulated protein

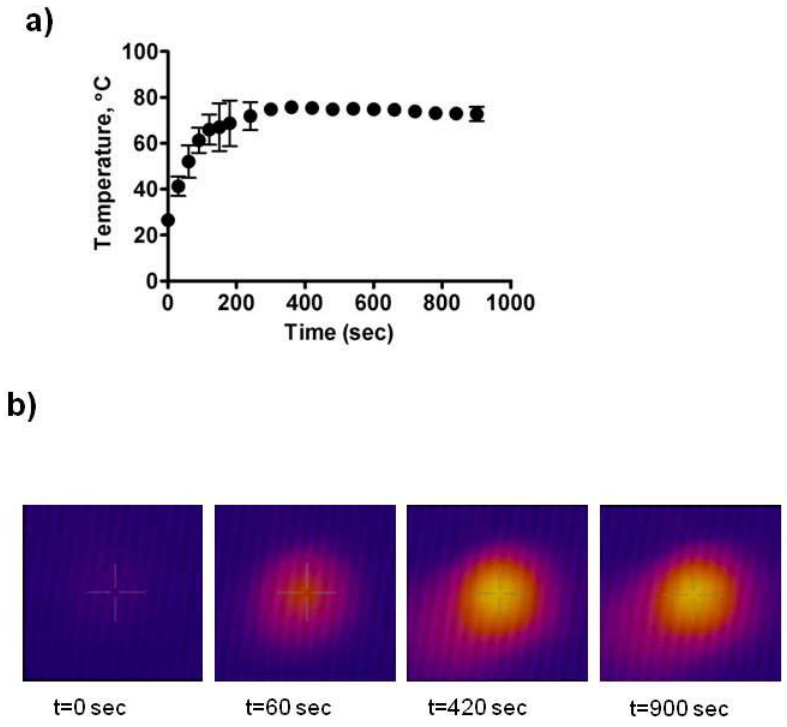


**Figure 5.4.** Demonstration of heating capabilities of the nanocomposite hydrogels when exposed to the AMF. They hydrogels were exposed to a magnetic field amplitude of 19.9 kA/m for 15 min on an induction power supply equipped with a solenoid (1.5 cm diameter, 5 turns) a) and the temperature was plotted at each time point, and (b) A picture was taken with an IR camera every 30 sec. The IR images of four time points (0 sec, 60 sec, 420, and 900 sec) are shown.

absence of the AMF. The control chloride concentration was then subtracted from the values found in the samples exposed to the field to ensure that the enzyme activity was due to the field and not to other environmental factors. As expected, as the field amplitude increased, the activity of the enzyme increased; however, as the amplitude passed 26.2 kA/m, the activity decreased (Figure 5.5a). This is consistent with previous data where the activity of free L-$HAD_{ST}$ decreased after the temperature increased over 70 °C, possibly due to protein denaturation (278). Although this study does not allow for direct correlation of field amplitude to temperature, it demonstrated that the activity of the enzyme followed a similar trend in the presence of the AMF as it did when heated in the water bath. Therefore, it was determined that the optimum activity was obtained at a field amplitude of 26.2 kA/m, which was used for all subsequent activity experiments. Characterization of the remotely heated hydrogels was performed by determining enzymatic activity after a 10 min incubation time at 26.2 kA/m in the presence of various substrate concentrations (Figure 6.5b). From this study, the enzyme was determined to have a $k_{cat}$ of 31.3 ± 8.1 × $10^{-5}$ $s^{-1}$ and a $K_m$ of 0.30 ± 0.07 mM. The catalytic efficiency of L-2-$HAD_{ST}$ was found to be 10.11 ± 3.52 × $10^{-4}$ $mM^{-1}$ $s^{-1}$ (Table 5.1). The $k_{cat}$ increased when the hydrogel was heated with an AMF and the $K_m$ decreased. This suggests that the affinity of the substrate to the enzyme increased when heated with the AMF, which indicates the remote heating is a more efficient heating method for optimal activity as compared to external approaches. Furthermore, the increase in $k_{cat}$ demonstrates that the product turnover is higher when heated in the AMF as compared to the water bath.

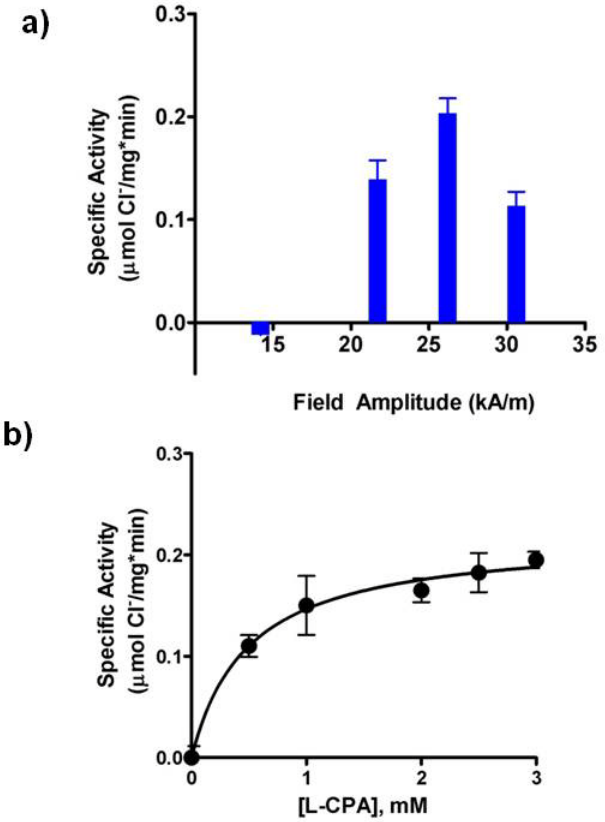


**Figure 5.5.** Investigating the AFM power setting for the activation of L-2-HAD$_{ST}$. a) To find an optimal power setting on the alternating magnetic field, the hydrogels were incubated in the specified field strength for 10 minutes in the presence of 0.5 mM CPA. The optimum field amplitude was determined to be 26.2 kA/m. b) The hydrogels were then placed at this field strength in the presence of various substrate concentrations. After 10 min incubation, the chloride concentrations were measured to calculate the specific activity of the enzyme. Data are blank subtracted and shown as averages ± one standard deviation (n=3).

This is interesting because the time of exposure, and thus the heating, in the AMF (10 min) is three times less than in the water bath (30 min), which indicates that the enzyme reaches and maintains the optimal temperature more rapidly in the AMF. Interestingly, compared to the free protein, the $k_{cat}$ of the immobilized enzyme does decrease. Such results were previously observed when the enzyme was immobilized *via* the lysine

residues on sepharose beads. The *kcat* of the free enzyme is roughly 10 times greater than the encapsulated materials, which, as discussed previously, likely arises from the diffusion limitation of the substrate through the porous hydrogel and the modification of the enzyme for hydrogel encapsulation. It is important to note, however, that the purpose of this study was not to compare the activity of the free and hydrogel-encapsulated protein, but to evaluate the efficiency of remotely controlling the heating of the enzyme in a system that is easily recoverable. Therefore, the more significant value in this work is the comparison of the $k_{cat}$ of the hydrogel-encapsulated enzyme heated in the water bath *versus* heated in the AMF.

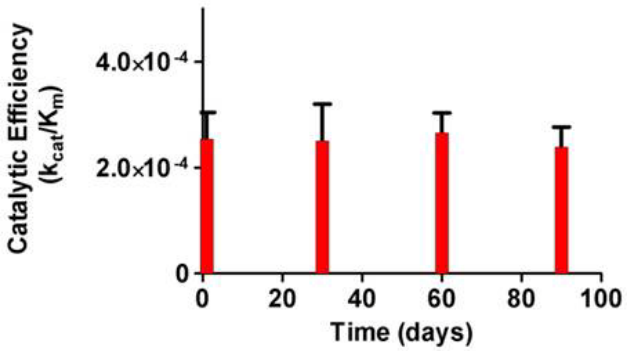


**Figure 5.6.** Demonstration of long-term stability of hydrogel encapsulated enzyme over a three month period. Each month, the hydrogels were incubated with varying substrate concentrations and heated *via* a water bath at 70 °C. Data are shown as averages ± one standard deviation (n=3).

To study the long-term stability of the enzyme-encapsulated hydrogel, the same nanocomposite systems were used over a three month period. The specific activity was calculated and plotted every month for three months. Enzymatic activity was maintained even after storage at 4 °C in glycine buffer for the three month period (Figure 5.6). As evident, no decrease in activity was observed over this time period indicating potential long-term stability.

Based on our results, numerous enhancements over conventional enzymatic applications can be achieved using the nanocomposite system. First, the data show that the catalytic efficiency increased two-fold when the hydrogels were heated *via* the AMF instead of the water bath at 70 °C. Furthermore, the sample incubation time for the AMF system required heating for only 10 min, as compared to 30 min required by the water bath. The system not only has efficient localized heating, but also requires less time to achieve higher catalytic output as compared to the hydrogel in the water bath. This is because the AMF exposure generates highly localized heating at the reaction location in the system. Due to the encapsulated $Fe_3O_4$ nanoparticles, the system reaches higher internal temperatures more rapidly than when using traditional heating methods. Unfortunately, the internal temperature of the hydrogel could not be determined, but this could be predicted through modeling/simulations[33] or determined after the development of an appropriate measurement technique. Second, based upon the design of the composite system, recyclability of the functional materials can be readily achieved. By having magnetic materials encapsulated in the hydrogel, magnetic separation can be applied to extract the functional materials from complex mixtures. This is important for the long-term recyclability, while minimizing the need to produce excessive amounts of enzyme. To that end, multiple sets of the composite material were functional for at least a 3 month period.

**5.4 Conclusions**

In conclusion, the formation of a novel composite system for remote controlled enzymatic activity has been demonstrated. This system consists of a hydrogel, a thermophilic enzyme, and magnetic nanoparticles for remote heating in the presence of

an AMF. The activity of the system was enhanced *via* AMF-based heating as compared to conventional heating methods due to the composite nature of the materials. Such materials can be readily dispersed in environmental systems for facile, remote contaminant degradation that is difficult to achieve using current technologies. It is envisioned that our approach can be applied to the creation of other materials that incorporate biological or synthetic elements that can be activated *via* an "on/off" switch and used in a variety of industrial, environmental and medical applications.

## Chapter 6. Conclusions and Future Perspectives

Nature has endowed us with cellular and molecular entities that can act as tools to perform biological recognition and actuation events by binding to analytes with high specificity, performing difficult reactions with ease via enzymes, and being adaptable to various environmental insults such as extreme temperatures and pH. With current advancements in technology, these proteins and cells can be exploited for a plethora of environmental and biomedical applications. Further, they can be genetically and chemically modified to further expand their use in bionanotechnology. The goals of this dissertation were to exploit the exquisite molecular recognition and actuation properties of biological systems by designing biosensing and bioremediation systems for a host of biomedical and environmental applications.

Chapter two demonstrates the utility of whole-cell biosensors to explore interkingdom communication between a mammalian host and its microbiome. It is well established that the microbiome plays a key yet still mostly unknown role in human physiological functions. Previous work has demonstrated that mammalian signaling molecules, such as epinephrine and norepinephrine, can interfere with bacterial quorum sensing, and thus play a role in bacterial communication (152). In this chapter, we focused on investigating whether a key mammalian neurotransmitter, namely serotonin, play a role in the mammalian host-microbiome interactions. Specifically, we investigated the potential Janus behavior of serotonin to act both as a mammalian neurotransmitter and as a quorum sensing molecule for the opportunistic pathogen *P. aeruginosa*, thus potentially crossing the mammalian and bacterial Kingdoms, and being identified as an interkingdom communication molecule. Using both an *E. coli* whole-cell biosensor based

on the regulatory protein LasR from the *P. aeruginosa* quorum sensing network and *P. aerugniosa* cells lacking the synthase for quorum sensing molecules, we were able to demonstrate that serotonin is able to act as a quorum sensing molecule on the *las* quorum sensing pathway. This is the first demonstration that serotonin not only acts as a mammalian neurotransmitter, but also plays a role in bacterial signaling. Although our work demonstrates serotonin's ability to interfere with quorum sensing *in vitro*, more studies need to be performed *in vivo* to fully understand the implications of this finding. A mammalian model has been developed by our lab to assess the presence of serotonin on *P. aeruginosa* infections. Further, serotonin agonists and antagonists, which have been employed for the treatment of diseases such as IBS (285), will be administered to determine what effect, if any, these have on the progression of infection. This can be monitored by determining cytokine expression daily and performing histology studies in the infected animals. A challenge related to understanding the mechanism by which serotonin interacts with LasR is the difficulty in purifying functional LasR. This may be overcome by employing two different strategies. First, the quorum sensing regulatory protein, QscR, which binds to the same ligand as LasR and has been isolated (286), can be used to perform binding studies with potential QSMs. This may give insight into the interaction of serotonin with the quorum sensing proteins of the bacterial communications circuitry. Second, the structure of LasR can be truncated and used in an analogous manner as that of the above-mentioned whole-cell sensing system. By truncating LasR, portions of the amino acid sequence can be selectively removed, i.e., the cognate ligand binding site, and determine if the addition of serotonin still activates the sensor. This truncation method has been successfully demonstrated previously with LuxR

to elucidate which termini is responsible for autoinducer binding (287), thus, it seems only natural that it could also be employed in interkingdom communication studies that could aid in unraveling the role of serotonin as a part of the bacterial signaling circuit.

Chapter three describes the evolution of a whole-cell biosensing system. In this chapter, a model whole-cell based sensing system based on the ArsR regulatory protein is employed to demonstrate the versatility of whole-cell biosensing systems. Initially, the whole-cell biosensor was designed for the detection of arsenic both in solution and in environmental samples. The biosensor was then employed to detect organoarsenicals, a class of arsenical compounds known to be highly toxic and widely used in warfare. After demonstrating the feasibility of employing our biosensing systems in conventional platforms, i.e., test tubes, microtiter and CD microfluidic platforms, we developed a paper-based biosensing platform. The design of this paper platform involves using a computer program for precise design, such as the Computer Aided Design, CAD, of the needed fluidics for sensing. Once the design is ready, a wax printer is employed to print the design and obtain the desired paper microfluidic platform. We also explored the preservation of our cell-based biosensing system for long-term storage and transport of our biosensors. For that, the sensing cells were sporulated, deposited in the paper platform and kept until needed. When sensing was needed, the cells were germinated and employed for sensing of the target molecule, thus demonstrating a method for the preservation of the whole-cell biosensor. Moreover, this method of spore preservation immobilized on paper strips is not only a demonstration of a long-term storage of a biosensor, but also of an easy to transport portable platform. In an effort to demonstrate the ability of our whole-cell sensing systems as living detection systems, we explored the

possibility of employing nematodes as the sensing vehicles. The advantage of using entire organisms, such as nematodes, over whole cell bacterial sensing systems is their mobility once they are deployed in the detection area. The nematode that we chose to employ in our system is *C*. *elegans*. We constructed our living nematode biosensing systems by allowing a strain of genetically engineered *C*. *elegans* which have GFP fused to the Arsenite-inducible RNA-associated protein, which causes the worm to fluoresce in the presence of arsenic *elegans* to consume the whole-cell biosensor and then place the worms in a solution containing arsenic. The response of these living worm biosnesors may find applications that micro-and nano-scale whole-cell and protein-based sensors cannot reach. The many demonstrated uses of whole-cell biosensors inspired chapter four where we focus on an in-depth look at the design, preparation, and enablement of spore based paper strip testing devices. Although this technology was introduced in chapter three as a feasibility concept, it was not fully optimized. In chapter four, we fabricated paper strips using the wax-based printing method in conjuction with depositing bacterial spores harboring plasmid pMUTin-23. A series of conditions for the use of spores in storage as well as living biosensors were explored. For example, we were able to enhance germination time significantly and reduce assay time by 75% while maintaining the same detection limits by identifying key nutrients and optimal conditions for germination of the dormant spore biosensors. With the advances in molecular biology and directed evolution, whole-cell biosensors can be tailored for altered specificity, enhance signal detection, or create novel sensing systems (288). Additionally, due to the innate selectivity of whole-cell biosensors, multiple whole-cell biosensing systems which can each detect a different analyte of interest (i.e. arsenic, hydroxylated polychlorobiphenyls,

and zinc) can be immobilized on designer wax-printed platforms to develop multiplex assays. Further, if *B*. *subtilis* or other sporulating organisms are used, the sensor could be sporulated for long-term storage and germinated when needed for sensing. Other factors enhance germination time, such as high pressures and temperatures, and mechanisms to facilitate these factors could be implemented on devices used for sensing purposes (289). Other higher organisms, such as plants, can also be genetically manipulated or be in symbiosis with whole-cell sensing bacteria to sense their environment (290).

In chapter five, we demonstrate that the enzymatic function of a thermophilic enzyme can be activated and controlled remotely for sensing and bioremediation applications. This was achieved by conjugating the thermophilic enzyme L-2-halaoacid dehalogenase from the organism *Sulfolobus tokodaii* to a polymeric hydrogel network containing iron oxide nanoparticles that can be addressed and heated remotely. Specifically, the protein was immobilized and polymerized onto the hydrogel via chemical polymerization trough the acrylic acid functional groups of the acrylamide/bis-acrylamide hydrogel network that contained iron oxide nanoparticles. In the presence of an alternating magnetic field, the iron oxide nanoparticles are heated up, thus heating the thermophilic L-2-halaoacid dehalogenase enzyme. Our studies showed that the activity of the enzyme was directly dependent on the field strength of the alternating magnetic field. This was the first study to demonstrate the remote heating, and thus activation of activity, of an enzyme using an alternating magnetic field can be employed to perform a sensing and a biodegradation/bioremediation function. It should be noted that the biohybrid material prepared was functional upon storage for at least three months, making it amenable for field applications. Further, the enzyme immobilized in the biohybrid

material had a two-fold increase in specific activity as compared to the enzyme free in solution. Additionally, due to the ability of the iron oxide nanoparticles reach higher temperatures rapidly in the presence of an AMF, this efficiency was achieved in one-third of the time when the system was heated with an AMF as compared to conventional heating techniques. The iron oxide nanoparticles would also allow for facile magnetic separation of the biohybrid material from complex mixtures, which enhances the reusability of the system. Future directions in this work would include direct immobilization of the protein to the iron oxide nanoparticles, rather than the hydrogel network site specifically by modifying the protein amino acid sequence with natural or non-natural amino acids to facilitate the immobilization (291-292). The utility of the system in environmental samples from sites contaminated with polyhalogenated compounds also needs to be evaluated. Additionally, other thermophilic enzymes with environmental or biomedical relevance can be employed to develop novel materials which can be remotely turned on or off and have uses *in vivo*. By pairing an enzyme with a hydrogel which has its own temperature dependent properties (i.e., swelling or shrinking as a response to temperature), not only can one control the enzymatic activity, but also the accessibility of the substrate to the enzyme. Further, certain enzymes such as Taq polymerase can be incorporated into a hydrogel nanocomposite network to facilitate remotely controlled PCR and have a system in which the polymerase may be reusable (293). Other materials, such as gold nanorods and carbon nanotubes, which are heated using near infrared light can also be explored in conjunction with thermophilic proteins to develop nanocomposite materials for remote control of biological activity in a variety of biomedical and environmental applications.

## REFERENCES


1. Chang, J. C., Rosenthal, S. J. Single quantum dot imaging in living cells. Methods Mol Biol 991, 149-162, 2013.

2. Chang, J. C., Rosenthal, S. J. Quantum dot-based single-molecule microscopy for the study of protein dynamics. Methods Mol Biol 1026, 71-84, 2013.

3. Kovtun, O., Arzeta-Ferrer, X., Rosenthal, S. J. Quantum dot approaches for target-based drug screening and multiplexed active biosensing. Nanoscale 5, 12072-12081, 2013.

4. Gussin, H. A., Tomlinson, I. D., Cao, D., Qian, H., Rosenthal, S. J., Pepperberg, D. R. Quantum dot conjugates of GABA and muscimol: binding to alpha1beta2gamma2 and rho1 GABA(A) receptors. ACS Chem Neurosci 4, 435-443, 2013.

5. Talafova, K., Hrabarova, E., Chorvat, D., Nahalka, J. Bacterial inclusion bodies as potential synthetic devices for pathogen recognition and a therapeutic substance release. Microb Cell Fact 12, 16, 2013.

6. Wang, G. D., Han, J. X., Wang, S. L., Li, P. Expression and purification of recombinant human bone morphogenetic protein-7 in *Escherichia Coli*. Prep Biochem & Biotechnol 44, 16-25, 2014.

7. Shimomura, O., Johnson, F. H., Saiga, Y. Extraction, purification and properties of aequorin, a bioluminescent protein from the luminous hydromedusan, Aequorea. J Cell Comp Physiol 59, 223-239, 1962.

8. Chalfie, M., Tu, Y., Euskirchen, G., Ward, W. W., Prasher, D. C. Green fluorescent protein as a marker for gene expression. Science 263, 802-805, 1994.

9. Ormo, M., Cubitt, A. B., Kallio, K., Gross, L. A., Tsien, R. Y., Remington, S. J. Crystal structure of the *Aequorea victoria* green fluorescent protein. Science 273, 1392-1395, 1996.

10. Rajendran, M., Yapici, E., Miller, L. W. Lanthanide-based imaging of protein-protein interactions in live cells. Inorg Chem, 2013.

11. Vuojola, J., Syrjanpaa, M., Lamminmaki, U., Soukka, T. Genetically encoded protease substrate based on lanthanide-binding peptide for time-gated fluorescence detection. Anal Chem 85, 1367-1373, 2013.

12. Zacharias, D. A., Tsien, R. Y. Molecular biology and mutation of green fluorescent protein. Methods Biochem Anal 47, 83-120, 2006.

13. Biskup, C., Zimmer, T., Benndorf, K. FRET between cardiac Na+ channel subunits measured with a confocal microscope and a streak camera. Nat Biotechnol 22, 220-224, 2004.

14. He, L., Bradrick, T. D., Karpova, T. S., Wu, X., Fox, M. H., Fischer, R., McNally, J. G., Knutson, J. R., Grammer, A. C., Lipsky, P. E. Flow cytometric measurement of fluorescence (Forster) resonance energy transfer from cyan fluorescent protein to yellow fluorescent protein using single-laser excitation at 458 nm. Cytometry A 53, 39-54, 2003.

15. Lewis, J. C., Daunert, S. Dual detection of peptides in a fluorescence binding assay by employing genetically fused GFP and BFP mutants. Anal Chem 71, 4321-4327, 1999.

16. Karp, M., Oker-Blom, C. A streptavidin-luciferase fusion protein: comparisons and applications. Biomol Eng 16, 101-104, 1999.

17. Casey, J. L., Coley, A. M., Tilley, L. M., Foley, M. Green fluorescent antibodies: novel in vitro tools. Protein Eng 13, 445-452, 2000.

18. Goh, Y. Y., Frecer, V., Ho, B., Ding, J. L. Rational design of green fluorescent protein mutants as biosensor for bacterial endotoxin. Protein Eng 15, 493-502, 2002.

19. Goh, Y. Y., Ho, B., Ding, J. L. A novel fluorescent protein-based biosensor for gram-negative bacteria. Appl Environ Microbiol 68, 6343-6352, 2002.

20. Roda, A., Guardigli, M., Michelini, E., Mirasoli, M. Bioluminescence in analytical chemistry and in vivo imaging. Trac-Trends in Anall Chem 28, 307-322, 2009.

21. Sarter, S., Zakhia, N. Chemiluminescent and bioluminescent assays as innovative prospects for mycotoxin determination in food and feed. Luminescence 19, 345-351, 2004.

22. Rink, T. J. Receptor-mediated calcium entry. FEBS Lett 268, 381-385, 1990.

23. Menon, V., Ranganathn, A., Jorgensen, V. H., Sabio, M., Christoffersen, C. T., Uberti, M. A., Jones, K. A., Babu, P. S. Development of an aequorin luminescence calcium assay for high-throughput screening using a plate reader, the LumiLux. Assay Drug Dev Technol 6, 787-793, 2008.

24. Doleman, L., Davies, L., Rowe, L., Moschou, E. A., Deo, S., Daunert, S. Bioluminescence DNA hybridization assay for *Plasmodium falciparum* based on the photoprotein aequorin. Anal Chem 79, 4149-4153, 2007.

25. Wu, C., Kawasaki, K., Ogawa, Y., Yoshida, Y., Ohgiya, S., Ohmiya, Y. Preparation of biotinylated cypridina luciferase and its use in bioluminescent enzyme immunoassay. Anal Chem 79, 1634-1638, 2007.

26. Qu, X., Deo, S. K., Dikici, E., Ensor, M., Poon, M., Daunert, S. Bioluminescence immunoassay for angiotensin II using aequorin as a label. Anal Biochem 371, 154-161, 2007.

27. Shrestha, S., Salins, L. L., Mark Ensor, C., Daunert, S. Rationally designed fluorescently labeled sulfate-binding protein mutants: evaluation in the development of a sensing system for sulfate. Biotechnol Bioeng 78, 517-526, 2002.

28. Salins, L. L., Goldsmith, E. S., Ensor, C. M., Daunert, S. A fluorescence-based sensing system for the environmental monitoring of nickel using the nickel binding protein from Escherichia coli. Anal Bioanal Chem 372, 174-180, 2002.

29. Lundgren, J. S., Salins, L. L., Kaneva, I., Daunert, S. A dynamical investigation of acrylodan-labeled mutant phosphate binding protein. Anal Chem 71, 589-595, 1999.

30. Salins, L. L., Deo, S. K., Daunert, S. Phosphate binding protein as the biorecognition element in a biosensor for phosphate. Sens Actuators B Chem 97, 81-89, 2004.

31. Hirshberg, M., Henrick, K., Haire, L. L., Vasisht, N., Brune, M., Corrie, J. E., Webb, M. R. Crystal structure of phosphate binding protein labeled with a coumarin fluorophore, a probe for inorganic phosphate. Biochem 37, 10381-10385, 1998.

32. Salins, L. L., Ware, R. A., Ensor, C. M., Daunert, S. A novel reagentless sensing system for measuring glucose based on the galactose/glucose-binding protein. Anal Biochem 294, 19-26, 2001.

33. Douglass, P. M., Salins, L. L., Dikici, E., Daunert, S. Class-selective drug detection: fluorescently-labeled calmodulin as the biorecognition element for phenothiazines and tricyclic antidepressants. Bioconjug Chem 13, 1186-1192, 2002.

34. Dikici, E., Deo, S. K., Daunert, S. Drug detection based on the conformational changes of calmodulin and the fluorescence of its enhanced green fluorescent protein fusion partner. Anal Chim Acta 500, 237-245, 2003.

35. Baird, G. S., Zacharias, D. A., Tsien, R. Y. Circular permutation and receptor insertion within green fluorescent proteins. Proc Natl Acad Sci U S A 96, 11241-11246, 1999.

36. Teasley Hamorsky, K., Ensor, C. M., Wei, Y., Daunert, S. A bioluminescent molecular switch for glucose. Angew Chem Int Ed Engl 47, 3718-3721, 2008.

37. Hamorsky, K. T., Ensor, C. M., Pasini, P., Daunert, S. A protein switch sensing system for the quantification of sulfate. Anal Biochem 421, 172-180, 2012.

38. Scott, D., Hamorsky, K. T., Ensor, C. M., Anderson, K. W., Daunert, S. Cyclic AMP receptor protein-aequorin molecular switch for cyclic AMP. Bioconjug Chem 22, 475-481, 2011.

39. Elisseeff, J. Hydrogels: structure starts to gel. Nature Mat 7, 271-273, 2008.

40. Miyata, T., Asami, N., Uragami, T. A reversibly antigen-responsive hydrogel. Nature 399, 766-769, 1999.

41. Ehrick, J. D., Deo, S. K., Browning, T. W., Bachas, L. G., Madou, M. J., Daunert, S. Genetically engineered protein in hydrogels tailors stimuli-responsive characteristics. Nature Mat 4, 298-302, 2005.

42. Ehrick, J. D., Stokes, S., Bachas-Daunert, S., Moschou, E. A., Deo, S. K., Bachas, L. G., Daunert, S. Chemically tunable lensing of stimuli-responsive hydrogel microdomes. Adv Mat 19, 4024, 2007.

43. Ehrick, J. D., Luckett, M. R., Khatwani, S., Wei, Y., Deo, S. K., Bachas, L. G., Daunert, S. Glucose responsive hydrogel networks based on protein recognition. Macromol Biosci 9, 864-868, 2009.

44. Hassan, C. M., Doyle, F. J., Peppas, N. A. Dynamic behavior of glucose-responsive poly(methacrylic acid-g-ethylene glycol) hydrogels. Macromol 30, 6166-6173, 1997.

45. Miyata, T., Uragami, T., Nakamae, K. Biomolecule-sensitive hydrogels. Adv Drug Deliv Rev 54, 79-98, 2002.

46. Freudl, R., MacIntyre, S., Degen, M., Henning, U. Cell surface exposure of the outer membrane protein OmpA of *Escherichia coli* K-12. J Mol Biol 188, 491-494, 1986.

47. Charbit, A., Boulain, J. C., Ryter, A., Hofnung, M. Probing the topology of a bacterial membrane protein by genetic insertion of a foreign epitope; expression at the cell surface. EMBO J 5, 3029-3037, 1986.

48. Agterberg, M., Adriaanse, H., Tommassen, J. Use of outer membrane protein PhoE as a carrier for the transport of a foreign antigenic determinant to the cell surface of *Escherichia coli* K-12. Gene 59, 145-150, 1987.

49. Charbit, A., Molla, A., Saurin, W., Hofnung, M. Versatility of a vector for expressing foreign polypeptides at the surface of gram-negative bacteria. Gene 70, 181-189, 1988.

50. Isticato, R., Cangiano, G., Tran, H. T., Ciabattini, A., Medaglini, D., Oggioni, M. R., De Felice, M., Pozzi, G., Ricca, E. Surface display of recombinant proteins on *Bacillus subtilis* spores. J Bacteriol 183, 6294-6301, 2001.

51. Golden, A. L., Battrell, C. F., Pennell, S., Hoffman, A. S., J, J. L., Stayton, P. S. Simple fluidic system for purifying and concentrating diagnostic biomarkers using stimuli-responsive antibody conjugates and membranes. Bioconjug Chem, 2010.

52. Hu, M., He, Y., Song, S., Yan, J., Lu, H. T., Weng, L. X., Wang, L. H., Fan, C. DNA-bridged bioconjugation of fluorescent quantum dots for highly sensitive microfluidic protein chips. Chem Commun 46, 6126-6128, 2010.

53. Sai, N., Chen, Y., Liu, N., Yu, G., Su, P., Feng, Y., Zhou, Z., Liu, X., Zhou, H., Gao, Z., *et al.* A sensitive immunoassay based on direct hapten coated format and biotin-streptavidin system for the detection of chloramphenicol. Talanta 82, 1113-1121, 2010.

54. Kim, J. H., Lee, C. S., Kim, B. G. Spore-displayed streptavidin: a live diagnostic tool in biotechnology. Biochem Biophys Res Commun 331, 210-214, 2005.

55. Hinc, K., Ghandili, S., Karbalaee, G., Shali, A., Noghabi, K., Ricca, E., Ahmadian, G. Efficient binding of nickel ions to recombinant *Bacillus subtilis* spores. Res Microbiol, 2010.

56. McKenney, P. T., Driks, A., Eskandarian, H. A., Grabowski, P., Guberman, J., Wang, K. H., Gitai, Z., Eichenberger, P. A distance-weighted interaction map reveals a previously uncharacterized layer of the *Bacillus subtilis* spore coat. Curr Biol 20, 934-938, 2010.

57. Kwon, S. J., Jung, H. C., Pan, J. G. Transgalactosylation in a water-solvent biphasic reaction system with beta-galactosidase displayed on the surfaces of *Bacillus subtilis* spores. Appl Environ Microbiol 73, 2251-2256, 2007.

58. Zhu, G., Wang, P. Polymer-enzyme conjugates can self-assemble at oil/water interfaces and effect interfacial biotransformations. J Am Chem Soc 126, 11132-11133, 2004.

59. Duc le, H., Hong, H. A., Barbosa, T. M., Henriques, A. O., Cutting, S. M. Characterization of *Bacillus* probiotics available for human use. Appl Environ Microbiol 70, 2161-2171, 2004.

60. Hong, H. A., Duc le, H., Cutting, S. M. The use of bacterial spore formers as probiotics. FEMS Microbiol Rev 29, 813-835, 2005.

61. Potot, S., Serra, C. R., Henriques, A. O., Schyns, G. Display of recombinant proteins on *Bacillus subtilis* spores, using a coat-associated enzyme as the carrier. Appl Environ Microbiol 76, 5926-5933, 2010.

62. Costa, T., Steil, L., Martins, L. O., Volker, U., Henriques, A. O. Assembly of an oxalate decarboxylase produced under sigmaK control into the *Bacillus subtilis* spore coat. J Bacteriol 186, 1462-1474, 2004.

63. Kim, J. H., Roh, C., Lee, C. W., Kyung, D., Choi, S. K., Jung, H. C., Pan, J. G., Kim, B. G. Bacterial surface display of GFP(uv) on *Bacillus subtilis* spores. J Microbiol Biotechnol 17, 677-680, 2007.

64. Kim, H., Hahn, M., Grabowski, P., McPherson, D. C., Otte, M. M., Wang, R., Ferguson, C. C., Eichenberger, P., Driks, A. The *Bacillus subtilis* spore coat protein interaction network. Mol Microbiol 59, 487-502, 2006.

65. Isticato, R., Di Mase, D. S., Mauriello, E. M., De Felice, M., Ricca, E. Amino terminal fusion of heterologous proteins to CotC increases display efficiencies in the *Bacillus subtilis* spore system. Biotechniques 42, 151-152, 154, 156, 2007.

66. Isticato, R., Esposito, G., Zilhao, R., Nolasco, S., Cangiano, G., De Felice, M., Henriques, A. O., Ricca, E. Assembly of multiple CotC forms into the *Bacillus subtilis* spore coat. J Bacteriol 186, 1129-1135, 2004.

67. Thompson, B. M., Stewart, G. C. Targeting of the BclA and BclB proteins to the *Bacillus anthracis* spore surface. Mol Microbiol 70, 421-434, 2008.

68. Fernandez-Gacio, A., Uguen, M., Fastrez, J. Phage display as a tool for the directed evolution of enzymes. Trends Biotechnol 21, 408-414, 2003.

69. Gupta, N., Farinas, E. T. Directed evolution of CotA laccase for increased substrate specificity using *Bacillus subtilis* spores. Protein Eng Des Sel 23, 679-682, 2010.

70. Hullo, M. F., Moszer, I., Danchin, A., Martin-Verstraete, I. CotA of *Bacillus subtilis* is a copper-dependent laccase. J Bacteriol 183, 5426-5430, 2001.

71. Hinc, K., Isticato, R., Dembek, M., Karczewska, J., Iwanicki, A., Peszynska-Sularz, G., De Felice, M., Obuchowski, M., Ricca, E. Expression and display of UreA of *Helicobacter acinonychis* on the surface of *Bacillus subtilis* spores. Microb Cell Fact 9, 2, 2010.

72. Prieto-Samsonov, D. L., Vazquez-Padron, R. I., Ayra-Pardo, C., Gonzalez-Cabrera, J., de la Riva, G. A. *Bacillus thuringiensis*: from biodiversity to biotechnology. J Ind Microbiol Biotechnol 19, 202-219, 1997.

73. Du, C., Chan, W. C., McKeithan, T. W., Nickerson, K. W. Surface display of recombinant proteins on *Bacillus thuringiensis* spores. Appl Environ Microbiol 71, 3337-3341, 2005.

74. Park, T. J., Lee, K. B., Lee, S. J., Park, J. P., Lee, Z. W., Choi, S. K., Jung, H. C., Pan, J. G., Lee, S. Y., Choi, I. S. Micropatterns of spores displaying heterologous proteins. J Am Chem Soc 126, 10512-10513, 2004.

75. Lee, K. B., Jung, Y. H., Lee, Z. W., Kim, S., Choi, I. S. Biospecific anchoring and spatially confined germination of bacterial spores in non-biofouling microwells. Biomaterials 28, 5594-5600, 2007.

76. Daunert, S., Barrett, G., Feliciano, J. S., Shetty, R. S., Shrestha, S., Smith-Spencer, W. Genetically engineered whole-cell sensing systems: coupling biological recognition with reporter genes. Chem Rev 100, 2705-2738, 2000.

77. Liu, X. M., Germaine, K. J., Ryan, D., Dowling, D. N. Whole-cell fluorescent biosensors for bioavailability and biodegradation of polychlorinated biphenyls. Sensors 10, 1377-1398, 2010.

78. Yagi, K. Applications of whole-cell bacterial sensors in biotechnology and environmental science. Appl Microbiol Biotechnol 73, 1251-1258, 2007.

79. Struss, A. K., Pasini, P., Daunert, S., Biosensing systems based on genetically engineered whole cells. In "Recognition Receptors in Biosensors", Zourob, M., Ed. Springer New York, 565-598, 2010.

80. Kumari, A., Pasini, P., Deo, S. K., Flomenhoft, D., Shashidhar, H., Daunert, S. Biosensing systems for the detection of bacterial quorum signaling molecules. Anal Chem 78, 7603-7609, 2006.

81. Michelini, E., Guardigli, M., Magliulo, M., Mirasoli, M., Roda, A., Simoni, P., Baraldini, M. Bioluminescent biosensors based on genetically engineered living cells in environmental and food analysis. Anal Lett. 39, 1503-1515, 2006.

82. Gu, M. B., Mitchell, R. J., Kim, B. C. Whole-cell-based biosensors for environmental biomonitoring and application. Adv Biochem Eng Biotechnol 87, 269-305, 2004.

83. Machala, M., Blaha, L., Lehmler, H. J., Pliskova, M., Majkova, Z., Kapplova, P., Sovadinova, I., Vondracek, J., Malmberg, T., Robertson, L. W. Toxicity of hydroxylated and quinoid PCB metabolites: inhibition of gap junctional intercellular communication and activation of aryl hydrocarbon and estrogen receptors in hepatic and mammary cells. Chem Res Tox 17, 340-347, 2004.

84. McLean, M. R., Bauer, U., Amaro, A. R., Robertson, L. W. Identification of catechol and hydroquinone metabolites of 4-monochlorobiphenyl. Chem Res Tox 9, 158-164, 1996.

85. Turner, K., Xu, S., Pasini, P., Deo, S., Bachas, L., Daunert, S. Hydroxylated polychlorinated biphenyl detection based on a genetically engineered bioluminescent whole-cell sensing system. Anal Chem 79, 5740-5745, 2007.

86. Feliciano, J., Shifen, X., Xiyuan, G., Lehmler, H.-J., Bachas, L. G., Daunert, S. ClcR-based biosensing system in the detection of cis-dihydroxylated (chloro-)biphenyls. Anal Bioanal Chem 385, 807-813, 2006.

87. Stocker, J., Balluch, D., Gsell, M., Harms, H., Feliciano, J., Daunert, S., Malik, K. A., vanderMeer, J. R. Development of a set of simple bacterial biosensors for quantitative and rapid measurements of arsenite and arsenate in potable water. Environ Sci Technol 37, 4743-4750, 2003.

88. Chen, J., Sun, S., Li, C. Z., Zhu, Y. G., Rosen, B. P. Biosensor for organoarsenical herbicides and growth promoters. Environ Sci Technol, 2014.

89. Branco, R., Cristovao, A., Morais, P. V. Highly sensitive, highly specific whole-cell bioreporters for the detection of chromate in environmental samples. PLoS One 8, e54005, 2013.

90. Shing, W. L., Heng, L. Y., Surif, S. Performance of a cyanobacteria whole cell-based fluorescence biosensor for heavy metal and pesticide detection. Sensors 13, 6394-6404, 2013.

91. Dahl, A. L., Sanseverino, J., Gaillard, J. F. Bacterial bioreporter detects mercury in the presence of excess EDTA. Environ Chem 8, 552-560, 2011.

92. Pasco, N. F., Weld, R. J., Hay, J. M., Gooneratne, R. Development and applications of whole cell biosensors for ecotoxicity testing. Anal Bioanal Chem 400, 931-945, 2011.

93. Kumari, A., Pasini, P., Daunert, S. Detection of bacterial quorum sensing N-acyl homoserine lactones in clinical samples. Anal Bioanal Chem 391, 1619-1627, 2008.

94. Chambers, C. E., Visser, M. B., Schwab, U., Sokol, P. A. Identification of N-acylhomoserine lactones in mucopurulent respiratory secretions from cystic fibrosis patients. FEMS Microbiol Lett 244, 297-304, 2005.

95. Sartor, R. B. Therapeutic manipulation of the enteric microflora in inflammatory bowel diseases: antibiotics, probiotics, and prebiotics. Gastroenterol126, 1620-1633, 2004.

96. Raut, N., Pasini, P., Daunert, S. Deciphering bacterial universal language by detecting the quorum sensing signal, autoinducer-2, with a whole-cell sensing system. Anal Chem 85, 9604-9609, 2013.

97. Miller, M. B., Bassler, B. L. Quorum sensing in bacteria. Annu Rev Microbiol 55, 165-199, 2001.

98. Federle, M. J. Autoinducer-2-based chemical communication in bacteria: complexities of interspecies signaling. Contrib Microbiol 16, 18-32, 2009.

99. Bassler, B., Wright, M., Showalter, R., Silverman, M. Intercellular signalling in Vibrio harveyi: sequence and function of genes regulating expression of luminescence. Mol Microbiol 9, 773 - 786, 1993.

100. Kaufman, E., Lamster, I. B. The diagnostic applications of saliva- a review. Crit Rev Oral Biol Med 13, 197-212, 2002.

101. Hill, M. J., Drasar, B. S. The normal colonic bacterial flora. Gut 16, 318-323, 1975.

102. Campagna, S. R., Gooding, J. R., May, A. L. Direct quantitation of the quorum sensing signal, autoinducer-2, in clinically relevant samples by liquid chromatography-tandem mass spectrometry. Anal Chem 81, 6374-6381, 2009.

103. Manichanh, C., Rigottier-Gois, L., Bonnaud, E., Gloux, K., Pelletier, E., Frangeul, L., Nalin, R., Jarrin, C., Chardon, P., Marteau, P.*, et al.* Reduced diversity of faecal microbiota in Crohn's disease revealed by a metagenomic approach. Gut 55, 205-211, 2006.

104. Baumgart, M., Dogan, B., Rishniw, M., Weitzman, G., Bosworth, B., Yantiss, R., Orsi, R. H., Wiedmann, M., McDonough, P., Kim, S. G.*, et al.* Culture independent analysis of ileal mucosa reveals a selective increase in invasive Escherichia coli of novel phylogeny relative to depletion of Clostridiales in Crohn's disease involving the ileum. ISME J, 2007.

105. Daunert, S., Barrett, G., Feliciano, J. S., Shetty, R. S., Shrestha, S., Smith-Spencer, W. Genetically engineered whole-cell sensing systems: coupling biological recognition with reporter genes. Chem Rev 100, 2705-2738, 2000.

106. Feliciano, J., Pasini, P., Deo, S. K., Daunert, S. Photoproteins as reporters in whole-cell sensing. Wiley-VCH Verlag GmbH & Co. KGaA, Weinheim, Germany, p 131-154 2006

107. Yong, Y.-C., Zhong, J.-J. A genetically engineered whole-cell pigment-based bacterial biosensing system for quantification of N-butyryl homoserine lactone quorum sensing signal. Biosen Bioelect 25, 41-47, 2009.

108. Struss, A., Pasini, P., Ensor, C. M., Raut, N., Daunert, S. Paper strip whole cell biosensors: A portable test for the semiquantitative detection of bacterial quorum signaling molecules. Anal Chem 82, 4457-4463, 2010.

109. Yagi, K. Applications of whole-cell bacterial sensors in biotechnology and environmental science. ApplMicrobiol Biotechnol 73, 1251-1258, 2007.

110. Kumari, A., Pasini, P., Deo, S. K., Flomenhoft, D., Shashidhar, H., Daunert, S. Biosensing systems for the detection of bacterial quorum signaling molecules. Anal Chem 78, 7603-7609, 2006.

111. Seksik, P., Sokol, H., Lepage, P., Vasquez, N., Manichanh, C., Mangin, I., Pochart, P., Dore, J., Marteau, P. Review article: the role of bacteria in onset and perpetuation of inflammatory bowel disease. Aliment Pharmacol Therap24, 11-18, 2006.

112. Khan, K. J., Ullman, T. A., Ford, A. C., Abreu, M. T., Abadir, A., Marshall, J. K., Talley, N. J., Moayyedi, P. Antibiotic therapy in inflammatory bowel disease: a systematic review and meta-analysis. Am J Gastroenterol 106, 661-673, 2011.

113. Gillis, R. J., Iglewski, B. H. Azithromycin retards *Pseudomonas aeruginosa* biofilm formation. J Clin Microbiol 42, 5842-5845, 2004.

114. Nalca, Y., Jansch, L., Bredenbruch, F., Geffers, R., Buer, J., Haussler, S. Quorum-sensing antagonistic activities of azithromycin in *Pseudomonas aeruginosa* PAO1: a global approach. Antimicrob Agents Chemother 50, 1680-1688, 2006.

115. Struss, A. K., Pasini, P., Flomenhoft, D., Shashidhar, H., Daunert, S. Investigating the effect of antibiotics on quorum sensing with whole-cell biosensing systems. Anal Bioanal Chem 402, 3227-3236, 2012.

116. Winson, M. K., Swift, S., Fish, L., Throup, J. P., Jorgensen, F., Chhabra, S. R., Bycroft, B. W., Williams, P., Stewart, G. S. Construction and analysis of luxCDABE-based plasmid sensors for investigating N-acyl homoserine lactone-mediated quorum sensing. FEMS Microbiol Lett 163, 185-192, 1998.

117. Bala, A., Kumar, R., Harjai, K. Inhibition of quorum sensing in *Pseudomonas aeruginosa* by azithromycin and its effectiveness in urinary tract infections. J Med Microbiol 60, 300-306, 2011.

118. Skindersoe, M. E., Alhede, M., Phipps, R., Yang, L., Jensen, P. O., Rasmussen, T. B., Bjarnsholt, T., Tolker-Nielsen, T., Hoiby, N., Givskov, M. Effects of antibiotics on quorum sensing in *Pseudomonas aeruginosa*. Antimicrob Agents Chemother 52, 3648-3663, 2008.

119. Kai, T., Tateda, K., Kimura, S., Ishii, Y., Ito, H., Yoshida, H., Kimura, T., Yamaguchi, K. A low concentration of azithromycin inhibits the mRNA expression of N-acyl homoserine lactone synthesis enzymes, upstream of lasI or rhlI, in *Pseudomonas aeruginosa*. PulmonPharmacol Therap 22, 483-486, 2009.

120. Bottomley, M. J., Muraglia, E., Bazzo, R., Carfi, A. Molecular insights into quorum sensing in the human pathogen *Pseudomonas aeruginosa* from the structure of the virulence regulator LasR bound to its autoinducer. J Biol Chem 282, 13592-13600, 2007.

121. Bozoglu, F., Ozilgen, M., Bakir, U. Survival kinetics of lactic-acid starter cultures during and after freeze-drying. Enz Microbial Technol 9, 531-537, 1987.

122. Premkumar, J. R., Lev, O., Rosen, R., Belkin, S. Encapsulation of luminous recombinant *E-coli* in sol-gel silicate films. Adv Mat 13, 1773-1775, 2001.

123. Premkumar, J. R., Rosen, R., Belkin, S., Lev, O. Sol-gel luminescence biosensors: Encapsulation of recombinant *E-coli* reporters in thick silicate films. Anal Chimica Acta 462, 11-23, 2002.

124. Tessema, D. A., Rosen, R., Pedazur, R., Belkin, S., Gun, J., Ekeltchik, I., Lev, O. Freeze-drying of sol-gel encapsulated recombinant bioluminescent *E. coli* by using lyo-protectants. Sens Act B-Chem 113, 768-773, 2006.

125. Busto, M. D., Meza, V., Ortega, N., Perez-Mateos, M. Immobilization of naringinase from *Aspergillus niger* CECT 2088 in poly(vinyl alcohol) cryogels for the debittering of juices. Food Chem 104, 1177-1182, 2007.

126. Lopez-Fouz, M., Pilar-Izquierdo, M. C., Martinez-Mayo, I., Ortega, N., Perez-Mateos, M., Busto, M. D. Immobilization of *Rhodococcus fascians* cells in poly(vinyl alcohol) cryogels for the debittering of citrus juices. J Biotechnol 131, S104-S104, 2007.

127. Lindsay, A., Ahmer, B. M. M. Effect of sdiA on biosensors of N-acylhomoserine lactones. J Bacteriol 187, 5054-5058, 2005.

128. Kim, C., Kim, J., Park, H. Y., Park, H. J., Lee, J. H., Kim, C. K., Yoon, J. Furanone derivatives as quorum-sensing antagonists of *Pseudomonas aeruginosa*. Appl Microbiol Biotechnol 80, 37-47, 2008.

129. Zhou, L., Zheng, H., Tang, Y., Yu, W., Gong, Q. Eugenol inhibits quorum sensing at sub-inhibitory concentrations. Biotechnol Lett 35, 631-637, 2013.

130. Dong, Y. H., Zhang, X. F., Soo, H. M., Greenberg, E. P., Zhang, L. H. The two-component response regulator PprB modulates quorum-sensing signal production and global gene expression in *Pseudomonas aeruginosa*. Mol Microbiol 56, 1287-1301, 2005.

131. Andersen, J. B., Heydorn, A., Hentzer, M., Eberl, L., Geisenberger, O., Christensen, B. B., Molin, S., Givskov, M. gfp-Based N-acyl homoserine-lactone sensor systems for detection of bacterial communication. Appl Environ Microbiol 67, 575-585, 2001.

132. Farrand, S., Qin, Y., Oger, P. Quorum-sensing system of Agrobacterium plasmids: analysis and utility. Methods Enzymol 358, 452 - 484, 2002.

133. Zhu, J., Beaber, J. W., More, M. I., Fuqua, C., Eberhard, A., Winans, S. C. Analogs of the autoinducer 3-oxooctanoyl-homoserine lactone strongly inhibit activity of the TraR protein of *Agrobacterium tumefaciens*. J Bacteriol 180, 5398-5405, 1998.

134. Date, A., Pasini, P., Daunert, S. Fluorescent and bioluminescent cell-based sensors: Strategies for their preservation in Whole Cell Sensing Systems I: Reporter Cells and Devices 117, 57-75, 2010.

135. Date, A., Pasini, P., Sangal, A., Daunert, S. Packaging sensing cells in spores for long-term preservation of sensors: a tool for biomedical and environmental analysis. Anal Chem 82, 6098-6103, 2010.

136. Desnous, C., Guillaume, D., Clivio, P. Spore photoproduct: a key to bacterial eternal life. Chem Rev 110, 1213-1232, 2010.

137. Cano, R. J., Borucki, M. K. Revival and identification of bacterial spores in 25- to 40-million-year-old Dominican amber. Science 268, 1060-1064, 1995.

138. Setlow, P., Waites, W. M. Identification of several unique, low-molecular-weight basic proteins in dormant spores of clastridium bifermentans and their degradation during spore germination. J Bacteriol 127, 1015-1017, 1976.

139. Ghosh, S., Zhang, P., Li, Y. Q., Setlow, P. Superdormant spores of *Bacillus* species have elevated wet-heat resistance and temperature requirements for heat activation. J Bacteriol 191, 5584-5591, 2009.

140. Sonenshein, A. L. Bacteriophages: how bacterial spores capture and protect phage DNA. Curr Biol 16, R14-16, 2006.

141. Setlow, P. Spores of *Bacillus subtilis*: their resistance to and killing by radiation, heat and chemicals. J Appl Microbiol 101, 514-525, 2006.

142. Ball, D. A., Taylor, R., Todd, S. J., Redmond, C., Couture-Tosi, E., Sylvestre, P., Moir, A., Bullough, P. A. Structure of the exosporium and sublayers of spores of the *Bacillus cereus* family revealed by electron crystallography. Mol Microbiol 68, 947-958, 2008.

143. Knecht, L. D., Pasini, P., Daunert, S. Bacterial spores as platforms for bioanalytical and biomedical applications. Anal Bioanal Chem 400, 977-989, 2011.

144. Hudson, K. D., Corfe, B. M., Kemp, E. H., Feavers, I. M., Coote, P. J., Moir, A. Localization of GerAA and GerAC germination proteins in the *Bacillus subtilis* spore. J Bacteriol 183, 4317-4322, 2001.

145. Date, A., Pasini, P., Daunert, S. Construction of spores for portable bacterial whole-cell biosensing systems. Anal Chem 79, 9391-9397, 2007.

146. Date, A., Pasini, P., Sangal, A., Daunert, S. Packaging sensing cells in spores for long-term preservation of sensors: a tool for biomedical and environmental analysis. Anal. Chem. 82, 6098-6103, 2010.

147. Fantino, J. R., Barras, F., Denizot, F. Sposensor: a whole-bacterial biosensor that uses immobilized *Bacillus subtilis* spores and a one-step incubation/detection process. J Mol Microbiol Biotechnol 17, 90-95, 2009.

148. Date, A., Pasini, P., Daunert, S. Integration of spore-based genetically engineered whole-cell sensing systems into portable centrifugal microfluidic platforms. Anal Bioanal Chem 398, 349-356, 2010.

149. Sangal, A., Pasini, P., Daunert, S. Stability of spore-based biosensing systems under extreme conditions. Sens Actuators, B 158, 377-382, 2011.

150. Kaper, J. B., Sperandio, V. Bacterial cell-to-cell signaling in the gastrointestinal tract. Infect Immun 73, 3197-3209, 2005.

151. Alverdy, J., Holbrook, C., Rocha, F., Seiden, L., Wu, R. L., Musch, M., Chang, E., Ohman, D., Suh, S. Gut-derived sepsis occurs when the right pathogen with the right virulence genes meets the right host: evidence for in vivo virulence expression in *Pseudomonas aeruginosa*. Annals of Surgery 232, 480-489, 2000.

152. Sperandio, V., Torres, A. G., Jarvis, B., Nataro, J. P., Kaper, J. B. Bacteria-host communication: The language of hormones. Proc Natl Acad Sci USA 100, 8951-8956, 2003.

153. Jarvis, K. G., Giron, J. A., Jerse, A. E., McDaniel, T. K., Donnenberg, M. S., Kaper, J. B. Enteropathogenic *Escherichia coli* contains a putative type III secretion system necessary for the export of proteins involved in attaching and effacing lesion formation. PNAS 92, 7996-8000, 1995.

154. Gershon, M. D., Tack, J. The serotonin signaling system: from basic understanding to drug development for functional GI disorders. Gastroenterol 132, 397-414, 2007.

155. Shahkolahi, A. M., Donahue, M. J. Bacterial flora, a possible source of serotonin in the intestine of adult female *Ascaris suum*. J Parasitol 79, 17-22, 1993.

156. Clarke, G., Grenham, S., Scully, P., Fitzgerald, P., Moloney, R. D., Shanahan, F., Dinan, T. G., Cryan, J. F. The microbiome-gut-brain axis during early life regulates the hippocampal serotonergic system in a sex-dependent manner. Mol Psychiatry 18, 666-673, 2013.

157. Cryan, J. F., O'Mahony, S. M. The microbiome-gut-brain axis: from bowel to behavior. Neurogastroenterol Motil 23, 187-192, 2011.

158. Wikoff, W. R., Anfora, A. T., Liu, J., Schultz, P. G., Lesley, S. A., Peters, E. C., Siuzdak, G. Metabolomics analysis reveals large effects of gut microflora on mammalian blood metabolites. Proc Natl Acad Sci U S A 106, 3698-3703, 2009.

159. Lyte, M. Microbial endocrinology and infectious disease in the 21st century. Trends Microbiol 12, 14-20, 2004.

160. Oleskin, A. V., Kirovskaia, T. A., Botvinko, I. V., Lysak, L. V. [Effect of serotonin (5-hydroxytryptamine) on the growth and differentiation of microorganisms]. Mikrobiologiia 67, 305-312, 1998.

161. Anuchin, A. M., Chuvelev, D. I., Kirovskaia, T. A., Oleskin, A. V. [Effects of monoamine neuromediators on the growth-related variables of *Escherichia coli* K-12]. Mikrobiologiia 77, 758-765, 2008.

162. Strakhovskaia, M. G., Ivanova, E. V., Frainkin, G. [Stimulatory effect of serotonin on the growth of the yeast Candida guilliermondii and the bacterium *Streptococcus faecalis*]. Mikrobiologiia 62, 46-49, 1993.

163. Roshchina, V. V., Evolutionary considerations of neurotransmitters in microbial, plant, and animal cells. In "Interkingdom Signaling in Infectious Disease and Health", Lyte, M.; Freestone, P. P. E., Eds. Springer, Microbial Endocrinology New York, NY, 17-52, 2010.

164. Bassler, B. L., Losick, R. Bacterially speaking. Cell 125, 237-246, 2006.

165. Bassler, B. How bacteria talk to each other: regulation of gene expression by quorum sensing. Curr Opin Microbiol 2, 582 - 587, 1999.

166. Lee, J. H., Lequette, Y., Greenberg, E. P. Activity of purified QscR, a *Pseudomonas aeruginosa* orphan quorum-sensing transcription factor. Mol Microbiol 59, 602-609, 2006.

167. Smith, K. M., Bu, Y., Suga, H. Induction and inhibition of *Pseudomonas aeruginosa* quorum sensing by synthetic autoinducer analogs. Chem Biol 10, 81-89, 2003.

168. Erspamer, V. Occurence of indolealkylamines in nature. Springer-Verlag, 1966.

169. Steck, N., Mueller, K., Schemann, M., Haller, D. Bacterial proteases in IBD and IBS. Gut 61, 1610-1618, 2012.

170. Miwa, J., Echizen, H., Matsueda, K., Umeda, N. Patients with constipation-predominant irritable bowel syndrome (IBS) may have elevated serotonin concentrations in colonic mucosa as compared with diarrhea-predominant patients and subjects with normal bowel habits. Digestion 63, 188-194, 2001.

171. Fuqua, C. The QscR quorum-sensing regulon of *Pseudomonas aeruginosa*: an orphan claims its identity. J Bacteriol 188, 3169 - 3171, 2006.

172. Pearson, J. P., Pesci, E. C., Iglewski, B. H. Roles of *Pseudomonas aeruginosa* las and rhl quorum-sensing systems in control of elastase and rhamnolipid biosynthesis genes. J Bacteriol 179, 5756-5767, 1997.

173. Smith, K., Bu, Y., Suga, H. Induction and inhibition of *Pseudomonas aeruginosa* quorum sensing by synthetic autoinducer analogs. Chem Biol 10, 81 - 89, 2003.

174. De Kievit, T. R., Gillis, R., Marx, S., Brown, C., Iglewski, B. H. Quorum-sensing genes in *Pseudomonas aeruginosa* biofilms: Their role and expression patterns. Appl Environ Microbiol 67, 1865-1873, 2001.

175. Davies, D. G., Parsek, M. R., Pearson, J. P., Iglewski, B. H., Costerton, J. W., Greenberg, E. P. The involvement of cell-to-cell signals in the development of a bacterial biofilm. Science 280, 295-298, 1998.

176. Garner, A. L., Struss, A. K., Fullagar, J. L., Agrawal, A., Moreno, A. Y., Cohen, S. M., Janda, K. D. 3-Hydroxy-1-alkyl-2-methylpyridine-4(1H)-thiones: Inhibition of the *Pseudomonas aeruginosa* virulence factor LasB. ACS Med ChemLett 3, 668-672, 2012.

177. Leid, J. G., Willson, C. J., Shirtliff, M. E., Hassett, D. J., Parsek, M. R., Jeffers, A. K. The exopolysaccharide alginate protects *Pseudomonas aeruginosa* biofilm bacteria from IFN-gamma-mediated macrophage killing. J Immunol 175, 7512-7518, 2005.

178. Ramsey, D. M., Wozniak, D. J. Understanding the control of *Pseudomonas aeruginosa* alginate synthesis and the prospects for management of chronic infections in cystic fibrosis. Mol Microbiol 56, 309-322, 2005.

179. Beatson, S. A., Whitchurch, C. B., Sargent, J. L., Levesque, R. C., Mattick, J. S. Differential regulation of twitching motility and elastase production by Vfr in *Pseudomonas aeruginosa*. J Bacteriol 184, 3605-3613, 2002.

180. Chauveau, J., Fert, V., Morel, A. M., Delaage, M. A. Rapid and specific enzyme immunoassay of serotonin. Clin Chem 37, 1178-1184, 1991.

181. Toimentseva, A. A., Sharipova, M. R. [Genetic mechanisms of the Bacillus adaptation]. Mikrobiologiia 82, 259-273, 2013.

182. Kim, C. S., Choi, B. H., Seo, J. H., Lim, G., Cha, H. J. Mussel adhesive protein-based whole cell array biosensor for detection of organophosphorus compounds. Biosen Bioelect 41, 199-204, 2013.

183. Date, A., Pasini, P., Daunert, S. Integration of spore-based genetically engineered whole-cell sensing systems into portable centrifugal microfluidic platforms. Anal Bioanal Chem 398, 349-356, 2010.

184. Kwon, H. J., Balcer, H. I., Kang, K. A. Sensing performance of protein C immuno-biosensor for biological samples and sensor minimization. Comp Biochem Physiol A Mol Integr Physiol 132, 231-238, 2002.

185. Tessaro, M. J., Soliman, S. S., Raizada, M. N. Bacterial whole-cell biosensor for glutamine with applications for quantifying and visualizing glutamine in plants. Appl Environ Microbiol 78, 604-606, 2012.

186. Bahl, M. I., Hansen, L. H., Licht, T. R., Sorensen, S. J. In vivo detection and quantification of tetracycline by use of a whole-cell biosensor in the rat intestine. Antimicrob Agents Chemother 48, 1112-1117, 2004.

187. WHO Arsenic in Drinking Water. http://www.who.int/mediacentre/factsheets/fs372/en/.

188. Date, A., Pasini, P., Daunert, S. Construction of spores for portable bacterial whole-cell biosensing systems. Anal Chem 79, 9391-9397, 2007.

189. Harwood, C. R., Cutting, S. M. Molecular Biological Methods for Bacillus. Wiley: New York, 1990.

190. Brenner, S. Genetics of *Caenorhabditis elegans*. Genetics 77, 71-94, 1974.

191. Sultson, J., Hodgkin, J., Methods. In "The nematode *Caenorhabditis elegans*", Wood, W. B., Ed. Cold Spring Harbor Laboratory, Cold Spring Harbor, 587-606, 1988.

192. Rothert, A., Deo, S. K., Millner, L., Puckett, L. G., Madou, M. J., Daunert, S. Whole-cell-reporter-gene-based biosensing systems on a compact disk microfluidics platform. AnalBiochem 342, 11-19, 2005.

193. Tisa, L. S., Rosen, B. P. Molecular characterization of an anion pump. The ArsB protein is the membrane anchor for the ArsA protein. J Biol Chem 265, 190-194, 1990.

194. Sato, T., Kobayashi, Y. The ars operon in the skin element of *Bacillus subtilis* confers resistance to arsenate and arsenite. J Bacteriol 180, 1655-1661, 1998.

195. Gladysheva, T. B., Oden, K. L., Rosen, B. P. Properties of the arsenate reductase of plasmid R773. Biochem 33, 7288-7293, 1994.

196. EPA. Arsenic in Drinking Water. http://water.epa.gov/lawsregs/rulesregs/sdwa/arsenic/,

197. Rahman, M. M., Chen, Z., Naidu, R. Extraction of arsenic species in soils using microwave-assisted extraction detected by ion chromatography coupled to inductively coupled plasma mass spectrometry. Environ Geochem Health 31 Suppl 1, 93-102, 2009.

198. Huang, J. H., Kretzschmar, R. Sequential extraction method for speciation of arsenate and arsenite in mineral soils. Anal Chem 82, 5534-5540, 2010.

199. Georgiadis, M., Cai, Y., Solo-Gabriele, H. M. Extraction of arsenate and arsenite species from soils and sediments. Environ Pollut 141, 22-29, 2006.

200. Pait, A. S., Whitall, D. R., Jeffrey, C. F., Caldow, C., Mason, A. L., Lauenstein, G. G., Christensen, J. D. Chemical contamination in southwest Puerto Rico: an assessment of organic contaminants in nearshore sediments. Mar Pollut Bull 56, 580-587, 2008.

201. Paul Sturm, R. V., Rob Ferguson, Tom Moore. Addressing land based sources of pollution in Guánica, Puerto Rico Proceedings of the 12th International Coral Reef Symposium, Cairns, Australia, 9-13 July 2012 21A Watershed Management and Reef Pollution 2012.

202. Plan, E. C. P. EPA Region 2 Coral Reef Protection Plan – Fiscal Year 2014, September 2013 http://www.epa.gov/region02/water/oceans/coral_protection_plansept2013final.pdf, 2013.

203. Cortinas, I., Field, J. A., Kopplin, M., Garbarino, J. R., Gandolfi, A. J., Sierra-Alvarez, R. Anaerobic biotransformation of roxarsone and related N-substituted phenylarsonic acids. Environ Sci Technol 40, 2951-2957, 2006.

204. Stolz, J. F., Perera, E., Kilonzo, B., Kail, B., Crable, B., Fisher, E., Ranganathan, M., Wormer, L., Basu, P. Biotransformation of 3-nitro-4-hydroxybenzene arsonic acid (roxarsone) and release of inorganic arsenic by Clostridium species. Environ Sci Technol 41, 818-823, 2007.

205. Yoshinaga, M., Cai, Y., Rosen, B. P. Demethylation of methylarsonic acid by a microbial community. Environ Microbiol 13, 1205-1215, 2011.

206. Terzic, O., Bartenbach, S., de Voogt, P. Determination of Lewisites and their hydrolysis products in aqueous and multiphase samples by in-sorbent tube butyl thiolation followed by thermal desorption-gas chromatography-full scan mass spectrometry. J Chromatogr A 1304, 34-41, 2013.

207. Chen, J., Qin, J., Zhu, Y. G., de Lorenzo, V., Rosen, B. P. Engineering the soil bacterium Pseudomonas putida for arsenic methylation. Appl Environ Microbiol 79, 4493-4495, 2013.

208. Liana, D. D., Raguse, B., Gooding, J. J., Chow, E. Recent advances in paper-based sensors. Sensors 12, 11505-11526, 2012.

209. Martinez, A. W., Phillips, S. T., Butte, M. J., Whitesides, G. M. Patterned paper as a platform for inexpensive, low-volume, portable bioassays. Angew Chem Int Ed Engl 46, 1318-1320, 2007.

210. Martinez, A. W., Phillips, S. T., Wiley, B. J., Gupta, M., Whitesides, G. M. FLASH: a rapid method for prototyping paper-based microfluidic devices. Lab Chip 8, 2146-2150, 2008.

211. Bruzewicz, D. A., Reches, M., Whitesides, G. M. Low-cost printing of poly(dimethylsiloxane) barriers to define microchannels in paper. Anal Chem 80, 3387-3392, 2008.

212. Abe, K., Kotera, K., Suzuki, K., Citterio, D. Inkjet-printed paperfluidic immuno-chemical sensing device. Anal BioanalChem398, 885-893, 2010.

213. Abe, K., Suzuki, K., Citterio, D. Inkjet-printed microfluidic multianalyte chemical sensing paper. Anal Chem 80, 6928-6934, 2008.

214. Carrilho, E., Martinez, A. W., Whitesides, G. M. Understanding wax printing: a simple micropatterning process for paper-based microfluidics. Anal Chem 81, 7091-7095, 2009.

215. Yetisen, A. K., Akram, M. S., Lowe, C. R. Paper-based microfluidic point-of-care diagnostic devices. Lab Chip 13, 2210-2251, 2013.

216. Singh, J., Mittal, S. K. Chlorella sp based biosensor for selective determination of mercury in presence of silver ions. Sens Actuat B-Chem 165, 48-52, 2012.

217. Hakkila, K., Green, T., Leskinen, P., Ivask, A., Marks, R., Virta, M. Detection of bioavailable heavy metals in EILATox-Oregon samples using whole-cell luminescent bacterial sensors in suspension or immobilized onto fibre-optic tips. J Appl Toxicol 24, 333-342, 2004.

218. Nguyen-Ngoc, H., Tran-Minh, C. Fluorescent biosensor using whole cells in an inorganic translucent matrix. Anal Chimica Acta 583, 161-165, 2007.

219. Date, A., Pasini, P., Daunert, S. Fluorescent and Bioluminescent Cell-Based Sensors: Strategies for Their Preservation. Adv. Biochem. Eng. /Biotechnol. 117, 57-75, 2010.

220. Fantino, J. R., Barras, F., Denizot, F. Sposensor: a whole-bacterial biosensor that uses immobilized Bacillus subtilis spores and a one-step incubation/detection process. J. Mol. Microbiol. Biotechnol. 17, 90-95, 2009.

221. Kaletta, T., Hengartner, M. O. Finding function in novel targets: *C. elegans* as a model organism. Nat Rev Drug Discov 5, 387-398, 2006.

222. Shtonda, B. B., Avery, L. Dietary choice behavior in *Caenorhabditis elegan*s. J Exp Biol 209, 89-102, 2006.

223. Rankin, C. H. Nematode behavior: the taste of success, the smell of danger! Curr Biol 16, R89-91, 2006.

224. Abada, E. A., Sung, H., Dwivedi, M., Park, B. J., Lee, S. K., Ahnn, J. *C. elegans* behavior of preference choice on bacterial food. Mol Cells 28, 209-213, 2009.

225. Liao, V. H., Yu, C. W. *Caenorhabditis elegans* gcs-1 confers resistance to arsenic-induced oxidative stress. Biometals 18, 519-528, 2005.

226. Roh, J. Y., Lee, J., Choi, J. Assessment of stress-related gene expression in the heavy metal-exposed nematode *Caenorhabditis elegans*: a potential biomarker for metal-induced toxicity monitoring and environmental risk assessment. Environ Toxicol Chem 25, 2946-2956, 2006.

227. Sok, J., Calfon, M., Lu, J., Lichtlen, P., Clark, S. G., Ron, D. Arsenite-inducible RNA-associated protein (AIRAP) protects cells from arsenite toxicity. Cell Stress Chaperones 6, 6-15, 2001.

228. Belkin, S. Microbial whole-cell sensing systems of environmental pollutants. Curr Opin Microbiol 6, 206-212, 2003.

229. Vreeland, R. H., Rosenzweig, W. D., Powers, D. W. Isolation of a 250 million-year-old halotolerant bacterium from a primary salt crystal. Nature 407, 897-900, 2000.

230. Rehman, K., Naranmandura, H. Double-edged effects of arsenic compounds: anticancer and carcinogenic effects. Curr Drug Metab 14, 1029-1041, 2013.

231. Thomas, D. J. The die is cast: arsenic exposure in early life and disease susceptibility. Cheml Res Toxicol 26, 1778-1781, 2013.

232. Jiang, J. Q., Ashekuzzaman, S. M., Jiang, A. L., Sharifuzzaman, S. M., Chowdhury, S. R. Arsenic contaminated groundwater and its treatment options in Bangladesh. Intern J Environ Res Public Health 10, 18-46, 2013.

233. McCarty, K. M., Hanh, H. T., Kim, K. W. Arsenic geochemistry and human health in South East Asia. Rev Environ Health 26, 71-78, 2011.

234. Arora, M., Megharaj, M., Naidu, R. Arsenic testing field kits: some considerations and recommendations. Environ Geochem Health 31 Suppl 1, 45-48, 2009.

235. Zhang, A. L., Zha, Y. Fabrication of paper-based microfluidic device using printed circuit technology. Aip Advances 2, 2012.

236. Dungchai, W., Chailapakul, O., Henry, C. S. A low-cost, simple, and rapid fabrication method for paper-based microfluidics using wax screen-printing. Analyst 136, 77-82, 2011.

237. Songjaroen, T., Dungchai, W., Chailapakul, O., Laiwattanapaisal, W. Novel, simple and low-cost alternative method for fabrication of paper-based microfluidics by wax dipping. Talanta 85, 2587-2593, 2011.

238. Lu, Y., Shi, W., Jiang, L., Qin, J., Lin, B. Rapid prototyping of paper-based microfluidics with wax for low-cost, portable bioassay. Electrophor 30, 1497-1500, 2009.

239. Carrilho, E., Phillips, S. T., Vella, S. J., Martinez, A. W., Whitesides, G. M. Paper microzone plates. Anal Chem 81, 5990-5998, 2009.

240. Sullivan, C. A., Meigh, J. R., Giacomello, A. M., Fediw, T., Lawrence, P., Samad, M., Mlote, S., Hutton, C., Allan, J. A., Schulze, R. E.*, et al.* The water poverty index: Development and application at the community scale. Natural Resources Forum 27, 189-199, 2003.

241. Hossain, S. M., Brennan, J. D. beta-Galactosidase-based colorimetric paper sensor for determination of heavy metals. Anal Chem 83, 8772-8778, 2011.

242. Abernathy, C. O., Liu, Y. P., Longfellow, D., Aposhian, H. V., Beck, B., Fowler, B., Goyer, R., Menzer, R., Rossman, T., Thompson, C.*, et al.* Arsenic: Health effects, mechanisms of actions, and research issues. Environ Health Perspect 107, 593-597, 1999.

243. Setlow, B., Atluri, S., Kitchel, R., Koziol-Dube, K., Setlow, P. Role of dipicolinic acid in resistance and stability of spores of *Bacillus subtilis* with or without DNA-protective alpha/beta-type small acid-soluble proteins. J Bacteriol 188, 3740-3747, 2006.

244. Paidhungat, M., Setlow, B., Driks, A., Setlow, P. Characterization of spores of *Bacillus subtilis* which lack dipicolinic acid. J Bacteriol 182, 5505-5512, 2000.

245. Matys, S., Raff, J., Soltmann, U., Selenska-Pobell, S., Bottcher, H., Pompe, W. Calcium dipicolinate induced germination of *Bacillus* spores embedded in thin silica layers: Novel perspectives for the usage of biocers. Chem Mat 16, 5549-5551, 2004.

246. Pelczar, P. L., Igarashi, T., Setlow, B., Setlow, P. Role of GerD in germination of *Bacillus subtilis* spores. J Bacteriol 189, 1090-1098, 2007.

247. Shetty, R. S., Deo, S. K., Shah, P., Sun, Y., Rosen, B. P., Daunert, S., Luminescence-based whole-cell-sensing systems for cadmium and lead using genetically engineered bacteria.Anal Bioanal Chem 376, 11-17, 2003.

248. Pan, Y., Du, X., Zhao, F., Xu, B. Magnetic nanoparticles for the manipulation of proteins and cells. Chem Soc Rev 41, 2912-2942, 2012.

249. Huschka, R., Zuloaga, J., Knight, M. W., Brown, L. V., Nordlander, P., Halas, N. J. Light-induced release of DNA from gold nanoparticles: nanoshells and nanorods. J Am Chem Soc 133, 12247-12255, 2011.

250. Alkilany, A. M., Thompson, L. B., Boulos, S. P., Sisco, P. N., Murphy, C. J. Gold nanorods: their potential for photothermal therapeutics and drug delivery, tempered by the complexity of their biological interactions. Adv Drug Deliv Rev 64, 190-199, 2012.

251. Schroeder, A., Goldberg, M., Kastrup, C., Levins, C. G., Langer, R. S., Anderson, D. G. Remotely-activated protein-producing nanoparticles. Nano Lett, 12, 2685-2689, 2012.

252. Fabbro, A., Villari, A., Laishram, J., Scaini, D., Toma, F. M., Turco, A., Prato, M., Ballerini, L. Spinal cord explants use carbon nanotube interfaces to enhance neurite outgrowth and to fortify synaptic inputs. ACS Nano 6, 2041-2055, 2012.

253. Park, J. H., von Maltzahn, G., Xu, M. J., Fogal, V., Kotamraju, V. R., Ruoslahti, E., Bhatia, S. N., Sailor, M. J. Cooperative nanomaterial system to sensitize, target, and treat tumors. Proc Natl Acad Sci U S A 107, 981-986, 2010.

254. Dreaden, E. C., Alkilany, A. M., Huang, X., Murphy, C. J., El-Sayed, M. A. The golden age: gold nanoparticles for biomedicine. Chem Soc Rev 41, 2740-2779, 2012.

255. Morton, J. G., Day, E. S., Halas, N. J., West, J. L. Nanoshells for photothermal cancer therapy. Methods Mol Biol 624, 101-117, 2010.

256. Wijaya, A., Schaffer, S. B., Pallares, I. G., Hamad-Schifferli, K. Selective release of multiple DNA oligonucleotides from gold nanorods. ACS Nano 3, 80-86, 2009.

257. Miyako, E., Nagata, H., Hirano, K., Hirotsu, T. Laser-triggered carbon nanotube microdevice for remote control of biocatalytic reactions. Lab Chip 9, 788-794, 2009.

258. Ntziachristos, V., Ripoll, J., Weissleder, R. Would near-infrared fluorescence signals propagate through large human organs for clinical studies? Errata. Opt Lett 27, 1652, 2002.

259. Frimpong, R. A., Fraser, S., Hilt, J. Z. Synthesis and temperature response analysis of magnetic-hydrogel nanocomposites. J Biomed Mater Res A 80, 1-6, 2007.

260. Satarkar, N. S., Biswal, D., Hilt, J. Z. Hydrogel nanocomposites: a review of applications as remote controlled biomaterials. Soft Matter 6, 2364-2371, 2010.

261. Hamad-Schifferli, K., Schwartz, J. J., Santos, A. T., Zhang, S., Jacobson, J. M. Remote electronic control of DNA hybridization through inductive coupling to an attached metal nanocrystal antenna. Nature 415, 152-155, 2002.

262. Tietze, R., Lyer, S., Durr, S., Alexiou, C. Nanoparticles for cancer therapy using magnetic forces. Nanomed 7, 447-457, 2012.

263. Al Faraj, A., Gazeau, F., Wilhelm, C., Devue, C., Guerin, C. L., Pechoux, C., Paradis, V., Clement, O., Boulanger, C. M., Rautou, P. E. Endothelial cell-derived microparticles loaded with iron oxide nanoparticles: Feasibility of MR imaging monitoring in mice. Radiol, 2012.

264. Burtea, C., Laurent, S., Mahieu, I., Larbanoix, L., Roch, A., Port, M., Rousseaux, O., Ballet, S., Murariu, O., Toubeau, G.*, et al.* In vitro biomedical applications of functionalized iron oxide nanoparticles, including those not related to magnetic properties. Contrast Media Mol Imaging 6, 236-250, 2011.

265. Tartaj, P., Morales, M. D., Veintemillas-Verdaguer, S., Gonzalez-Carreno, T., Serna, C. J. The preparation of magnetic nanoparticles for applications in biomedicine. J Phys D: Appl Phys 36, R182-R197, 2003.

266. Thomas, C. R., Ferris, D. P., Lee, J. H., Choi, E., Cho, M. H., Kim, E. S., Stoddart, J. F., Shin, J. S., Cheon, J., Zink, J. I. Noninvasive remote-controlled release of drug molecules in vitro using magnetic actuation of mechanized nanoparticles. J Am Chem Soc 132, 10623-10625, 2010.

267. Stanley, S. A., Gagner, J. E., Damanpour, S., Yoshida, M., Dordick, J. S., Friedman, J. M. Radio-wave heating of iron oxide nanoparticles can regulate plasma glucose in mice. Science 336, 604-608, 2012.

268. Haraguchi, K., Takehisa, T. Nanocomposite hydrogels: a unique organic-inorganic network structure with extraordinary mechanical, optical, and swelling/deswelling properties. Adv Mater 14, 1120-1124, 2002.

269. Pardo-Yissar, V., Gabai, R., Shipway, A. N., Bourenko, T., Willner, I. Gold nanoparticle/hydrogel composites with solvent-switchable electronic properties. Adv Mater 13, 1320-1323, 2001.

270. Satarkar, N. S., Johnson, D., Marrs, B., Andrews, R., Poh, C., Gharaibeh, B., Saito, K., Anderson, K. W., Hilt, J. Z. Hydrogel-MWCNT nanocomposites: Synthesis, characterization, and heating with radiofrequency fields. J Appl Polym Sci 117, 1813-1819, 2010.

271. Zhao, X., Ding, X., Deng, Z., Zheng, Z., Peng, Y., Tian, C., Long, X. A kind of smart gold nanoparticle-hydrogel composite with tunable thermo-switchable electrical properties. New J Chem 30, 915-920, 2006.

272. Hilt, J. Z., Byrne, M. E., Peppas, N. A. Microfabrication of intelligent biomimetic networks for recognition of D-glucose. Chem Mat 18, 5869-5875, 2006.

273. Liedl, T., Dietz, H., Yurke, B., Simmel, F. Controlled trapping and release of quantum dots in a DNA-switchable hydrogel. Small 3, 1688-1693, 2007.

274. Wei, B., Cheng, I., Luo, K. Q., Mi, Y. Capture and release of protein by a reversible DNA-induced sol-gel transition system. Angew Chem Int Ed Engl 47, 331-333, 2008.

275. Hao, R., Xing, R., Xu, Z., Hou, Y., Gao, S., Sun, S. Synthesis, Functionalization, and biomedical applications of multifunctional magnetic nanoparticles. Adv Mater, 2010.

276. Satarkar, N. S., Hilt, J. Z. Magnetic hydrogel nanocomposites for remote controlled pulsatile drug release. J Controlled Release 130, 246-251, 2008.

277. Satarkar, N. S., Zhang, W., Eitel, R. E., Hilt, J. Z. Magnetic hydrogel nanocomposites as remote controlled microfluidic valves. Lab Chip 9, 1773-1779, 2009.

278. Bachas-Daunert, P. G., Law, S. A., Wei, Y. Charicterization of a recombinant thermostable dehalogenase isolated from the hot spring thermophile *Sulfolobus tokodaii*. Appl Biochem Biotechnol 159, 382-393, 2009.

279. Satarkar, N. S., Meenach, S. A., Anderson, K. W., Hilt, J. Z. Remote actuation of hydrogel nanocomposites: Heating analysis, modeling, and simulations. Aiche Journal 57, 852-860, 2011.

280. Cude, M. P., Gwenin, C. D. Development of gold coated superparamagnetic iron oxide nanoparticles for nitroreductase delivery. ECS Trans 33, 79-89, 2011.

281. Ren, Y. H., Rivera, J. G., He, L. H., Kulkarni, H., Lee, D. K., Messersmith, P. B. Facile, high efficiency immobilization of lipase enzyme on magnetic iron oxide nanoparticles via a biomimetic coating. BMC Biotechnol 11, 2011.

282. Bachas-Daunert, P. G., Sellers, Z. P., Wei, Y. Detection of halogenated organic compounds using immobilized thermophilic dehalogenase. Anal Bioanal Chem 395, 1173-1178, 2009.

283. Cardenas-Fernandez, M., Lopez, C., Alvaro, G., Lopez-Santin, J. L-Phenylalanine synthesis catalyzed by immobilized aspartate aminotransferase. Biochem Eng J 63, 15-21, 2012.

284. Grosova, Z., Rosenberg, M., Rebros, M., Sipocz, M., Sedlackova, B. Entrapment of beta-galactosidase in polyvinylalcohol hydrogel. Biotechnol Lett 30, 763-767, 2008.

285. Creed, F. How do SSRIs help patients with irritable bowel syndrome? Gut 55, 1065-1067, 2006.

286. Chugani, S. A., Whiteley, M., Lee, K. M., D'Argenio, D., Manoil, C., Greenberg, E. P. QscR, a modulator of quorum-sensing signal synthesis and virulence in *Pseudomonas aeruginosa*. PNAS 98, 2752-2757, 2001.

287. Hanzelka, B. L., Greenberg, E. P. Evidence that the N-terminal region of the *Vibrio fischeri* LuxR protein constitutes an autoinducer-binding domain. J Bacteriol 177, 815-817, 1995.

288. Checa, S. K., Zurbriggen, M. D., Soncini, F. C. Bacterial signaling systems as platforms for rational design of new generations of biosensors. Curr Opin Biotechnol 23, 766-772, 2012.

289. Reineke, K., Mathys, A., Knorr, D. The impact of high pressure and temperature on bacterial spores: inactivation mechanisms of *Bacillus subtilis* above 500 MPa. J Food Sci 76, M189-197, 2011.

290. Joyner, D. C., Lindow, S. E. Heterogeneity of iron bioavailability on plants assessed with a whole-cell GFP-based bacterial biosensor. Microbiol 146, 2435-2445, 2000.

291. Sperling, R. A., Parak, W. J. Surface modification, functionalization and bioconjugation of colloidal inorganic nanoparticles. Philos Trans A Math Phys Eng Sci 368, 1333-1383, 2010.

292. Chatterjee, A., Sun, S. B., Furman, J. L., Xiao, H., Schultz, P. G. A versatile platform for single- and multiple-unnatural amino acid mutagenesis in *Escherichia coli*. Biochem 52, 1828-1837, 2013.

293. Miyako, E., Nagata, H., Hirano, K., Hirotsu, T. Laser-triggered carbon nanotube microdevice for remote control of biocatalytic reactions. Lab Chip 9, 788-794, 2009.

# VITA

Leslie D. Knecht was born in Vallejo, California. She moved to Barbourville, Kentucky at the age of three where she graduated Salutatorian of her class from Knox Central High School in 2002. She then attended college at the University of Kentucky and earned a B.S. in Biology and Chemistry in 2006. After working as an undergraduate with Dr. Sylvia Daunert, she joined her research lab in Fall of 2006 at the University of Kentucky. She later transferred to the University of Miami with Dr. Daunert in 2011. Leslie is the recipient of numerous fellowships, including the National Science Foundation Integrative Graduate Education Research Traineeship, the Wethington Fellowship, and the Lyman T. Johnson Fellowship. Leslie has also received many awards during her time in graduate school including the 100% plus award from the University of Kentucky Department of Chemistry, 2$^{nd}$ place in the 2013 Superfund Research Program Poster Competition, 2014 Graduate Student Exemplar Award from the University of Miami, and was the subject of a film which won the Tribeca Film Festival Outstanding Role Model Award. During her time in graduate school, she has published several original research articles in peer reviewed journals.